Technische Universität München

Max-Planck-Institut für Biochemie

Small-molecule inhibitors of cyclin-dependent kinase 2 (CDK2) and the p53-Mdm2 interaction

Przemyslaw Jacek Ozdowy

Vollständiger Abdruck der von der Fakultät für Chemie der Technischen Universität München zur Erlangung des akademischen Grades eines

Doktors der Naturwissenschaften

genehmigten Dissertation.

Vorsitzender:	Univ.-Prof. Dr. Thomas Kiefhaber
Prüfer der Dissertation:	1. apl. Prof. Dr. Luis Moroder
	2. Univ.-Prof. Dr. Michael Groll

Die Dissertation wurde am 16. Juli 2008 bei der Technischen Universität München eingereicht und durch die Fakultät für Chemie am 18. September 2008 angenommen.

Acknowledgements

I would like to thank all of those who have contributed to this work. In particular, I am most grateful to Professor Robert Huber for giving me the opportunity to work in his department and for access to all his laboratories and facilities, and to Professor Luis Moroder for being my Doktorvater. This thesis was only possible because of the support of Doctor Tad A. Holak to whom I am indebted not just for his scientific contribution but also for his motivating words, day after day, his help, financial support and his friendship.

My thank goes to all of the NMR friendly team for their help and advice, physicists: Dr. Loyola D'Silva and Marcin Krajewski, as well as people who worked with me in the lab: Dr. Madhumita Ghosh, Dr. Narashimha Rao Nalabothula, Dr. Igor Siwanowicz, Dr. Paweł Śmiałowski, Dr. Joma Kanikadu Joy, Sudipta Majumdar, Aleksandra Mikolajka, Dr. Grzegorz Popowicz, Ulli Rothweiler, Mahavir Singh, Tomasz Sitar.

My apologies to the others who I have not mentioned by name, I am indebted to them for the many ways they helped me.

Finally, I would like to pay tribute to the constant support of my family and my friends, without their love over the many months none of this would have been possible and whose sacrifice I can never repay.

Publications

Parts of this thesis have been or will be published in due course:

1. D'Silva, L.; Ozdowy, P.; Krajewski, M.; Rothweiler, U.; Singh, M.; Holak, T. A.; Monitoring the effects of antagonists on protein-protein interactions with NMR spectroscopy *J. Am. Chem. Soc*.; 2005; *127*; 13220-13226.

2. Krajewski M., Ozdowy P., D'Silva, L.; Holak, T. A.; NMR indicates that the small molecule RITA does not block the p53-MdmM2 binding in vitro *Nature Med.* 2005; 11; 1135-1136

MANUSCRIPT IN PREPARATION:

1. Ozdowy P.; D'Silva, L.; Holak, T. A.; Small-molecule inhibitors of the p53-Mdm2 interaction.

Contents

Chapter 1

Introduction

1.1 Overview

Protein–protein interactions are essential for many biological processes and for that reason represent a large and important class of targets for human therapeutics. Protein–protein interactions have been of great interest to drug discovery; however, developing small-molecule antagonists has been a difficult task. A number of factors can challenge the identification of small organic compounds that inhibit protein–protein interactions. These include the general lack of small-molecule starting points for drug design, the typical flatness of the interface, and the difficulty of distinguishing real from artifactual binding, and the size and characteristics of typical small-molecule libraries. Selection of a tractable protein–protein system is also important. Good targets for small-molecule inhibition are those that have small hot spots that can be covered by a drug-sized molecule. Drug discovery is also crucially augmented by the availability of orthogonal methods of characterization; such methods include biophysics, mutagenesis, epitope mapping and structural biology (Table 1, Appendix). A novel molecule can be described as ‘validated’ when it has been shown to bind noncovalently with 1:1 binding stoichiometry to the target of interest. NMR and X-ray crystallography play key roles in identification of small organic compounds that inhibit protein–protein interactions. Crystallography is used to identify the binding site or to generate hypotheses for structure-based design. NMR spectroscopy techniques are attractive for characterization a macromolecular complexes. The full range of biological and chemical methods to uniformly or selectively label ligands and/or active site residues will often be needed in order for NMR spectroscopy to contribute to structure based drug design projects in timely manner. It should be noted that combinations of chemical and

biological approaches do provide valuable information. Often, it is the combination of methods, rather than any one experiment, that propel a drug-discovery project forward.

1.2 p53-Mdm2

The human p53 tumor suppressor protein is a tetrameric nuclear phosphoprotein that is 393 amino acids long (*Figure 1*). The central region of p53 contains a DNA-binding domain, the N-terminus contains a transcription activation domain, and the C-terminal domain is involved in oligomerization. The central domain of p53 is activated by cellular stress or DNA-damage and binds specifically to DNA (Zauberman et al., 1993).

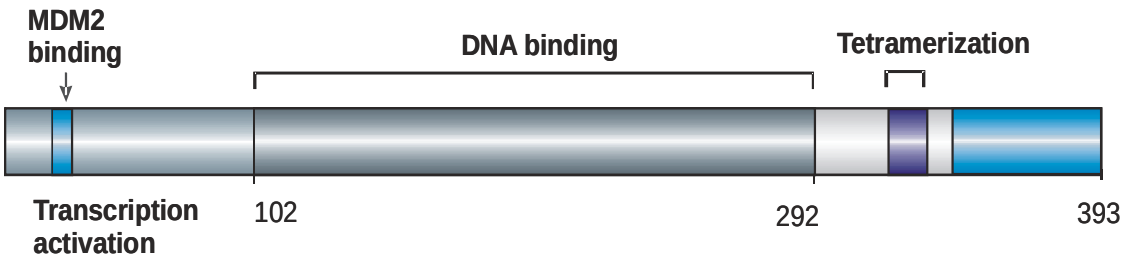

Figure 1 Schematic representation of the human full-length p53 protein.

p53 can prevent tumor cell proliferation by programmed cell death or by arresting the cell cycle (Chen et al., 1994; Gotz and Montenarh, 1995). The cellular stress response pathway regulated by p53 is critical for the maintenance of genomic integrity and for the prevention of oncogenic transformation (Momand et al., 2000; O'Connor et al., 1997). Mutants of p53, frequently seen in a large number of different human cancers, fail to bind to the DNA and hence cause the loss of tumor suppressor activity (May and May, 1995; Pan and Haines, 2000). Loss of p53 function through mutations is involved in ~50% of human cancers.

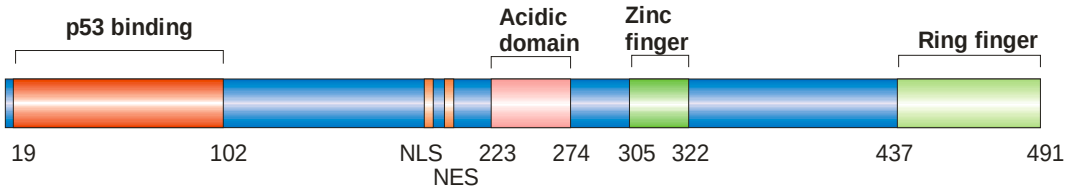

Figure 2 Schematic representation of the full-length Mdm2.

Wild-type p53 is also inactivated through interaction with the Mdm2 protein (*Figure 2*) (Deb, 2002; Jones et al., 1998). Mdm2 is a principal cellular antagonist of p53 that interacts through its 100 residue amino terminal domain with the N-terminal transactivation domain of p53 (Oliner et al., 1993). The rescue of the impaired p53 function by disrupting the Mdm2-p53 wild type interaction offers new avenues for anticancer therapeutics and several lead compounds have recently been reported which inhibit this interaction (Arkin and Wells, 2004; Klein and Vassilev, 2004).

1.3 The Mdm2-p53 interaction

The crystal structure of the p53-Mdm2 complex shows that the N-terminal part of the transactivation domain of p53 forms an amphipathic α-helix, which inserts its hydrophobic face (Phe19, Trp23, and Leu26) into a deep groove in Mdm2 (Kussie et al., 1996). Molecular mechanisms of the interaction between Mdm2 and p53 were also investigated using peptide libraries (Schon et al., 2002).

1.4 Mdm2 inhibitors

The first class of reported Mdm2-p53 inhibitors was chalcones (*Figure 3,* compound 1) (Stoll et al., 2001). Biochemical assays showed that these compounds could disrupt the p53-Mdm2 protein complex with the highest inhibitory activity for Mdm2 of 40 µM. Boronic derivatives of chalcones were also reported to inhibit the growth of human breast cell lines at micromolar concentrations. More recent NMR studies, however, showed that these compounds are very weak binders of Mdm2 (D'Silva et al., 2005). In general, anticancer role of chalcones may also be a consequence of their antioxidant properties, mediated via inhibition or induction of metabolic enzymes (Go et al., 2005). Zhao et al. introduced non-peptidic inhibitors derived form the substituted bicyclo[2.2.1]heptanes (Zhao et al., 2002). Cellular assays show some of these inhibitors have affinity for Mdm2. For example, compound syc-7 (*Figure 3,* compound 2) can activate the p53 pathway, by stimulating p53 accumulation in cell lines, and induce apoptosis. Another non-peptidic inhibitor was obtained by techniques based on a computationally derived pharmacophore model of the Mdm2 binding (Galatin and Abraham, 2004). In these studies the sulfonamide compounds inhibited the physical interaction of recombinant p53 and Mdm2 in vitro. In a more recent study, we showed that the sulfonamide inhibitor (*Figure 3,* compound 3) precipitated Mdm2 and released a folded p53 (D'Silva et al., 2005).

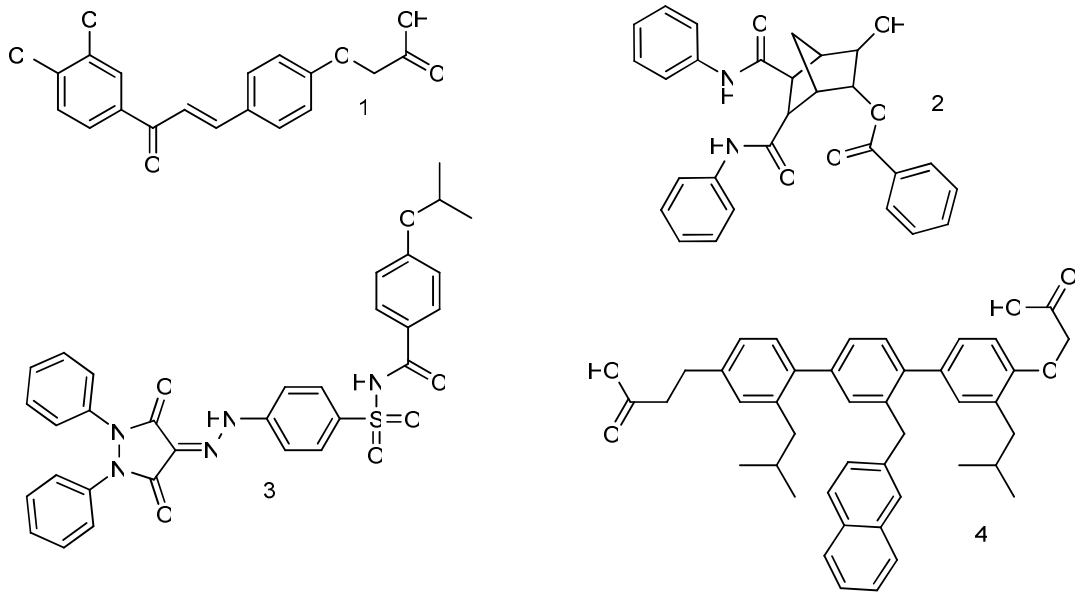

Figure 3 Chemical structures of the Mdm2 inhibitors. (1) chalcone, (2) bicyclo[2.2.1]heptane, (3) the sulfonamide compound, (4) terphenyl derivative,

Terphenyl derivatives were obtained by using a similar strategy and showed to be potent Mdm2 antagonists (Yin H et al., 2005). These compounds were designed to mimic one face of the α-helical p53 peptide. NMR assays indicated that one of the derivatives (with 2-naphthylmethylene at the middle phenyl ring) (*Figure 3,* compound 4) interacts with Mdm2 in a manner similar to p53 peptides.

The first convincing evidence for drug-like molecules of the p53-Mdm2 interaction was reported by Vassilev et al. (2004) when they introduced a series of cis-imidazoline compounds, named Nutlins, which were capable to activate selectively the p53 pathway both in vitro and, importantly, in vivo in human tumor cell lines, which contain wild-type p53 and overexpress Mdm2, thus leading to growth inhibition and apoptosis. Nutlin-3 (*Figure 4,* compound 5) was shown to inhibit the p53-Mdm2 interaction with an IC_{50} of 0.09 µM (Vassilev et al., 2004). The NMR and X-ray structures of a complex between

Mdm2 and Nutlin-3 showed that it binds to Mdm2 at the p53 protein binding site (Fry et al., 2004). Also, studies preformed by our group on Nutlins showed that Nutlin-3 is capable of releasing p53 from the Mdm2-p53 complex. The free p53 is folded and the Mdm2-Nutlin-3 complex stays in solution (e.g. Nutlin-3 did not induce precipitation of Mdm2) (D'Silva et al., 2005). Caylin-1 and Caylin-2 produced by the Cayman Chemical Company are the Nutlin-3 analogues that are 7-fold and 10-fold less potent, respectively, than Nutlin-3 in the same assays (*Figure 4,* compounds 6 and 7) (Cat nr: 10005002, 10004985; www.caymanchem.com).

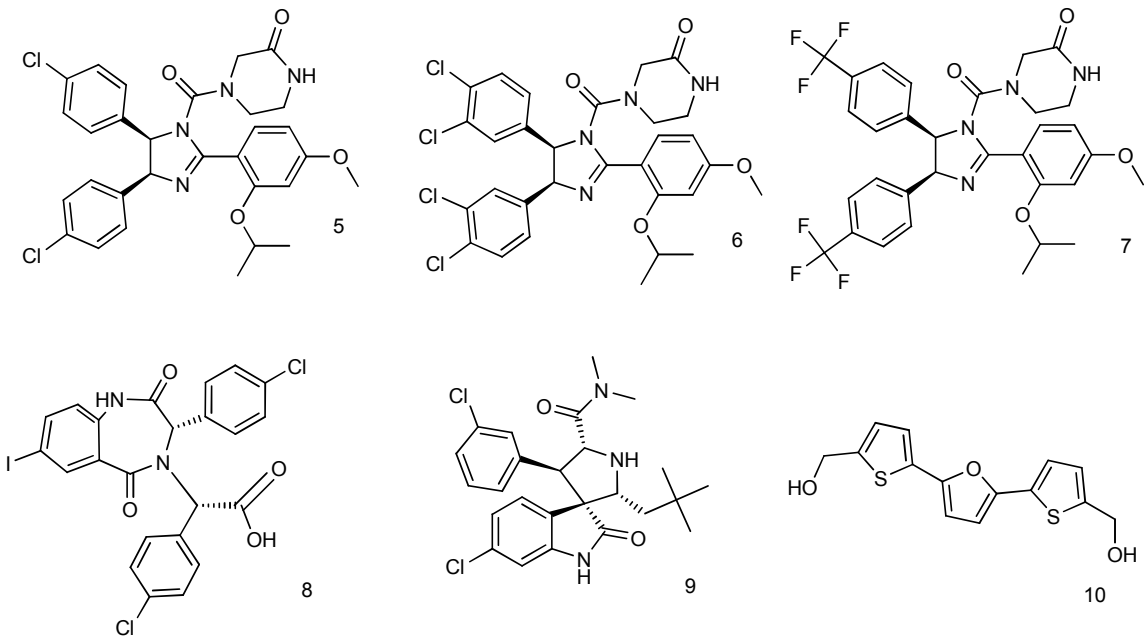

Figure 4 Nutlins and inhibitors with high affinity to Mdm2. (5) Nutlin-3, (6) Caylin-1 and (7) Caylin-2. (8) benzodiazepinedione, (9) oxindole, and (10) RITA.

A second class of small molecules based on benzodiazepinedione, a different chemotype then the Nutlins, was recently reported to bind to Mdm2 with high affinity and to show functional agonism of p53 in cells (Grasberger et al., 2005). The crystal

structure of compound 9 complexed to Mdm2 showed that it occupies the same pocket as the p53 peptide (*Figure 4*). Finally, Ding et al., used a substructure search technique in natural products to find motifs that could mimic the interaction of Trp23 of p53 with Mdm2. Oxindole was found to perfectly mimic the side-chain of Trp23 for interaction with Mdm2 (*Figure 4,* compound 9) (Ke Ding et al., 2005). The capability of these compounds to disrupt the interaction between Mdm2 and p53 was established by fluorescent polarization-based binding assays.

Suppression of Mdm2 can be obtained not only by a direct inhibition of the p53-Mdm2 complex formation (*Figure 5,* **A**), but also in principle by conformational changes in proteins involved in the complex (*Figure 5,* **B** and **C**).

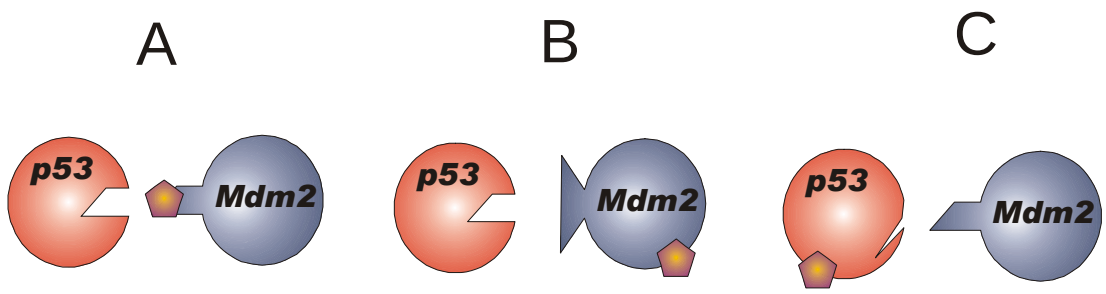

Figure 5 Disrupting p53–Mdm-2 interactions by small molecules. (**A**) Inhibitor prevents the p53 Mdm2 complex formation by interaction with the p53 Mdm2 binding site (**B**), (**C**) Inhibition by conformational or/and functional changes of the partners.

Issaeva et al. (2004) introduced a small molecule compound, RITA (*Figure 4,* compound 10), that rescues impaired p53 function by blocking p53's interaction with Mdm2. In in vitro studies, these authors claimed that RITA is a p53-binding compound that disrupted the p53–Mdm2 interaction by causing a two-step conformational change

in p53 (Issaeva et al., 2004). Direct binding of RITA to p53 in vitro was however not observed in our recent NMR studies (Krajewski et al., 2005).

In recent studies, a new way of inhibition of the p53-Mdm2 complex has been presented, by blocking the p53 degradation by the E3 ligase activity of Mdm2 (Yang et al., 2004). For example, Berkson et al. (2005) screened a large library of small molecules and found three candidates that can inhibit Mdm2 autoubiquitylation (Berkson et al., 2005). These compounds were tested in the cell-based reporter system. One of them showed mild cytotoxicity and is a good inducer of p53 dependent transcription (*Figure 6*, compound 11). This result seems to open a novel way for the p53/Mdm2 interaction based cancer therapeutics. A second group of E3 functional inhibitors have also been described recently (*Figure 6,* compounds 12, 13, and 14) (Yili Yang et al., 2005). These compounds have low solubility and need large therapeutic concentrations, but could serve as initial inhibitors for future optimization studies.

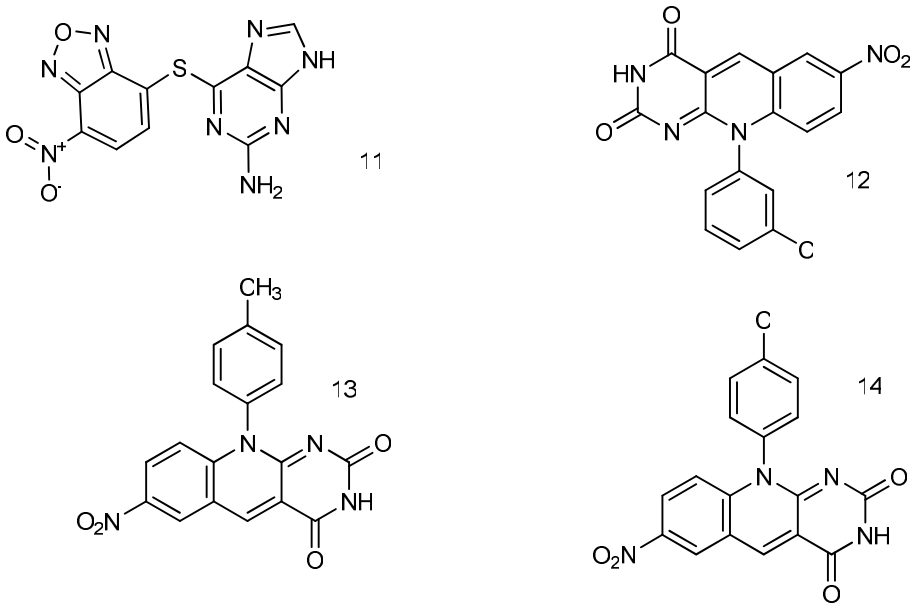

Figure 6 Chemical structures of E3 functional inhibitors.

The Mdm2 oncoprotein has been validated as a potential target for cancer drug development. Mdm2 amplification and/or overexpression occur in a wide variety of human cancers, several of which can be treated experimentally with Mdm2 antagonists. Mdm2 interacts primarily with the p53 tumor suppressor protein in an autoregulatory negative feedback loop to attenuate p53's cell cycle arrest and apoptosis functions. Inhibition of the p53-Mdm2 interaction has been shown to cause selective cancer cell death, as well as sensitize cancer cells to chemotherapy or radiation effects. Consequently, this interaction has been the main focus of anticancer drug discovery targeted to Mdm2. The promotion of the proteasomal degradation of the p53 protein by Mdm2 is central to its repression of the tumor suppressor functions of p53, and many proteins impinge upon this activity, either enhancing or inhibiting it. Mdm2 also has oncogenic activity independent of its interaction with p53, but this has so far not been explored for drug discovery. Among the approaches for targeting Mdm2 for cancer therapy, small molecule antagonists have recently featured as effective anticancer agents in experimental models, although the repertoire is currently limited and none has yet entered human clinical trials. As shown on previous pages, small molecules that have been reported to disrupt the p53-Mdm2 binding, thereby enhancing p53 activity to elicit anticancer effects include the following: synthetic chalcones, norbornane derivatives, cis-imidazoline derivatives (Nutlins), a pyrazolidinedione sulfonamide and 1,4-benzodiazepine-2,5-diones, as well as tryptophan derivatives. In addition to compounds disrupting p53pMdm2 binding, three compounds have been discovered that are effective in inhibiting the E3 ligase activity of Mdm2 towards p53, and should serve as leads for drug discovery targeting this aspect of the p53-Mdm2 interaction as well.

These compounds were discovered from library screening and/or structure-based rational drug design strategies.

1.5 Cyclin-dependent kinase 2 (CDK2)

Cyclin-dependent kinase 2 (CDK2) is a Ser/Thr protein kinase that belongs to the cyclin-dependent kinase family (Elledge and Spottswood, 1991) (*Figure 7*). Protein kinases become active when they associate with their respective cyclin subunits (Tsai et al., 1991). Cyclins appear and disappear during the cell division cycle. Today 13 CDKs have been discovered (Shapiro, 2006). CDKs were originally studied for their cell cycle functions. Cell cycle progression is mediated by activation and deactivation through phosphorylation of various tumor suppressor proteins (Nevins, 1992), transcription factors (Harbour et al., 1999; Pagano et al., 1992) and other proteins that are important for DNA replication and cell division (Guadagno et al., 1993; Xiong et al., 1992). In normal cells, progression from one phase of the cycle to the next can be initiated only after passage through checkpoints, where correct completion of the preceding steps is controlled. Tumor cells possess faulty checkpoints and can proliferate despite a compromised genome. Very often the mechanisms by which transformed cells can override checkpoints are closely related to CDK function (Zhu et al., 2004). For this reason, restoration of cell cycle control through pharmacological inhibition of CDKs has been actively pursued over the last decade as a new strategy for the treatment of cancer (Balasubramanian et al., 2005; Owa et al., 2001).

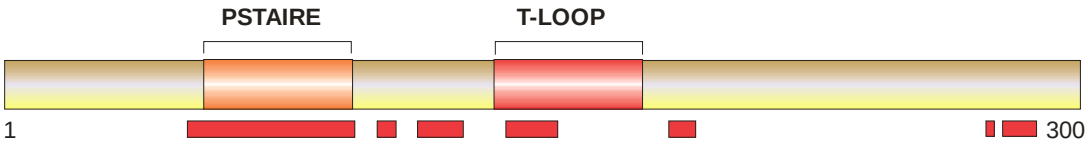

Figure 7 Schematic representation of the full-length CDK2 protein. The CDK2 sequence was taken from the crystal structure (PDB entry 1FIN). The sequence regions corresponding to the PSTAIRE helix and the T-loop are indicated. The regions that contact the respective cyclin molecule in the structures are represented by red boxes.

1.6 Inhibitors of CDK2

Many low molecular weight compounds with very high potency in vitro are available but in many cases this biochemical potency does not translate into cellular potency, perhaps due to unknown mechanistic reasons. In many studies CDK2 has been shown as potential target for small molecular substances. Inhibitors of this protein can be classified into several classes. The biggest class represents substituted purines and pyrimidines. They are most structurally similar to adenosine 5'-triphosphate (ATP) whose binding they antagonize. Surprisingly, however, all known purine-based inhibitors for which co-crystal structures with CDK2 have been solved, do not bind to the kinase in a way that mimics ATP (Fischer and Lane, 2000). Substituted adenines yielded the first CDK-selective protein kinase inhibitors (De Azevedo et al., 1997).

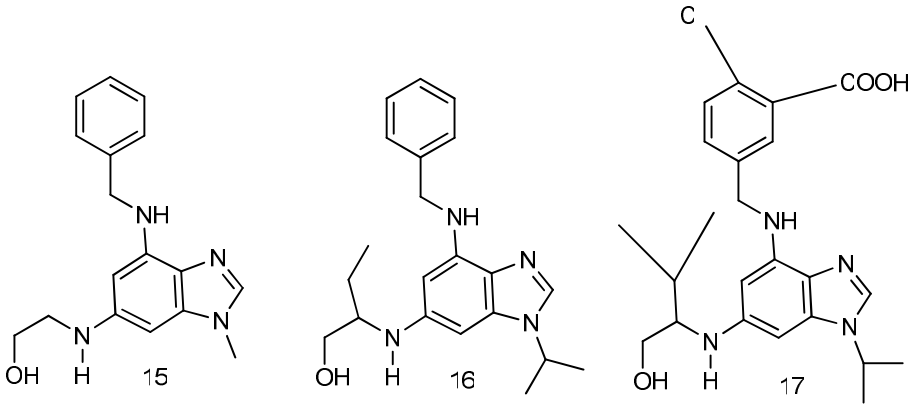

Figure 8 Chemical structures of Olomucine family inhibitors.

Olomoucine (*Figure 8*, compound 15) is a weak inhibitor of CDK2; examples of close analogs with improved potency are roscovitine and N9-isopropylolomoucine (*Figure 8*, compound 16) (Alessi et al., 1998; Glab et al., 1994; Schutte et al., 1997). Roscovitine inhibits cyclin complexes of CDK2 with high nanomolar IC_{50} values. The purvalanols display a similar selectivity profile (Meijer and Raymond, 2003). They are among the most potent CDK2 inhibitors reported to date; thus purvalanol B (*Figure 8*, compound 17) inhibits CDK2 with IC_{50} values of < 10 nM (Gray et al., 1999; Gray et al., 1998). Potent purine-based CDK inhibitors, such as CGP79807 and CGP74514 (*Figure 9*, compound 18 and 19), with cyclic hydroxy- or amino-alkylamino groups present at C2, have also been described (Dreyer et al., 2001; Furet et al., 2000) .

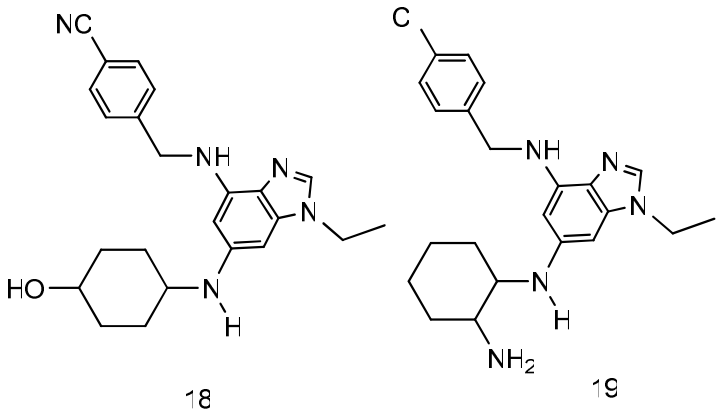

Figure 9 Chemical structures of Olomucine family inhibitors.

Guanine derivatives compounds NU2058 and NU6102 (*Figure 10*, compound 20 and 21), represent yet another subgroup of purine-derived inhibitors (Arris et al., 2000). Compound NU2058 is modestly potent against CDK2. Structure-based design starting from this compound led to the identification of NU6102, which possesses both increased potency and aqueous solubility (Davies et al., 2002a; Davies et al., 2002b; Hardcastle et al., 2002).

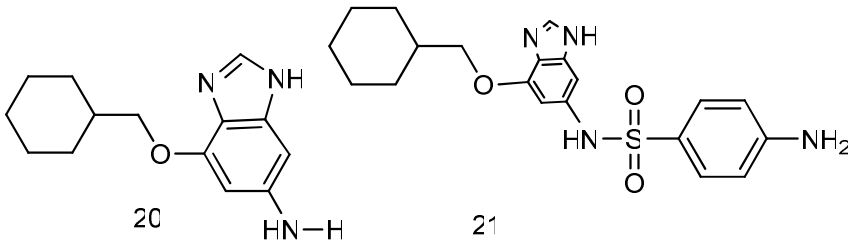

Figure 10 Chemical structures of guanine derivatives.

Pyrimidine derivatives like phenylaminopyrimidines CGP60474 (*Figure 11*, compound 22) have been shown as selective inhibitors of CDK2 (Furet et al., 2000; Toogood, 2001). NU6027 (*Figure 11*, compound 23) was designed as an alternative to

the corresponding purine-based compound NU2058 and the designed mimicry was confirmed crystallographically (Hardcastle et al., 2002).

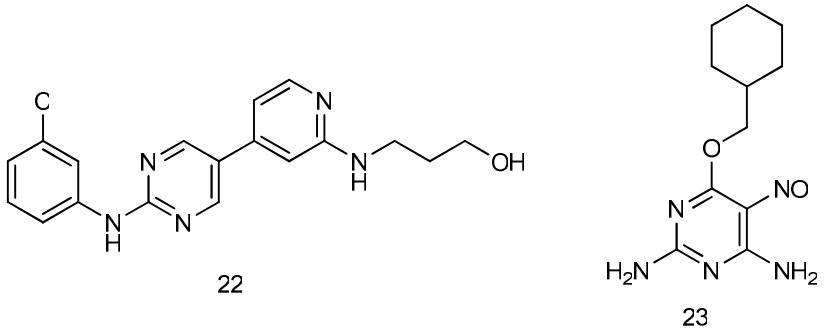

Figure 11 Chemical structures of phenylaminopyrimidines derivatives

Another type of pyrimidine inhibitors represent thiazolopyrimidines (Fischer, 2004) such as structures 24, 25, and 26 (*Figure 12*). Thiazolopyrimidine 26 is an extremely potent CDK2 inhibitor (IC50 < 1 nM).

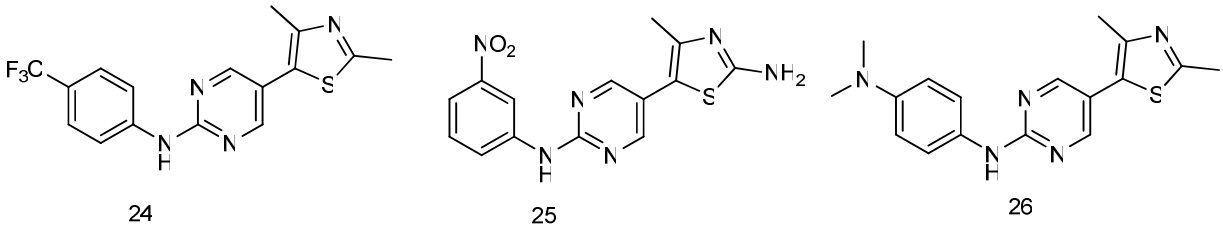

Figure 12 Chemical structures of thiazolopyrimidine derivatives

Heterocyclic compounds are yet another group of CDK2 inhibitors. An oxindole group represented by indirubin-3'-monoxime (*Figure 13*, compound 27) and indirubin 5-sulfonate (*Figure 13*, compound 28), that contains two fused oxindole groups, are potent and apparently selective inhibitors of CDK2 (Davies et al., 2001).

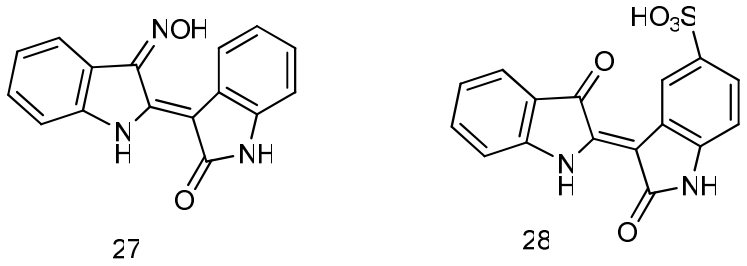

Figure 13 Chemical structures of oxindole derivatives with fused oxidole groups

Numerous oxindole-based CDK2 inhibitors have been described and an extensive study was published showing both phenylhydrazone (*Figure 14*, compound 29 and 30) and anilinomethylene (*Figure 14*, compound 31) oxindoles (Bramson et al., 2001).

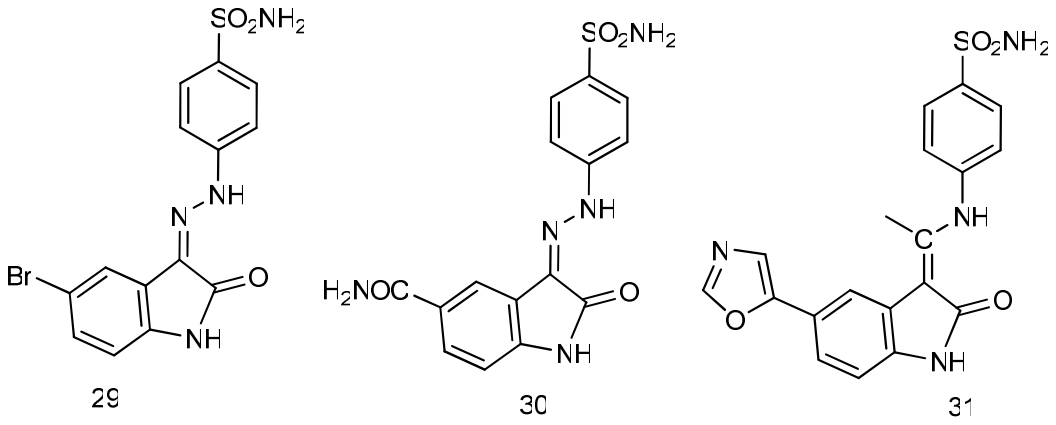

Figure 14 Chemical structures of oxindole derivatives.

Structurally related to the oxindoles are the indenopyrazoles (*Figure 15*), which have also been shown to be CDK inhibitors with potency and selectivity against CDK2. Compounds 32 and 33 are examples for which an anti-proliferative effect, consistent with CDK inhibition, has been demonstrated (Nugiel et al., 2002; Yue et al., 2002).

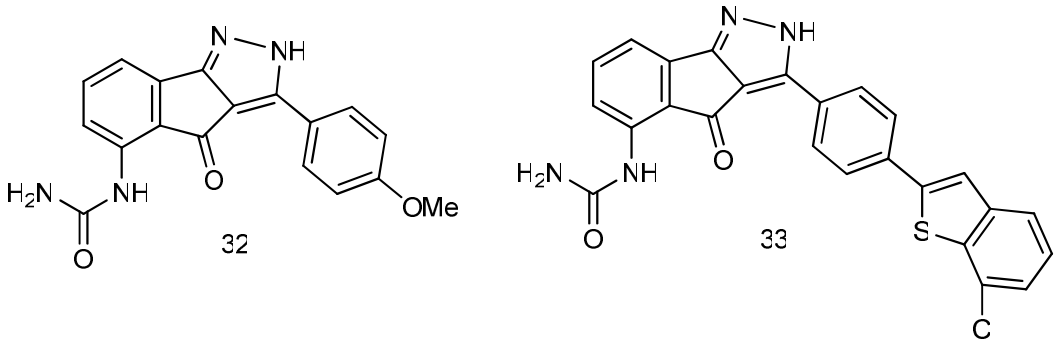

Figure 15 Chemical structures of indenopyrazoles derivatives.

Last classes of CDK2´s heterocyclic inhibitors are anilinoquinazolines and aminothiazole compounds (*Figure 16*, compound 34 and 35), (Kim et al., 2002; Sielecki et al., 2001).

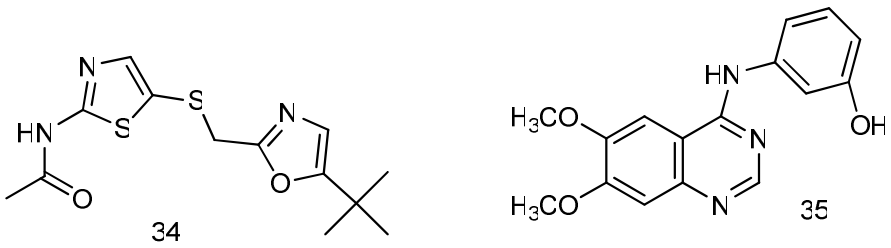

Figure 16 Chemical structures of anilinoquinazolines and aminothiazole derivatives.

Other CDK2 inhibitors are paullones. Classes of these compounds were found to be potent selective inhibitors of CDK2 and kenpaullone (*Figure 17*, compound 36) with

nanomolar activity (Zaharevitz et al., 1999). The most potent derivative in this series was named alsterpaullone (*Figure 17*, compound 37) (Soni and Jacobberger, 2004). Another compound with potent CDK2 inhibition properties is butyrolactone-I (*Figure 17*, compound 38) (Kitagawa et al., 1994; Kitagawa et al., 1993).

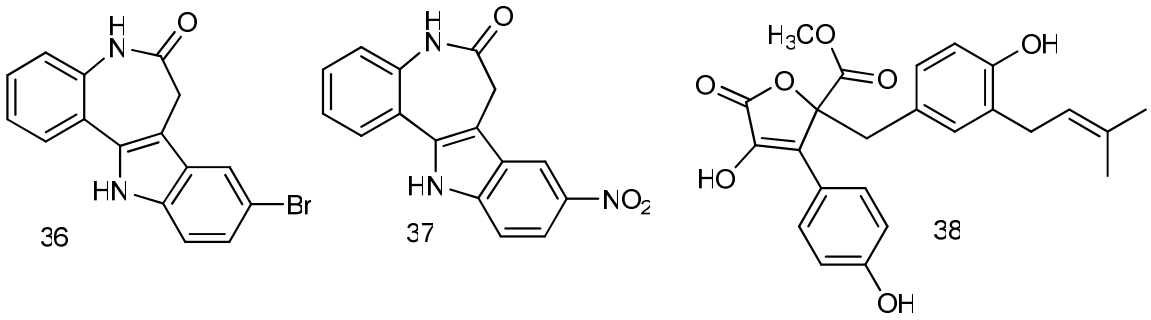

Figure 17 Chemical structures of paullones derivatives and butyrolactone-I.

The most recently reported are heterocyclic analogues of flavopiridol; 8-amidoflavone, 8-sulfonamidoflavone, 8-amido-7-hydroxyflavone (Ahn et al., 2007).

1.7 Chalcones

Chalcones (benzylideneacetophenone) and chalcone derivatives have been shown to exhibit cytotoxic activity against cancer cells and may have potential applications in cancer treatment (Makita et al., 1996; Satomi, 1993; Yamamoto et al., 1991). Natural and synthetic chalcones have been shown to have anticancer activity in various tumor cells. De Vincenzo et al. (2000) presented the effect of 15 different natural and synthetic chalcones on the proliferation of both established and primary ovarian cancer cells. Another study showed the tumour reducing and antioxidant activity of synthetic

chalcones and structurally related compounds. Methyl and hydroxy substituted chalcones were found to be cytotoxic in vitro, whereas only hydroxy substituted chalcones could reduce ascites tumours in animals (Anto et al., 1995). Z-1,1-dichloro-2,3-diphenylcyclopropane have been shown to inhibit proliferation of both estrogen-responsive and -nonresponsive human breast cancer cells (ter Haar et al., 1997). A series of chalcones and (E)-4-(4'-hydroxyphenyl)but-3-en-2-one were tested for their ability to inhibit cell growth in vitro. This study indicated their ability to bind to tubulin and the disruption of microtubule assembly (Lawrence et al., 2000). A total of 150 chemically-defined natural and synthetic polyphenols (flavonoids, dibenzoylmethanes, dihydrostilbenes, dihydrophenanthrenes and 3-phenylchromen-4-ones), with molecular weights ranging from 224 to 824, were investigated for cytotoxic activity against human oral squamous cell carcinoma HSC-2 and salivary gland tumor HSG cell lines compared to normal human gingival fibroblasts HGF. Many of the compounds have shown the cytotoxic activity (Fukai et al., 2000). A natural chalcone extracted from a licorice root, Licochalcone-A, showed some anti-tumor activity. This compound has estrogenic activity, anti-tumor activity, and modulated the apoptotic protein Bcl-2 in human cell lines derived from acute leukemia, breast cancer, and prostate cancer (Rafi et al., 2000). In another study with breast cancer cells and the T-leukemic Jurkat cell lines, new chalcones have been identified as interesting compounds having chemopreventive and antitumor properties (De Vincenzo et al., 2000). However, the exact mechanisms by which chalcone compounds exert their cytotoxic effects in cancer cells remains unclear. Recent studies show several possibilities. Chalcones have a potent estrogenic activity and modulate the apoptotic protein Bcl-2 (Rafi et al., 2000). In another study, a group of hydroxychalcones that exhibited anticancer effects were examined for toxicity.

The cytotoxic mechanism of all of the hydroxychalcones was partly due to mitochondrial uncoupling as evident from an observed increase in oxygen consumption together with a collapse in the mitochondrial membrane potential, and this was associated with GSH oxidation. The highest pKa chalcones were the most effective at collapsing the mitochondrial membrane potential which suggests that the cytotoxic activity of hydroxychalcones are likely due to their ability to uncouple mitochondria (Sabzevari et al., 2004). Licochalcone (LA) induced modest level of apoptosis but had more pronounced effect on cell cycle progression arresting cells in G2/M, accompanied by suppression of cyclin B1 and Cdc2. It also inhibited phosphorylation of pRb (specifically phosphorylation of S780 with no change of phosphorylation status of T821), decreased expression of the transcription factor E2F concurrent with reduction of cyclin D1, down-regulation of CDKs 4 and 6, but increased cyclin E expression. These findings provide mechanistic explanation for LA activity and suggest that it may be considered as a chemopreventive agent and its anticancer properties should be further explored (Fu et al., 2004). We and others showed that carboxylic chalcones may disrupt the Mdm2-p53 interaction (Stoll et al., 2001) and that boronic chalcone derivatives induce an accumulation of p53 and p21 proteins and exhibit significantly greater growth inhibitory effect on human breast cancer cell lines than on normal breast epithelial cells.

1.8 Synthesis

1,3-Diphenylpropenone (benzylideneacetophenone) and its derivatives (ArCH=CHC(=O)Ar, chalcones) can be prepared by an aldol condensation between a benzaldehyde and an acetophenone in the presence of sodium hydroxide as a catalyst (*Figure 18*).

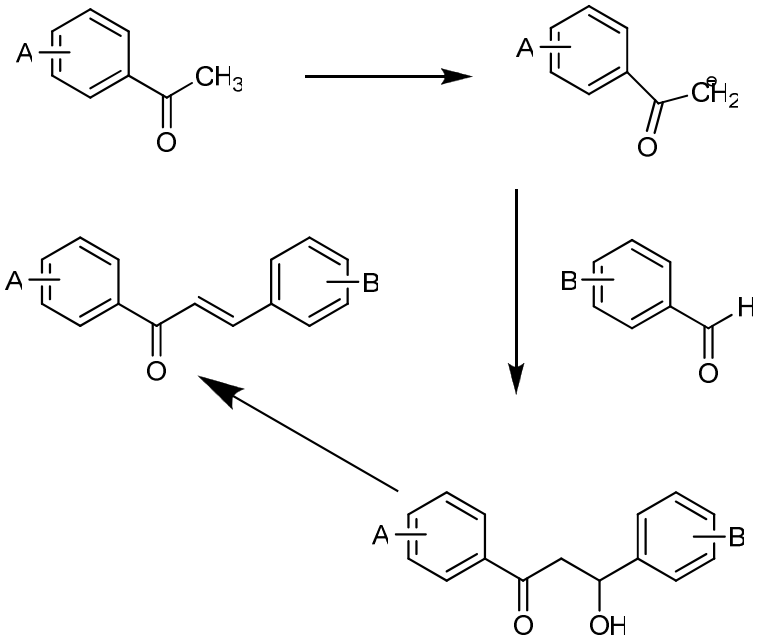

Figure 18 The aldol condensation: chalcone synthesis.

This reaction has been found to work also without any solvent at all - a solid-state reaction (Toda et al., 1990). The reaction between substituted benzaldehydes and acetophenones has been used to demonstrate green chemistry in undergraduate chemistry education (Palleros, 2004).

1.9 Onco-, tumorsuppressor and stem cell proteins: molecular targets for small-molecule antagonists

1.9.1 E7

E7 is the oncoprotein of human papillomavirus type 16 (Howley et al., 1989). This protein promotes cell proliferation in the presence of antiproliferative signals (Hawley-Nelson et al., 1989). Three regions, conserved regions CR1 and CR2 and a C-terminal zinc finger, are required for protein pathogenic activity (Gulliver et al., 1997) (*Figure 19*).

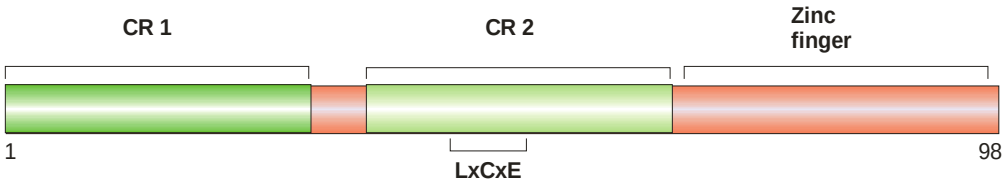

Figure 19 Schematic representation of the full-length protein E7 (Human papillomavirus type 91)

Additionally, a LxCxE motif was found in the conserved region 2 (Radulescu et al., 1995). Using this motif, viral E7 protein binds to the retinoblastoma tumor suppressor protein (pRb) and inactivates the growth suppressive functions of Rb and facilitates cell immortalization (Bringold and Serrano, 2000). Particulary, a high-affinity binding to the retinoblastoma tumor repressor (pRb) was shown in several studies (Dyson et al., 1992; Lee et al., 1998; McIntyre et al., 1996). The third region is a C-terminal zinc finger that functions in E7 dimerization (Zwerschke et al., 1996). There are two mechanisms proposed for the inactivation of Rb by E7. One is that E7 physically interferes with pRb-E2F binding; the second mechanism proposes the inactivation of pRb by the E7 targeted destabilization of pRb. The LxCxE motif of E7 is important for interference with

pRb-E2F binding (Chellappan et al., 1992), but role of E7 sequences outside of the LxCxE motif in blocking the association of pRb and E2F is not well defined. Expression of E7 reduces pRb levels in a number of cell types (Berezutskaya et al., 1997; Webster et al., 2001). Also, both the LxCxE motif (Chan et al., 2001) and CR1 (Gulliver et al., 1997; Martin et al., 1998), have been shown to be necessary for efficient reduction of pRb levels. This correlation may indicate that Rb destabilization is a secondary effect of E7 expression.

1.9.2 Model of the retinoblastoma protein

Up to now, in many studies the Rb protein (pRb) has been shown to be a tumor suppressor. It has been shown also that this protein plays a crucial role in the negative control of the cell cycle and in tumor progression. pRb is responsible for a major G1 checkpoint, blocking S-phase entry and cell growth. Three members, Rb/p105, p107 and Rb2/p130 are representing the retinoblastoma family (Stiegler and Giordano, 2001), and are known also as “pocket proteins”. Pocket domains A (aa 379-578), B (aa 642-791), C (aa 791-928) are indicated in *Figure 20*.

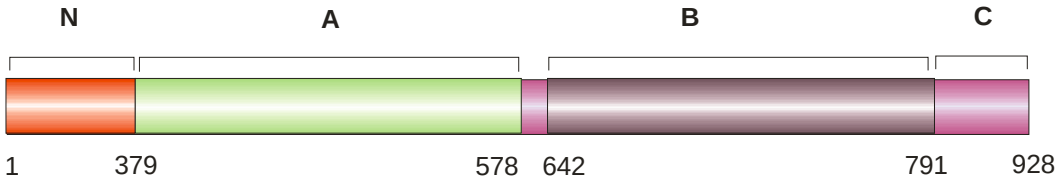

Figure 20 Schematic representation of the human full-length protein pRb

The mechanism of the pRb negatively regulating the transition from G_1 to S phase is by repressing genes responsive to the E2F family of transcription factors (Zhu et al., 1995). pRb binds E2F and inhibits transcription by blocking the E2F transcriptional

activation domain (Lang et al., 2001; Xiao et al., 2003), or also by factors such as histone deacetylase 1(HDAC1) (Nikolaev et al., 2004; Singh et al., 2005; Zini et al., 2001). During cell cycle, pRb is inactivated through phosphorylation by several cyclin--dependent kinase (CDK) complexes (Dyson, 1998). Loss of pRb functions through chromosomal mutations or by viral oncoprotein binding is one of the principal reasons for retinoblastoma tumor development (Giacinti and Giordano, 2006).

1.9.3 Nucleostemin

Nucleostemin (NSC) is a protein found in the nucleoli of embryonic stem cells, adult CNS stem cells (Tsai and McKay, 2002), and several cancer cell lines (Liu et al., 2004). It contains an N-terminal basic domain B and two GTP-binding motifs: G4 and G1 (*Figure 21*).

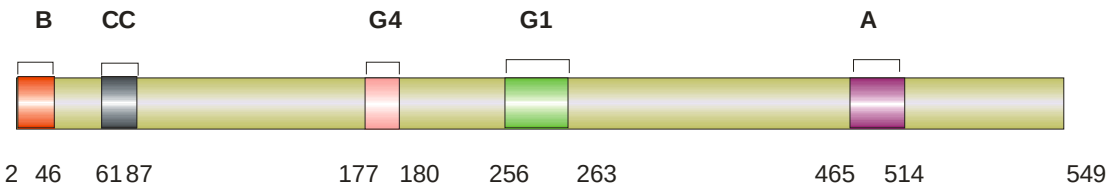

Figure 21 Schematic representation of the full-length protein nucleostemin

It has been shown through mutation analysis of this protein that mutants that lack the GTP-regulatory domain prevent cells from entering mitosis and cause apoptosis in a p53-dependent manner (Tsai and McKay, 2002, 2005),. The N-terminal basic domain is responsible for nucleolar localization (Normile, 2002). Additionally, nucleostemin was characterised as a stem cell marker present in many stem cells, like mesenchymal

(Baddoo et al., 2003) or neural stem cells (NSC) (Cai et al., 2004). This fact implicates that studies of nucleostemine may help in the development of protocols for stem cell based therapies. This protein has been involved in a novel nucleolar mechanism that controls the cell-cycle progression in stem cells and cancer cells (Han et al., 2005; Wang et al., 2004; Xu et al., 2004) and it has been suggested to have an important role in controlling the cell-cycle progression in stem cells and cancer cells (Beekman et al., 2006; Misteli, 2005; Schwartz et al., 2005; Yaghoobi et al., 2005).

1.10 Goal of studies

The molecular machinery that controls cell-cycle progression is based on the sequential activity of a family of protein kinases known as cyclin-dependent kinases or CDKs. A precise model for the interaction between CDKs and their binding partners can be created based on high-resolution 3-D structures of the interacting proteins. A binding site would place at our disposal a means to regulate the actions of the CDKs, arguably one of the most important cell cycle regulators. Numerous cases of CDK deregulation, because of mutation in these endogenous inhibitors in human cancers, prompted us to study several small molecule inhibitors with NMR spectroscopy, focusing on the ATP/inhibitor binding site of CDK2. Design and in silico modeling of novel, low molecular weight ligands with therapeutic potential should be possible based on new interaction sites revealed in this study.

Another important group of proteins are tumor suppressors and oncogenes. The retinoblastoma tumor suppressor protein (pRb) is the main substrate of the CDK4–6/D kinases. In its unphosphorylated or hypophosphorylated form, pRb associates with several transcription factors, silencing their transactivation functions. Of great relevance

among the pRb-regulated transcription factors are the E2F proteins. Similarly, viral oncoproteins such as SV40 large T antigen, adenoviral E1a protein, or herpes virus E7 protein, inactivate the growth suppressive functions of Rb and facilitate immortalization.

The tumor suppressor protein p53 is inactivated in approximately half of all human cancers. Activation of p53 involves complex post-translational modifications that include phosphorylation and acetylation, and leads to an increased half-life (hours) and to a conformation compatible with DNA binding and transactivation. Several targets of p53 have been identified that are involved in a variety of processes, such as cell-cycle arrest and apoptosis. p53 levels are determined mainly by the rate of p53 ubiquitination and subsequent proteolytic degradation. The main ubiquitin ligase E3-type enzyme for p53 is the oncogene Mdm2 (also known as HDM2 when referring specifically to the human gene). Mdm2 is an oncogene frequently amplified or overexpressed in sarcomas and in some other human cancers.

Nucleostemin (NSC) is a protein found in the nucleoli of embryonic stem cells, adult CNS stem cells. This protein has been involved in a novel nucleolar mechanism that controls the cell-cycle progression in stem cells and cancer cells

The important aim of this doctoral thesis was the expression of highly soluble recombinant proteins in *E. coli,* either unlabeled or labeled with ^{15}N. A preparative purification protocol for these proteins was established to obtain concentrated solutions suitable for analysis using NMR spectroscopic methods, and in the case of pRB, for crystallization trials. Furthermore, we were interested in the inhibitors of CDKs and of the p53-Mdm2 complex. Hence, another goal of this thesis was to review possible inhibitory compounds for these systems. Based on that, the most promising compound was analyzed by NMR. Finally, these experiments led to the development of new NMR

approaches to monitor protein-protein interactions in the presents of small molecular weight compounds.

Chapter 2

Materials and Methods

2.1 Organisms:

Bacterial strains: *Escherichia coli* Top 10, Xl Blue, BL21, BL21(DE3)

2.2 DNA techniques

2.2.1 The isolation of plasmid DNA

Preparation of plasmid DNA: The isolation of plasmid DNA from E. coli was carried out using plasmid purification kits from Qiagen. The kits employ a standard alkalina lysis of the precipitated bacteria in the presence of RNAse and strong ionic detergent, SDS, followed by neutralization/DNA renaturation with acetate. For purification, a crude cell elute was loaded onto a silica gel column, washed with an ethanol-containing buffer, and eluted in a small volume, yielding up to 20 µg of the plasmid DNA. A polymerase chain reaction was employed to amplify desired DNA fragments and genes, introduce restriction sites, STOP codons and sequences encoding restriction protease cleavage sites. The primers were prepared according to standardized principles regarding the length, GC-content.

2.2.2 PCR conditions

Reaction was prepared accordingly:

5 µl 10x buffer

0,5 µl dNTP 100 mM

50 or 100 ng template DNA

2,5 µl sens_primer 10 pmol/µl

2,5 µl antisens_primer 10 pmol/µl

water (up to 47,5 µl)

2,5 µl PWO polymerase from Peqlab (after initial heating)

PCR cycler was programmed depending on the oligonucleotide properties

2.2.3. Digestion with restriction enzymes

Usually, 1-2 units of each restriction enzyme were used per 1 µg of plasmid DNA to be digested. The digestion was performed in a buffer specified by the manufacturer at the optimal temperature (37℃) for 2-16 h. The frag ments ends that occurred after digestion were cohesive.

2.2.4 Purification of PCR and restriction digestion products

DNA obtained after restriction digestion was purified from primers, nucleotides, enzymes, buffering substances, mineral oil, salts, agarose, ethidium bromide, and other impurities, using a silica-gel column (QIAquick PCR purification Kit, Qiagen) or Gel Extraction Kit, Qiagen. The QIAquick system uses a simple bind-wash-elute procedure. A binding buffer was added directly to the PCR sample or other enzymatic reaction, and the mixture was applied to the spin column. Nucleic acids absorbed to the silica-gel membrane in the high-salt conditions provided by the buffer. Impurities and short fragments of single or double-stranded DNAs were removed by the wash step and pure DNA was eluted with a small volume of 10 mM Tris pH 8.0.

2.2.5 Agarose gel electrophoresis of DNA

For verification of the presence and length of PCR or restriction digestion products, agarose gel electrophoresis was performed. For this purpose 1% agarose in TBE buffer plus ethidium bromide was prepared. The solution was poured into a horizontal gel chamber to polymerise. The DNA samples were mixed with 6× sample buffer prior loading. Electrophoresis was carried out at 100-120 V DC. Results were evaluated using UV illumination (*Figure 22*).

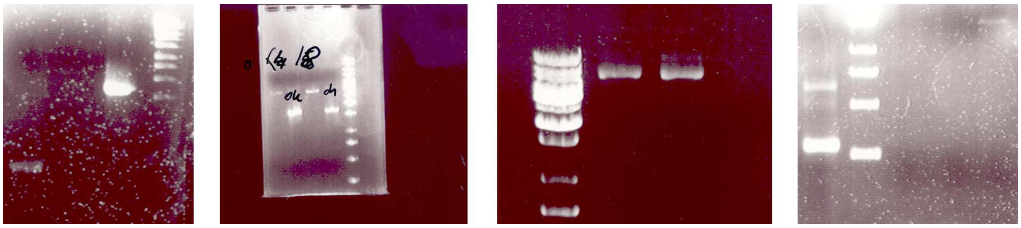

Figure 22 1% agraose gel photographs. Cloning of nucleostemin.

2.2.6 Plasmids for protein expression:

	Construct	Description	Reference
1	p53	pQE40 (QIAGEN, FRG) with inserted p53 fragment (1-312 aa)	Helin et al., 1993a
2	Mdm2	pQE40 (QIAGEN, FRG) with inserted Mdm2 fragment (1-118 aa).	Stoll et al., 2001
3	E7	pET vector with full length gene of HPV16 E7	
4	pRB	pRSET with inserted A/B pocket (379-772 aa) and long N-terminus His-Tag listet by side.	MRGSHHHHHHGMASMTG GQQMRDLYDDDDKDPSS RSAAGTMEFMNTIQQLMMI LNS

5	Nucleostemin	pQE40, pET 29, different constructs	Figure 37, **B**
6	CDK2	pET40 (NOVAGEN) with inserted full length CDK2 (298 aa).	Majumdar et al., in preparation

2.3 Proteins

Hen egg white lysozyme, RNaseA, DNaseI, BSA, BamHI, EcoRI, HindIII, XhoI, Pfu turbo DNA polymerase, T4 DNA ligase

2.4 Antibiotics:

• Ampicillin

• Kanamycin

2.5 Chemicals

All chemicals used in the work were supplied from Merck (Darmstadt, FRG) or Sigma (Deisenhofen, FRG), unless otherwise indicated.

• Acetic acid

• Acrylamide

• L-Arginine

• Ammonium chloride, NH_4Cl

• Ammonium persulfate, APS

• Biotin

• Boric acid, H_3BO_3

• Citric acid

- Cobalt (II) chloride, $CoCl_2$
- Coomassie brillant blue R-250
- Dimethylsulfoxide, DMSO
- Dipotassium hydrogenphosphate, K_2HPO_4
- Disodium hydrogenphosphate, Na_2HPO_4
- Dithiothreitol, DTT
- Ethanol
- Ethylendiamintetraacetic acid, disodium salt, EDTA
- Ferrous citrate
- D-Glucose
- L-Glutathione, oxidized, GSSG
- L-Glutathione, reduced, GSH
- Glycerine
- Guanidine hydrochloride
- Hydrochloric acid, HCl
- Imidazole
- Isopropanol
- Isopropyl-β-D-thiogalactopyranoside, IPTG
- Magnesium chloride, $MgCl_2$
- Magnesium sulfate, $MgSO_4$
- Manganese (II) chloride, $MnCl_2$
- β-Mercaptoethanol
- Methanol

- N,N'-Methylenbisacrylamide
- Potassium chloride, KCl
- Potassium dihydrogenphosphate, KH_2PO_4
- Sodium acetate
- Sodium azide, NaN_3
- Sodium carbonate, Na_2CO_3
- Sodium chloride, NaCl
- Sodium dihydrogenphosphate, NaH_2PO_4
- Sodium dodecylsulphate, SDS
- Sodium hydrogencarbonate, $NaHCO_3$
- Sodium hydroxide, NaOH
- Sodium molybdate, Na_2MoO_4
- Sodium thiosulfate
- N,N,N',N'-Tetramethylenethylendiamine, TEMED
- Thiamin
- Tricine
- Trifluoroethanol, TFE
- Tris-(hydroxymethyl)-aminomethane, TRIS
- Triton X-100
- Tryptone
- Yeast Extract
- Zinc acetate, $Zn(Ac)_2$

2.6 Additional chemicals

Protease inhibitors:

- Complete protease inhibitors cocktail (Roche, FRG)

Isotopically enriched chemicals:

- ^{15}N-Ammonium chloride, NH_4Cl 99.9% (Campro Scientific, Berlin, FRG)
- Deuteriumoxide D_2O (Campro Scientific, Berlin, FRG)

Kits and reagents:

- QIAquick PCR Purification Kit Qiagen (Germany)
- QIAprep Spin Miniprep Kit Qiagen (Germany)
- Quick change site-directed mutagenesis kit Stratagene (USA)
- Pre-Crystallization Test (PCT) Hampton Research (USA)

Protein and nucleic acid markers

- Prestained Protein Marker: New England Bio Labs (USA)
- Broad Range (6-175 kDa) 1 kb DNA-Leiter: Peq Lab (Germany)

2.7 Buffers and media

All buffers, stock solutions, and media, if not mentioned here, were prepared exactly as described in Sambrook & Russell (2001).

2.7.1 LB Medium

Tryptone 10 g/l

Yeast extract 5 g/l

NaCl 5 g/l

For the preparation of agar plates the medium was supplemented with 15 g agar. Antibiotics were added after the medium has been cooled down to 50℃.

2.7.2 Minimal medium (MM) for uniform enrichment with ^{15}N

Stock solutions:

1. thiamine, 1%

2. antibiotic

3. $MgSO_4$, 1 M

4. Zn-EDTA solution:

EDTA 5 mg/ml

$Zn(Ac)_2$ 8.4 mg/ml

Dissolved separately in small water volumes, then mixed together.

5. trace elements solution:

H_3BO_3 2.5 g/l

$CoCl_2{*}H_2O$ 2.0 g/l

$CuCl_2{*}H_2O$ 1.13 g/l

$MnCl_2{*}2H_2O$ 9.8 g/l

$Na_2MoO_4{*}2H_2O$ 2.0 g/l

If difficult to dissolve, pH was lowered with citric acid or HCl.

6. glucose, 5 g/25 ml, separately autoclaved.

For 1 liter medium:

1. mixture was prepared:

a stirring element

NaCl 0.5 g

trace elements solution 1.3 ml

citric acid monohydrate 1 g

ferrous citrate 36 mg (dissolved in 120 µl conc. HCl, heated)

KH_2PO_4 4.02 g

$K_2HPO_4{*}3H_2O$ 7.82 g

Zn-EDTA solution 1 ml

NH_4Cl or $^{15}NH_4Cl$ 1 g

2. pH was adjusted to 7.0 with NaOH

3. the mixture was autoclaved

4. 25 ml separately autoclaved glucose was added

5. other compounds were added (previously sterile filtered):

thiamine 560 µl

antibiotica (half of the usual amount for LB-medium)

$MgSO_4$, 1 M 2 ml

2.8 Other stock solution

2.8.1 IPTG stock solution

IPTG was dissolved in water (2.38 g/10 ml) to the end concentration of 1 M. The stock solution was sterile filtered and stored in aliquots at –20℃ until used. The stock solution was diluted 1:1000 when added to the medium, unless otherwise indicated.

2.8.2 Ampicillin stock solution

Ampicillin was dissolved in water (1 g/10 ml) to the end concentration of 100 mg/ml. The stock solution was sterile filtered and stored in aliquots at –20℃ until used. The stock solution was diluted 1:1000 when added to the medium.

2.8.3 Kanamycin stock solution

Kanamycin was dissolved in water (0.5 g/10 ml) to the end concentration of 50 mg/ml. The stock solution was sterile filtered and stored in aliquots at –20℃ until used. The stock solution was diluted 1:1000 when added to the medium.

2.9 SDS polyacrylamide gel electrophoresis (SDS-PAGE)

SDS polyacrylamide gel electrophoresis was performed at various stages of purification to verify the purity of the samples, identify the eluted proteins in chromatography purification, progression of enzymatic digestion etc. in glycine-SDS-PAGE systems.

2.9.1 Visualization of separated proteins

For visualization of the protein bands, the gels were stained in a Coomassie-blue solution. Background was cleared by incubation of the gel in a destaining solution.

2.10 Laboratory equipment

2.10.1 Consumables

Centripreps YM3, YM10 Amicon, Witten, FRG

Dialysis tubing Spectra/Por MW 3500, 10000 Roth, Kleinfeld, Hannover, FRG

Falcon tubes, 15 ml, 50 ml Becton Dickinson, Heidelberg, FRG

Maxi-Prep, Plasmid Isolation Kit Qiagen, FRG

NMR-tubes, 5 mm Wilmad, Buena, NJ, USA

Parafilm American National, Canada

Pipette tips 10 µl, 200 µl,1000 µl Gilson, Villiers-le Bel, France

Plastic disposable pipettes 1 ml, 5 ml, 10 ml, 25 ml Falcon, FRG

Reaction cups 0.4 ml, 1.5 ml, 2 ml Eppendorf, FRG

Sterile filters Millex 0.22 µm, 0.45 µm Millipore, Molsheim, FRG

Syringes 1 ml, 2 ml, 10 ml, 20 ml, 60 ml Braun, Melsungen FRG

Ultrafiltration membranes YM3, YM10 Amicon, Witten, FRG

2.10.2 Chromatography equipment, columns and media:

ÄKTA explorer 10 Amersham Pharmacia, Freiburg, FRG

Peristaltic pump P-1 Amersham Pharmacia, Freiburg, FRG

Fraction collector RediFrac Amersham Pharmacia, Freiburg, FRG

Recorder REC-1 Amersham Pharmacia, Freiburg, FRG

UV flow through detector UV-1 Amersham Pharmacia, Freiburg, FRG

BioloLogic LP System Biorad, FRG

HiLoad 26/60 Superdex S75pg Amersham Pharmacia, Freiburg, FRG

HiLoad 10/30 Superdex S75pg Amersham Pharmacia, Freiburg, FRG

Mono Q HR 5/5, 10/10 Amersham Pharmacia, Freiburg, FRG

NiNTA-agarose QIAGEN, FRG

Buthyl Sepharose 4 FF Amersham Pharmacia, Freiburg, FRG

Q-Sepharose FF Amersham Pharmacia, Freiburg, FRG

SP-Sepharose FF Amersham Pharmacia, Freiburg, FRG

Glutathione Sepharose Amersham Pharmacia, Freiburg, FRG

2.10.3 Miscellaneous

Autoclave Bachofer, Reutlingen, FRG

Balances PE 1600, AE 163 Mettler, FRG

Centrifuge Avanti J-30I Beckman, USA

Centrifuge Microfuge R Beckman, USA

Centrifuge 3K15 Sigma, FRG

Centrifuge 5414 Eppendorf, FRG

Chambers for SDS PAGE and Western blotting MPI für Biochemie, FRG

MARresearch image plates, mar345 MARresearch, Hamburg, FRG

Magnetic stirrer Heidolph M2000 Bachofer, Reutlingen, FRG

NMR-spectrometer DRX500, DRX600 Bruker, Rheinstetten, FRG

pH-meter pHM83 Radiometer, Copenhagen, Denmark

Pipettes 2.5 µl, 10 µl, 20 µl, 200 µl, 1000 µl Eppendorf, FRG

Quarz cuvettes QS Hellma, FRG

Shaker Adolf-Kühner AG, Switzerland

Spectrophotometer Amersham Pharmacia, Freiburg, FRG

Ultrafiltration cells, 10 ml, 50 ml, 200 ml Amicon, Witten, FRG

Vortex Cenco, FRG

Molecular Biology Techniques

All employed molecular biology protocols, if not mentioned here, were used exactly like described in Sambrook & Russell (2001).

2.11 Protocols

2.11.1 Transformation of competent bacteria:

In a 1.5 ml sterile vial 1 µl of plasmid DNA solution in water/ KCM was mixed together with the 25 µl aliquot of chemical competent bacteria. Mixture was incubated on ice for 20 min and than 2 min in 42℃. 150 µl of the sterile pre-warmed (37℃) LB medium (without antibiotics) was added and shaked (800 rpm) at 37℃. After 1 h the cells were streaked on a LB agar plate with appropriate antibiotics.

2.11.2 Bacterial culture in LB medium

1. 50 ml LB was inoculated with a fresh single bacterial colony and incubated overnight at 37℃ with vigorous shaking (280 rpm) in a 100 ml flask.
2. Pre-warmed 1 l LB medium in a 3 l flask was inoculated with 10 ml of the overnight culture, supplemented with appropriate antibiotic, and incubated at 37℃ with shaking (150 rpm) until the OD_{600} reached the 0.7 value.
3. Induction by IPTG addition followed. 0.1-1 mM IPTG concentration was usually used. The cells were then grown until the expected OD was reached.

2.11.3 Bacterial culture in MM

1. 2 ml LB were inoculated with a single colony, and shaked (150 rpm) overday in a 15 ml falcon tube at 37℃.
2. 20 ml MM were inoculated with 50 µl the overday culture, and shaked (280 rpm) overnight in a 100 ml flask at 37℃.

3. 1 l MM was inoculated with 20 ml the overnight culture (1:50), and shaked (150 rpm) in a 3 l flask, until the expected optical density was reached.

2.11.4 Protein concentration

The concentration of proteins in solutions was estimated with the assistance of the Bradford reagent (BioRad; Bradford, 1976). 10 µl of the protein solution (or 1 µl, if the protein solution was very concentrated) to be measured were added to 625 µl of the BioRad-reagent working solution (the working solution was prepared by 1:5 dilution of a BioRad-reagent stock solution in PBS buffer or water, stored in the fridge). Then the mixture was diluted with 400 µl water. After thoroughly mixing the sample, the OD_{595} was measured. As a reference similar mixture was prepared with 10 µl water instead of the protein solution. OD was subsequently converted into the protein concentration on the basis of a BSA calibration curve.

2.11.5 Preparation of NMR samples

Typically, NMR samples contained up to 1 mM of protein in 50 mM KH_2PO_4, 50 mM Na_2HPO_4, 150 mM NaCl, pH 7.4, 5 mM DTT, 0.02% NaN_3. Before measuring, the sample was centrifuged in order to sediment aggregates and other macroscopic particles. 450 µl of the protein solution were mixed with 50 µl of D_2O (5-10%) and transferred to the NMR sample tube.

2.12 Protein crystallization (pRB)

I used sitting drop techniques for crystallization. Crystallization was set up in the following manner: more than a 95% pure protein sample was loaded on the preparative grade gel filtration column (S75) in 50 nM Tris, 150 mM NaCl buffer. The protein was concentrated to ~15-20 mg/ml and centrifuged at high rpm briefly. 2 µl of protein was mixed with 2 µl of reservoir buffer in the well filled with 200 µl of buffer. Crystallization plates were set up at two temperatures 4℃ and room temperature.

2.13 Chemical synthesis of alkoxylated chalcones

The general procedure for preparing alkoxylated chalcones is as follows. In a round-botton flask, a methanolic solution of NaOH (3% w/v, 10 ml) and a substituted aldehyde (10 mmol in 10 ml) were stirred together at room temperature. A methanolic solution of the substituted acetophenone (10 mmol in 10 ml) was added dropwise, and the mixture was stirred for 48 h. The product was obtained as a brightly colored precipitate. The precipitate was removed by filtration, washed with cold methanol, and recrystallized. Compounds were characterized by ^{13}C NMR and mass spectrometry analysis.

2.14 Indole-3-carbinol tetrameric derivative

The aim of this study was to synthesize a stable I3C (Indole-3-Carbinol) derivative and to test its inhibitor activity on cyclin-dependent kinase 6 (*Figure 30*). This molecule is able to inhibit the growth of both ER-positive and ER-negative breast cancer cells (Brandi et al., 2003). The reaction with acetic acid was preformed. The tetramer was purified by silica gel column chromatography (data not shown).

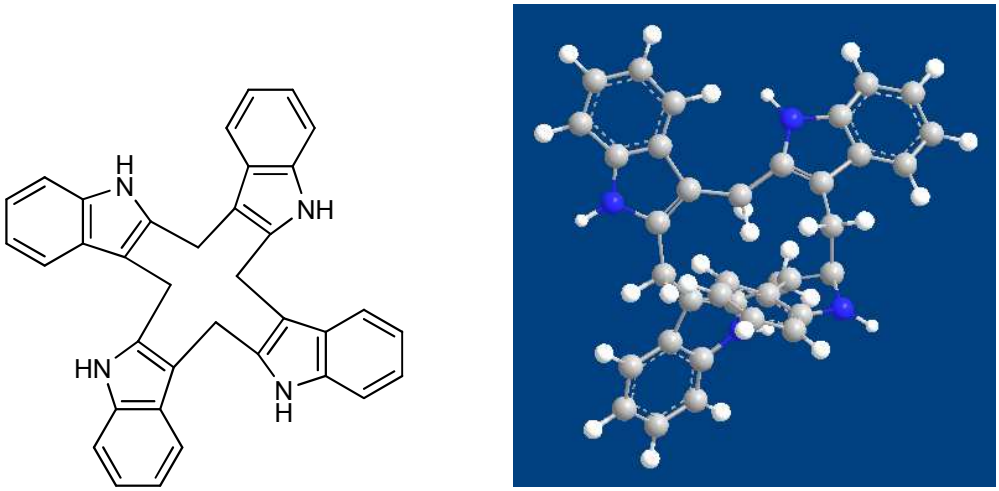

Figure 30 Chemical structure of tetrameric indole-3-carbinol and its 3D model

2.15 NMR experiments

All NMR spectra were acquired at 300 K on a Bruker DRX 600 MHz spectrometer equipped with a cryoprobe. For the ^{1}H -^{15}N HSQC spectrum, water suppression was carried out using the WATERGATE sequence. NMR data were processed using the Bruker program Xwin-NMR version 3.5.

2.15.1 Inhibitors of CDK2

For titration experiments, 0.1-0.3 mM of human CDK2 in 140 mM NaCl, 10 mM Na_2HPO_4, 2.7 mM KCl 0.05% NaN_3, 5 mM DTT was used. The inhibitors were lyophilized and finally dissolved in DMSO-d_6. No shifts were observed for 1% DMSO (the maximum concentration of DMSO used in all NMR experiments with the inhibitors). The complexes of human CDK2 and the inhibitors were prepared by mixing the protein

and the ligand in the NMR tube. Typically, NMR spectra were recorded 15 min after mixing at room temperature. An initial screening of all compounds used in this study was performed with a 10-fold molar excess of inhibitor to human CDK2. All subsequent titrations were carried out until no further shifts were observed in the spectra. Saturating conditions were achieved at a molar ratio of inhibitor to CDK2 of 6. Typically, the concentration of human CDK2 was 0.1 mM and the final concentration of the ligand was 50 mM in each titration. Quantitative analysis of induced chemical shifts was performed on the basis of spectra obtained at saturating conditions of each inhibitor. Selectively enriched samples of human CDK2 (^{15}N-Lys) were titrated with the inhibitor. Only $\Delta\delta_c(^1H, ^{15}N)$ values larger than 0.1 ppm were considered to be significant. Furthermore, all residues of human CDK2 involved in binding show significant shifts $\Delta\delta_c(^1H, ^{15}N)$.

2.15.2 Inhibitors of the p53-Mdm2 complex

Ligand binding experiments were carried out in an analogous way to that described in Stoll et al. (2001). 500 µl of the protein sample containing 10% D_2O, at a concentration of about 0.1 mM, and a 20 mM stock solution of each compound in DMSO-d_6 was used in all the experiments. Titrations were carried out with three inhibitors, namely, Nutlin-3 (Nutlin-3 was purchased from Cayman Chemical, MI, USA (Catalog No. 10004372), sulfonamide (obtained from the National Cancer Institute, NSC 279287) and a boronic chalcone. In case of the experiments with Nutlin-3, the titration was carried out until no further change in the 2D spectrum was observed, thus indicating saturation. The maximum concentration of DMSO at the end of titration experiments was about 2-3%. The pH was maintained constant during the entire

titration. As controls, in order to check the effect of DMSO on the proteins, we titrated the protein complex and proteins with DMSO. We found no significant changes in the chemical shifts, precipitation or denaturation of the proteins for DMSO concentrations used in the compound titrations (up to 3%). *Figure 31* shows the ^{1}H -^{15}N HSQC spectra of Mdm2 titrated with DMSO. The p53/ Mdm2 complex titrated up to 20% with DMSO partially precipitated (40% after 10 h). Preincubation of the p53/ Mdm2 complex with 15% DMSO at 310 K for 1.5 h, 10 degrees higher than the temperature at which NMR experiments were carried out (300 K), resulted in increased precipitation (50%), but no other changes in the spectrum of the soluble fraction were observed. The soluble complex was reacting with Nutlin-3. The p53 peaks of the ^{15}N labeled p53 shift little with higher concentrations of DMSO (c.a. 0.1 ppm in proton dimension for the Trp 23 sidechain signal at 20% DMSO). We thus conclude that the effect of DMSO on the proteins while titrating with different compounds can be ignored.

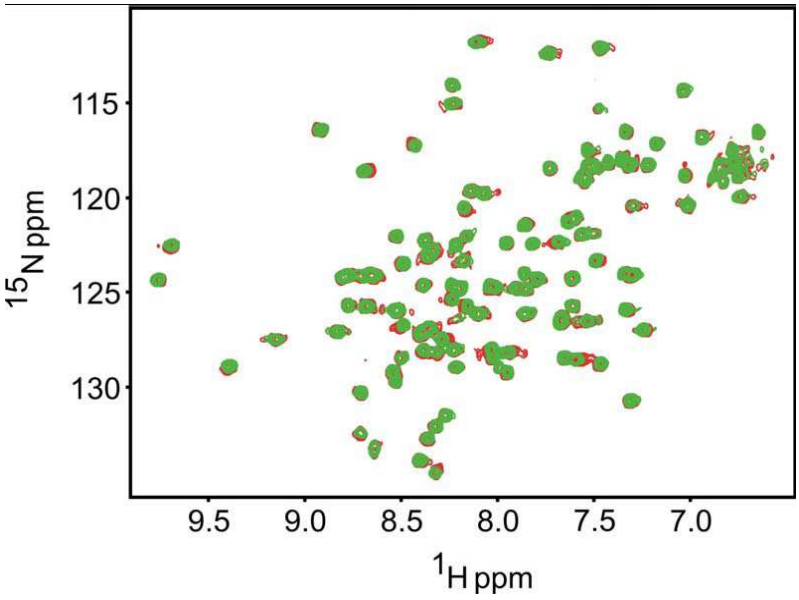

Figure 31 1H-^{15}N HSQC spectra of Mdm2 (in red) titrated with DMSO (in green). There were no significant chemical changes when DSMO is added upto about 5% in the NMR tube containing the protein sample. DMSO at this amount did not induce precipitation/denaturation of the protein as seen from the 2D spectra.

2.16 Protein expression and purification

2.16.1 CDK2

The recombinant human cyclin-dependent kinase 2 (CDK2) protein was obtained from an *Escherichia coli* BL21(DE3) expression system and contained the full length gene of human CDK2 (*Figure 7*) cloned in a pET46 vector (Novagen) (*Figure 23*). Factor Xa site was introduced before the start of the protein. The protein was purified under native conditions using a NiNTA (Qiagen) column. Eluted CDK2 was collected and concentrated down to 5 ml and loaded in the S75pg column for size exclusion chromatography (Amersham Pharmacia Biotech) in 140 mM NaCl, 10 mM Na_2HPO_4, 2.7 mM KCl 0.05% NaN_3,and 5 mM DTT.

histag
β3 sheet
MAHHHHHHVD DDDKM MENFQ KVEKIGEGTY GVVYKARNKL TGEVVALKKI RLDTETEGV
enterokinase site
33
α2 helix
PSTAIREISLL KELNHPNIVK LLDVIHTENK LYLVFEFLHQ DLKKFMDASA LTGIPLPLI
89

KSYLFQLLQGL AFCHSHRVLH RDLKPQNLLI NTEGAIKLAD FGLARAFGVP VRTYTHEVV

TLWYRAPEILL GCKYYSTAVD IWSLGCIFAE MVTRRALFPG DSEIDQLFRI FRTLGTPDE

VVWPGVTSMPD YKPSFPKWAR QDFSKVVPPL DEDGRSLLSQ MLHYDPNKRI SAKAALAHP

FFQDVTKPVPH LRL

Figure 23 Sequence of CDK2 protein construct, with the histidine-tag and the lysines marked by blue letters. Lys33 and Lys89 are highlighted according to their presence in the structure.

Protein eluted as a single monomeric peak. Fractions containing CDK2 were pooled and concentrated with an Amicon concentrating cell (cut-off 10 kDa) up to 1 mM for NMR spectroscopy (*Figure 24*).

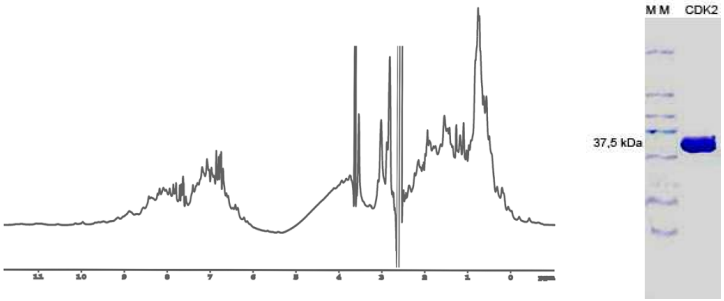

Figure 24 1D proton NMR spectrum of human CDK2 showing the folded nature of the protein. SDS PAGE showing the quality of CDK2 sample preparation.

2.16.2 p53

The recombinant human p53 protein was expressed in the *Escherichia coli* BL21 expression system and contained the first 312 residues of human p53 cloned in to a pQE-40 vector (Qiagen) with an N-terminal His-tag and T5 promotor. Inclusion bodies were washed twice with the PBS buffer containing 0.05% Triton X-100, with subsequent low-speed centrifugation (12000 G), and solubilized with 6 M guanidine hydrochloride in 100 mM tris-HCl, pH 8.0, including 10 mM β-mercaptoethanol (10 ml buffer per 1 g inclusion bodies). The protein was purified under denaturing conditions using a NiNTA (Qiagen) column. Eluted p53 was refolded at 10℃ by slowly diluting it into 0.1 M Tris (pH 8), 1 M arginine, 10% (v/v) glycerol, 5 mM DTT. It was concentrated using a ProVario ultra-filtration system (Pall Filtron), dialyzed against 50 mM Tris-HCl (pH 6.8), 50 mM KCl, 5 mM DTT, 10% glycerol and further purified using a combination of affinity

chromatography on a heparin HiTrap column (Amersham Phamacia Biotech) (eluted with a linear KCl gradient) and size exclusion chromatography on a High Load 26/60 Superdex 75 column (Amersham Pharmacia Biotech) in 50 mM sodium phosphate (pH 6.8), 150 mM KCl, 5 mM DTT (*Figure 25*)..

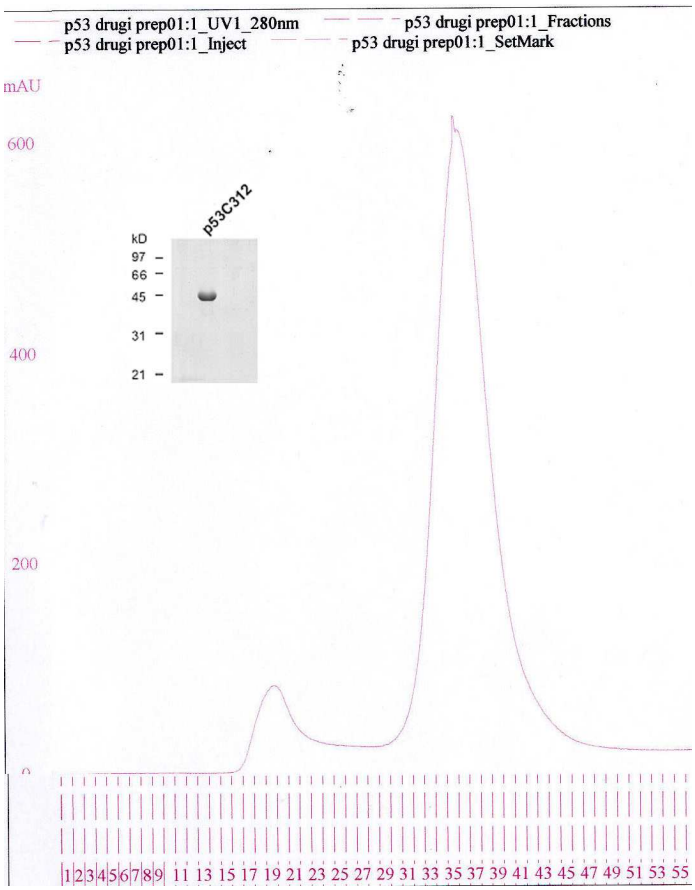

Figure 25 Chromatogram showing the elution profile of the p53 in the Superdex 75 gel chromatography, SDS PAGE showing the quality of p53 sample preparation.

Fractions containing p53 were pooled and concentrated with an Amicon concentrating cell (cut-off 3 kDa) up to 1 mM for NMR spectroscopy and rest of the protein was flash-frozen in liquid nitrogen and stored in aliquots at -80℃.

2.16.3 Mdm2

The recombinant human Mdm2 protein was expressed in *Escherichia coli* BL21 expression system and contained the first 118 N-terminal residues of human Mdm2 cloned in a pQE-40 vector (Qiagen). Inclusion bodies were washed twice with the PBS buffer containing 0.05% Triton X-100, with subsequent low-speed centrifugation (12000G), and solubilized with 6 M guanidine hydrochloride in 100mM tris-HCl, pH 8.0, including 1mM EDTA and 10 mM DTT (10 ml buffer per 1 g inclusion bodies). After lowering pH to 3-4, the protein was dialyzed at 4℃, against 4 M guanidine hydrochloride, pH 3.5, including 10 mM DTT, until equilibrium was reached. For renaturation the protein was diluted (1:100) into 10 mM tris-HCl, pH 7.0 including 1 mM EDTA and 10 mM DTT by adding the protein in several pulses. Refolding was performed for overnight at room temperature. Ammonium sulfate was added to a final concentration of 1 M and the refolded human Mdm2 was applied to hydrophobic interaction chromatography (batch purification) using Buthyl Sepharose 4 Fast Flow (Pharmacia, FRG). Because of the low binding capacity of the medium, 100 ml bead volume per 1 liter bacterial culture was used. The protein was eluted with 0.1 M Tris-HCl, pH 7.2 supplied with 5 mM DTT. Finally, all fractions containing Mdm2 were pooled, concentrated, and applied to a HiLoad 26/60 Superdex 75pg gel filtration column (Pharmacia, FRG) (*Figure 26 A*).

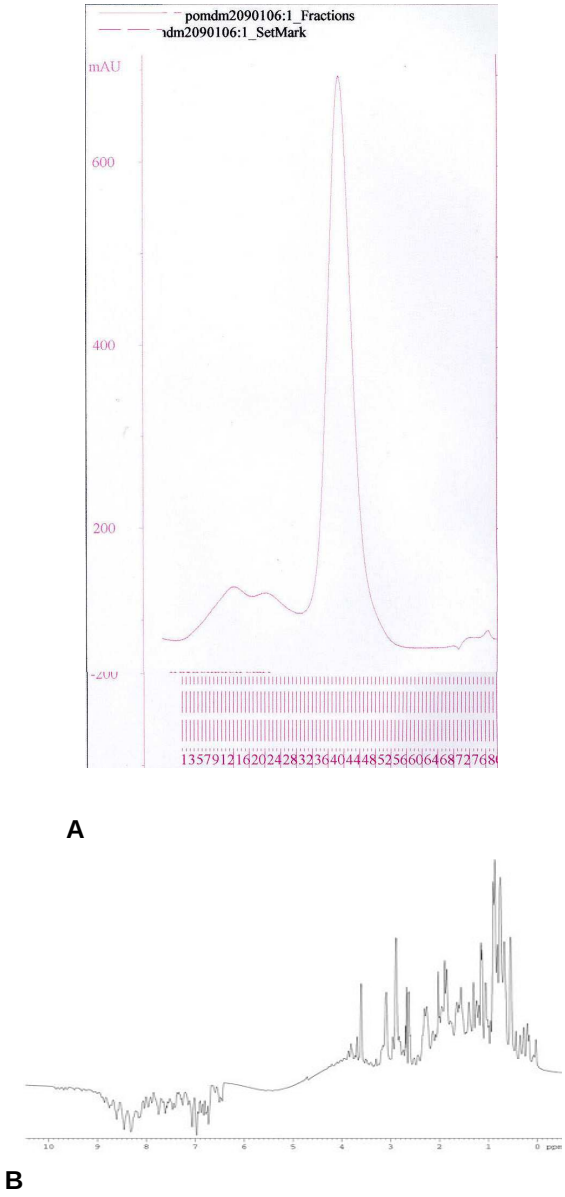

Figure 26 (**A**) Chromatogram showing the elution profile of the Mdm2 in the Superdex 75 gel chromatography, (**B**) 1D proton NMR spectrum of human Mdm2 showing the folded nature of the protein

The running buffer contained 50 mM KH_2PO_4, 50 mM Na_2HPO_4, pH 7.4, 150 mM NaCl, 5 mM DTT, 0.02% NaN_3, and protease inhibitors (Complete, Roche, FRG). All fractions

with monomeric human Mdm2 were pooled and concentrated with an Amicon concentrating cell (cut off 3 kDa) up to 1 mM for NMR spectroscopy (*Figure 26 B*). The protein was stored at -20℃.

2.16.4 Expression and purification of the A/B pocket of pRb

The recombinant human pRb protein was expressed in *Escherichia coli* BL21 Star (DE3) plysS expression system and contained the A/B pocket of human pRb cloned in a pRSET vector (Qiagen) with an N-terminal His-tag. A/B pocket of pRb was expressed at high levels at low temperature 14℃. Additionally s olubility of pRb was increased by cultured bacteria in LB-medium with presence of 200 mM potassium phosphate buffer pH 7.2 and 1 mM $MgSO_4$ and 1% of glucose. The protein was purified under native conditions using a NiNTA (Qiagen) column. Eluted pRb was collected and concentrated down to 5 ml and loaded in the Mono S column for cation exchange chromatography (Amersham Pharmacia Biotech) in 25 mM MES buffer pH 6.0 and was eluted with 1 M NaCl gradient (*Figure 27*).

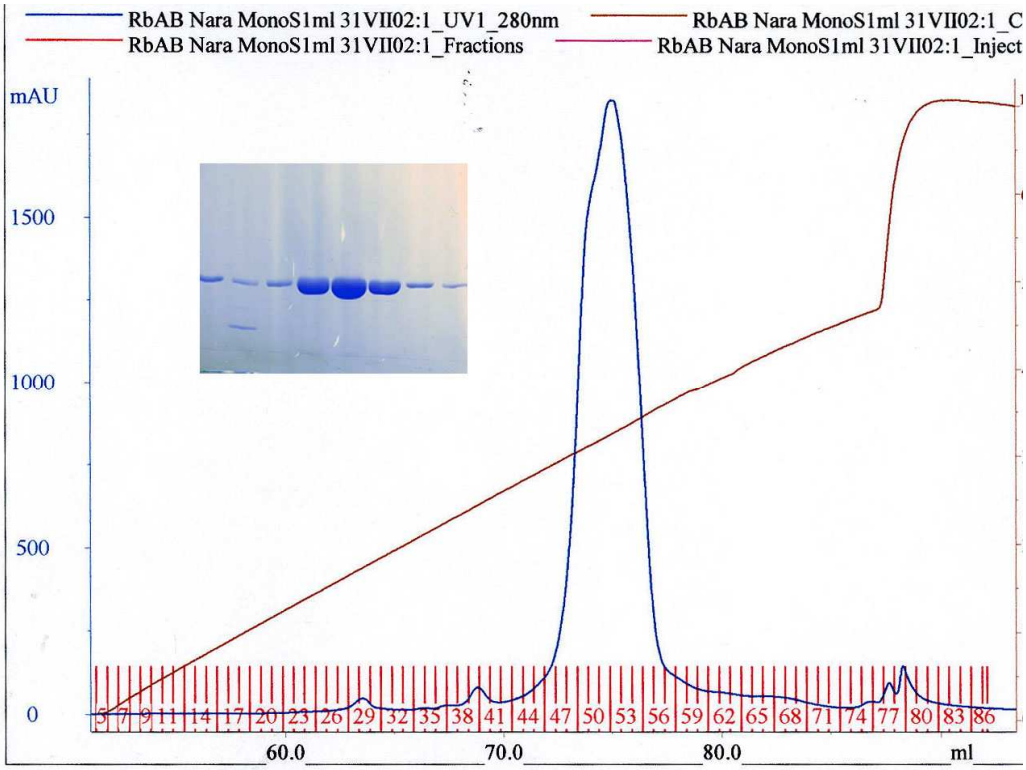

Figure 27 Purification of the native pRb (A/B) by cation exchange chromatography. The solid blue colored line shows the UV absorption curve of pRb; the brown line indicates gradient of NaCl, SDS PAGE of main pick.

Finally, all fractions containing pRb were pooled, concentrated, and applied to a HiLoad 26/60 Superdex 75pg gel filtration column (Pharmacia, FRG) HEPES 25 mM 150 mM NaCl 5 mM DTT pH 7.2 (crystallization buffer) (*Figure 28*).

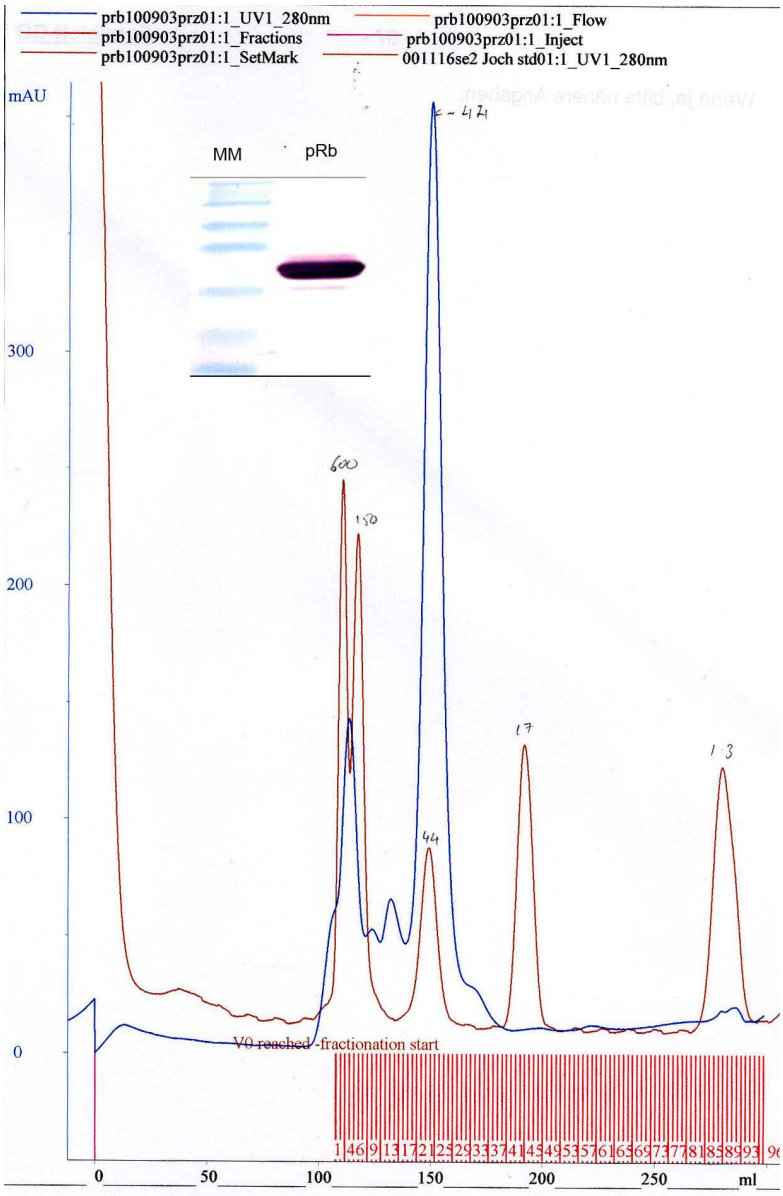

Figure 28 Purification of the native pRb (A/B) by gel filtration chromatography. The UV absorption curves were aligned with the curves of protein mass standards. The solid blue colored line shows the UV absorption curve of pRb; the brown line indicates the UV absorption curve of molecular mass standards; the mass of each protein used as a standard is indicated. The arrow mark represents the calculated mass of native pRb. Western blot of pRb (A/B). MM is molecular weight marker.

2.16.5 E7

The recombinant the full length HPV16 E7 protein was obtained from an *Escherichia coli* BL21(DE3) pLys S expression system and contained the full length gene of HPV16 E7 (*Figure 29 C*) cloned in a pET vector (Novagen). Bacteria pellets were washed with the PBS buffer and solubilized with 6 M guanidine hydrochloride in 100 mM tris-HCl, pH 8.0, including 10 mM β-mercaptoethanol (10 ml buffer per 1 liter of bacteria culture). The protein was purified under denaturing conditions using a NiNTA (Qiagen) column. Eluted E7 was refolded at 4℃ by slowly diluting (100 fold) it into 0.1 M NaPCl (mM NaH_2PO_4/Na_2HPO_4) buffer (pH 7.4), 300 mM NaCl, 2 mM MgCl, 30 uM ZnCl, 1 mM EGTA, 4 mM DTT. It was concentrated using a hydroxyapatite column, elution with 200 mM NaPCl (NaH_2PO_4/Na_2HPO_4) (*Figure 29 A*). Then size exclusion chromatography on a High Load 26/60 Superdex 200 column (Amersham Pharmacia Biotech) in 50 mM NaPCl (pH 7.4), 150 mM NaCl, 5 mM DTT. Protein eluted as a single monomeric peak. Fractions containing E7 were pooled and concentrated with an Amicon concentrating cell (cut-off 1 kDa) up to 1 mM for NMR spectroscopy (*Figure 29 B*).

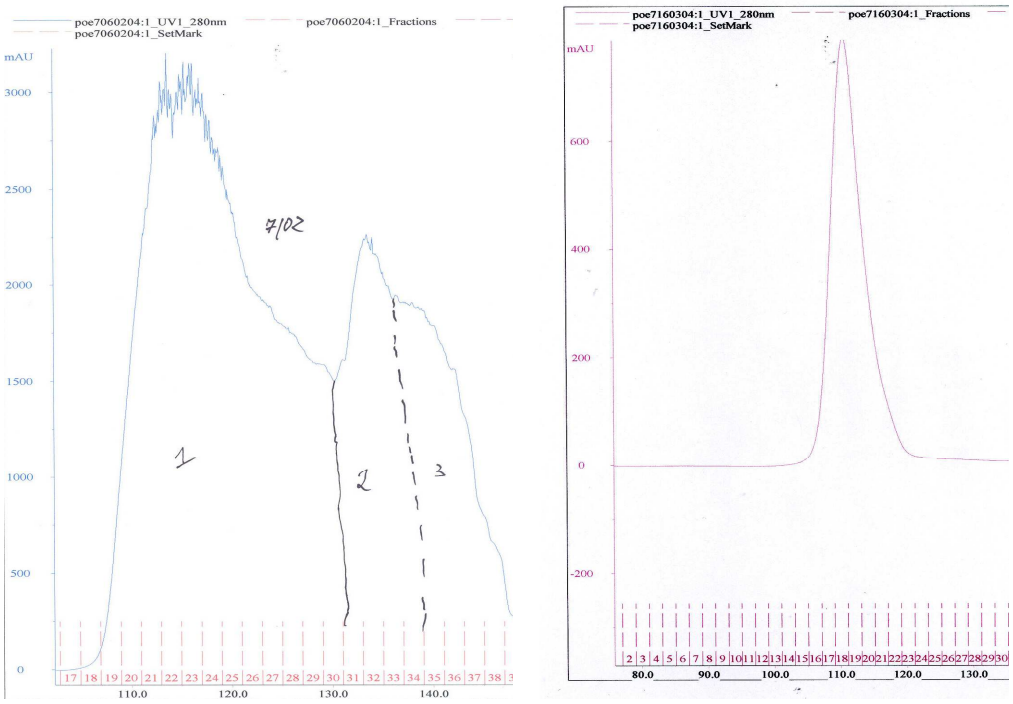

A **B**

```
  1 MHGDTPTLHE YMLDLQPETT DLYCYEQLND SSEEEDEIDG PAGQAEPDRA HYNIVTFCCK 60

 61 CDSTLRLCVQ STHVDIRTLE DLLMGTLGIV CPICSQKPHH HHHH 104
```

C

Figure 29 Purification of the native E7 protein (**A**) hydroxyapatite column, (**B**) gel filtration chromatography (the magenta colored line shows the UV absorption curve of E7, (**C**) sequence of the construct with a C-terminus His-tag.

2.17 Characterisation of small molecular compounds

2.17.1 Alkoxylated chalcones

Two alkoxylated chalcones 3,4-dichlorochalcones (*Figure 33*) and 3-dichlorochalcones (*Figure 32*) were synthesized and characterized by ^{13}C NMR and mass-spectrometry analysis.

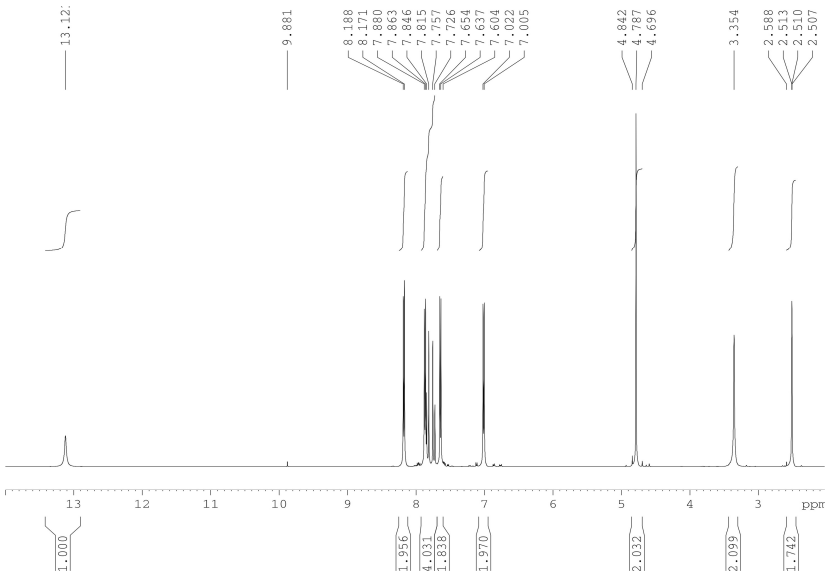

Spectrum 1 The ^{1}H 1D NMR spectrum of chalcone 1Cl in 100% DMSO-d_6 recorded on the DRX-400 MHz spectrometer at 298 K. The compound is at least 99% pure in terms of the proton containing impurities.

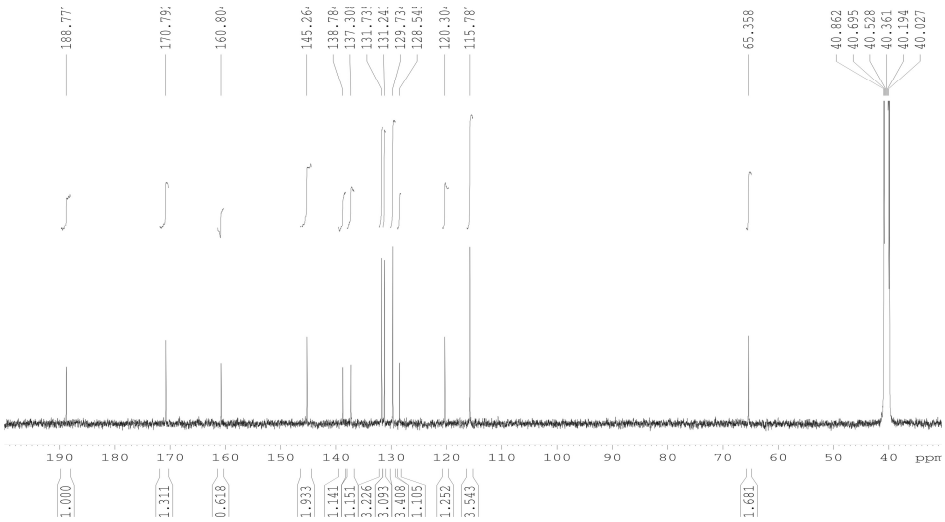

Spectrum 2 The ^{13}C 1D NMR spectrum of chalcone 1Cl 100% DMSO-d_6 recorded on the DRX-400 MHz spectrometer at 298 K. Since natural abundance of ^{13}C is 1% and no signals other than those from chalcone 1Cl, and DMSO are visible in the spectrum, concentrations of impurities must be below 1%, if any at all.

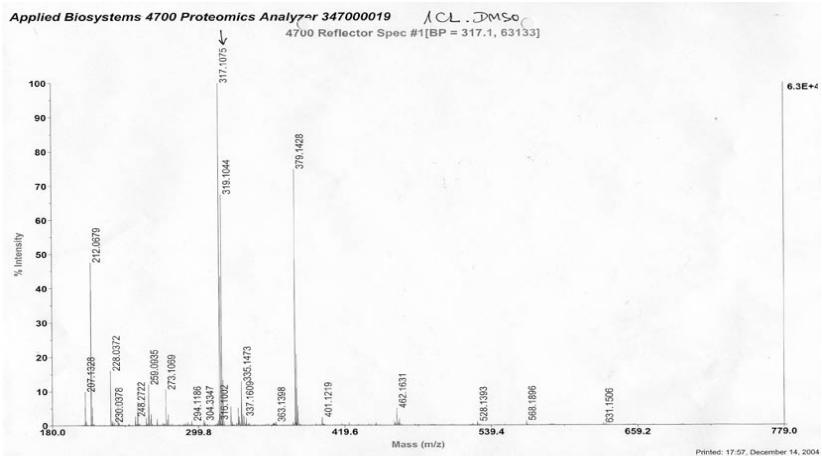

Spectrum 3 The mass spectrum of chalcone 1Cl in DMSO. The peak with correct molecular weight is marked.

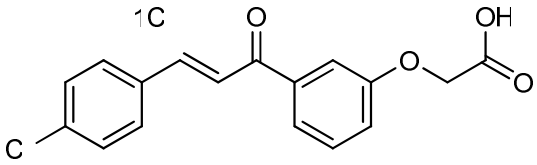

Figure 32 Chemical structures of (1Cl) 3,4-dichlorochalcones

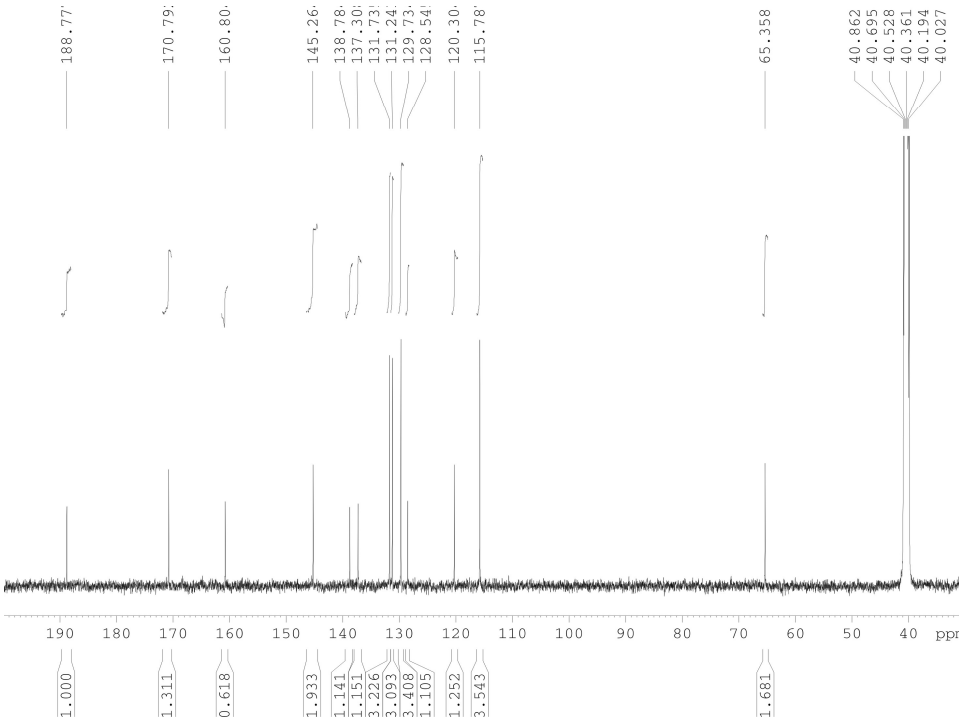

Spectrum 4 The ^{1}H 1D NMR spectrum of chalcone 2Cl in 100% DMSO-d_6 recorded on the DRX-400 MHz spectrometer at 298 K. The compound is at least 99% pure in terms of the proton containing impurities.

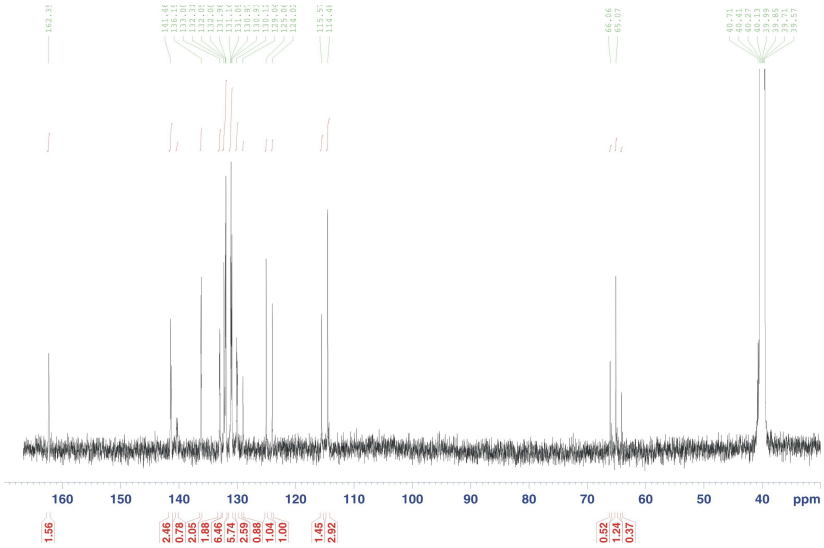

Spectrum 5 The ^{13}C 1D NMR spectrum of chalcone 2Cl 100% DMSO-d_6 recorded on the DRX-400 MHz spectrometer at 298 K. Since natural abundance of ^{13}C is 1% and no signals other than those from chalcone 1Cl, and DMSO are visible in the spectrum, concentrations of impurities must be below 1%, if any at all.

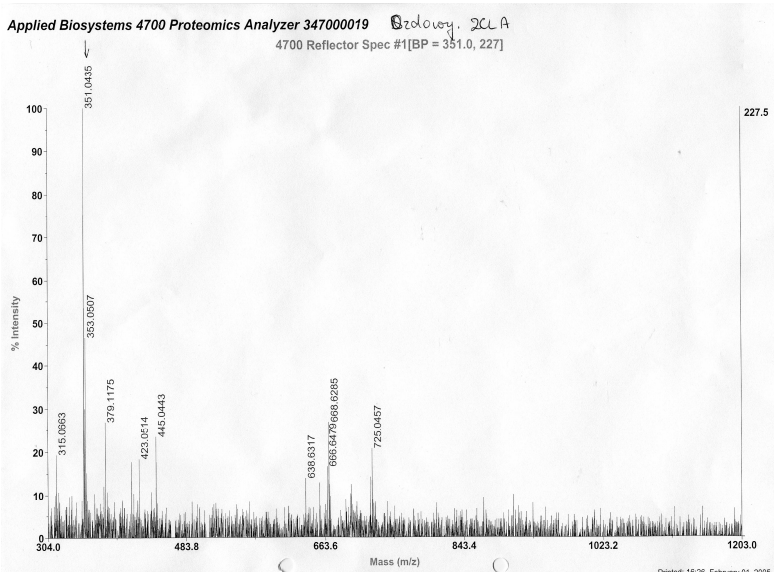

Spectrum 6 The mass spectrum of chalcone 2Cl in DMSO. The peak with correct molecular weight is marked.

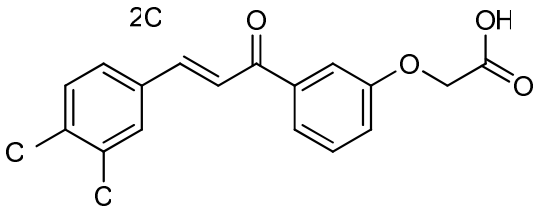

Figure 33 Chemical structures of (2Cl) 3,4-dichlorochalcones

2.17.2 RITA

RITA was characterized by a series of NMR experiments to confirm the purity and structure.

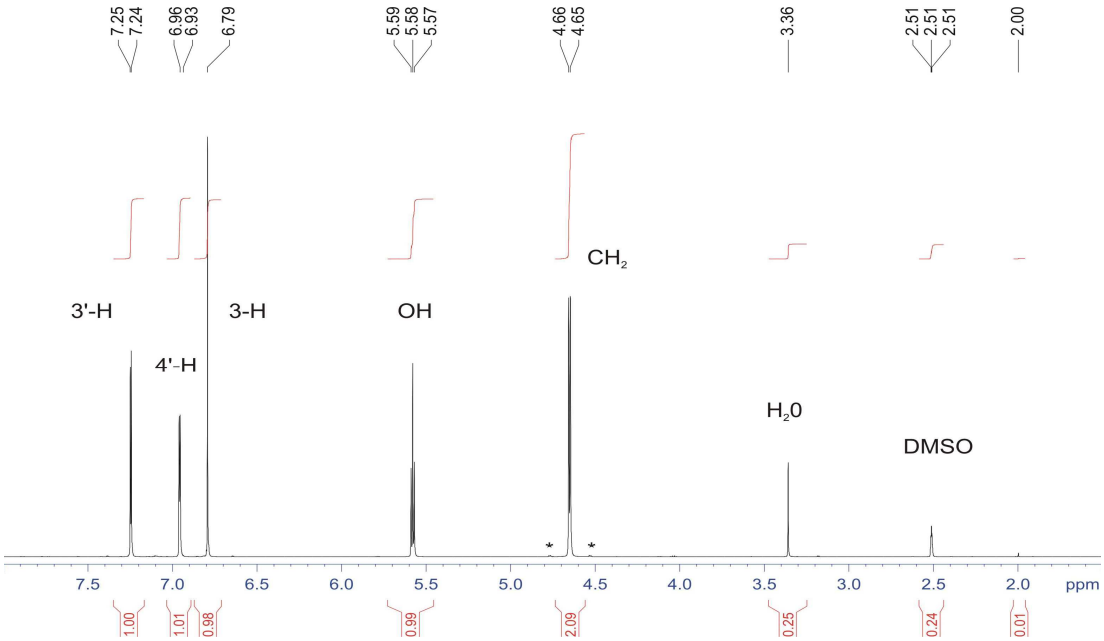

Spectrum 7 The proton NMR spectrum of RITA in DMSO. The ^{1}H 1D NMR spectrum of RITA in 100% DMSO-d_6 recorded on the DRX-600 MHz spectrometer at 298 K. The compound is at least 99% pure in terms of the proton containing impurities. The resonances have been assigned based on the 2D ^{1}H COSY spectrum 8 and on the water exchange experiments of spectrum 9.

Conclusion: The asterisks denote an example of ^{13}C satellites from the ^{1}H-^{13}C coupling. Since natural abundance of ^{13}C is 1% and no signals other than those from RITA, H_2O, and DMSO are visible in the spectrum, concentrations of impurities must be below 1%, if any at all.

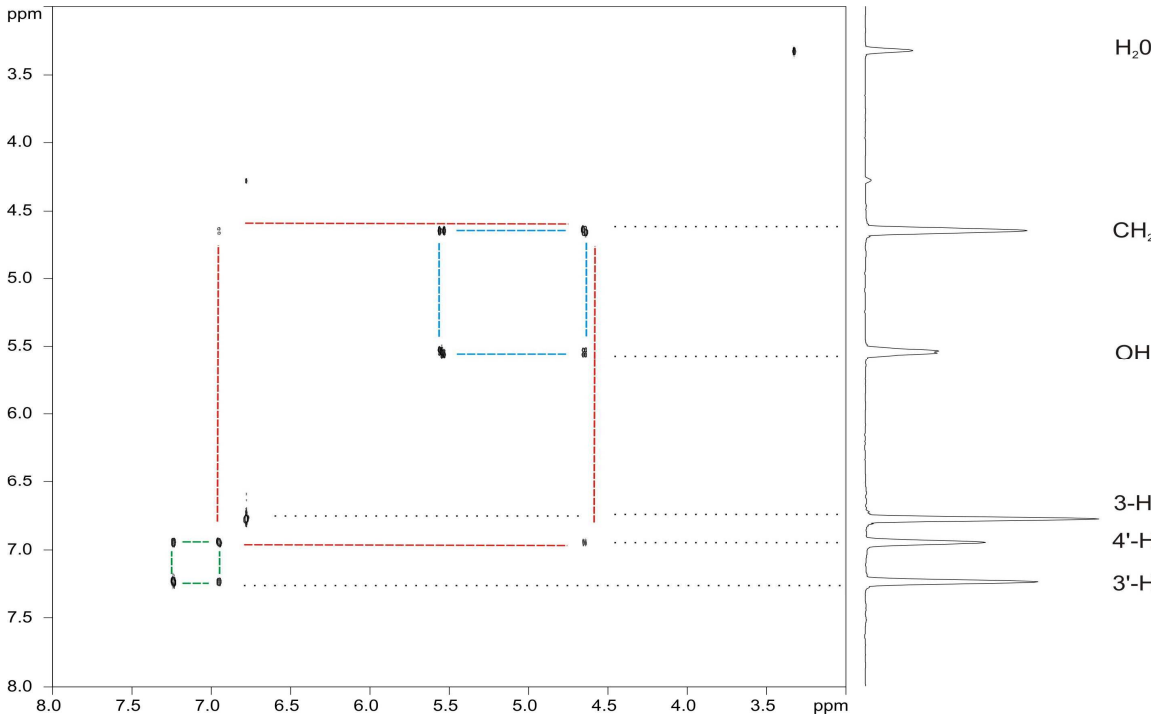

Spectrum 8 COSY spectrum of RITA in DMSO. On the basis of the COSY spectrum (AMX 400MHz, 300K) RITA resonances can be easily assigned: DMSO at 2.5 ppm, H_2O at 3.3 ppm, CH_2 at 4.65 ppm (connectivity to OH, blue lines), OH at 5.52 ppm (connectivity to CH_2, blue), 3-H at 6.8 ppm (no cross peaks present), 4'-H at 6.95 ppm (cross peaks to 3´, green, and to CH_2, red), 3'- H at 7.25 ppm (connected to 4´, green).

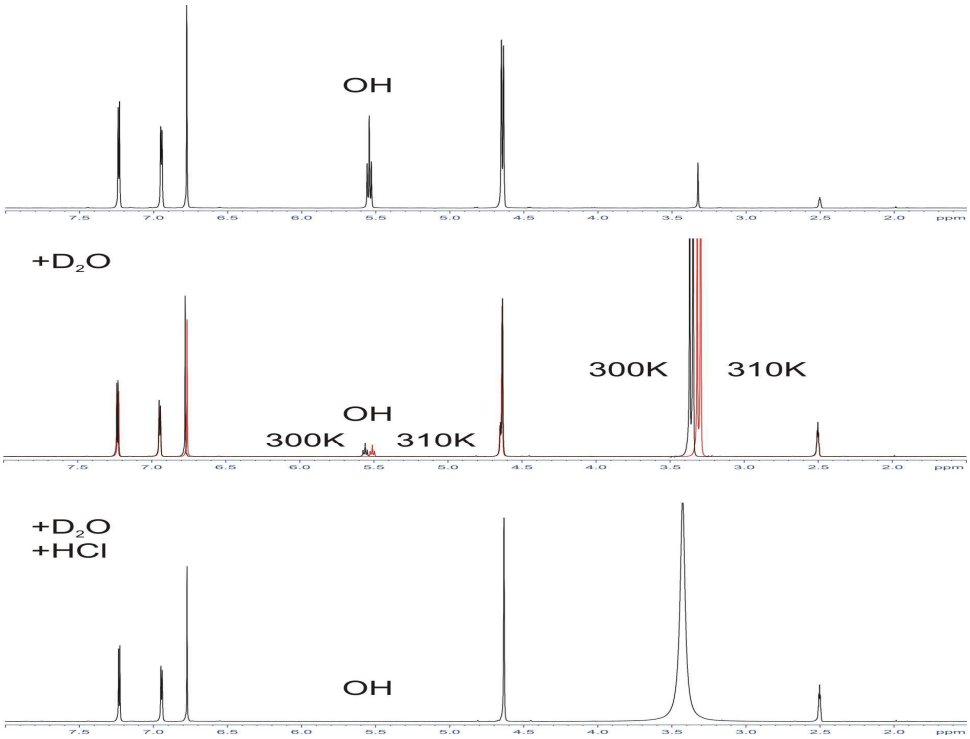

Spectrum 9 Verification of the OH assignment. Since the OH resonance should be sensitive to the chemical exchange with water, we have carried out the following experiments: (a) 5 □l (1% vol.) of D_2O was added to the sample of RITA in DMSO (100%), T = 300 K. The OH triplet is reduced, CH_2 is an unsymmetric doublet. (b) The temperature was changed to 310 K. A shift of H_2O and OH signals was observed. (c) T= 300 K, added 1 □l (0.2% vol.) of 3.7% HCl. The OH signal dissapeared, CH_2 is a singlet.

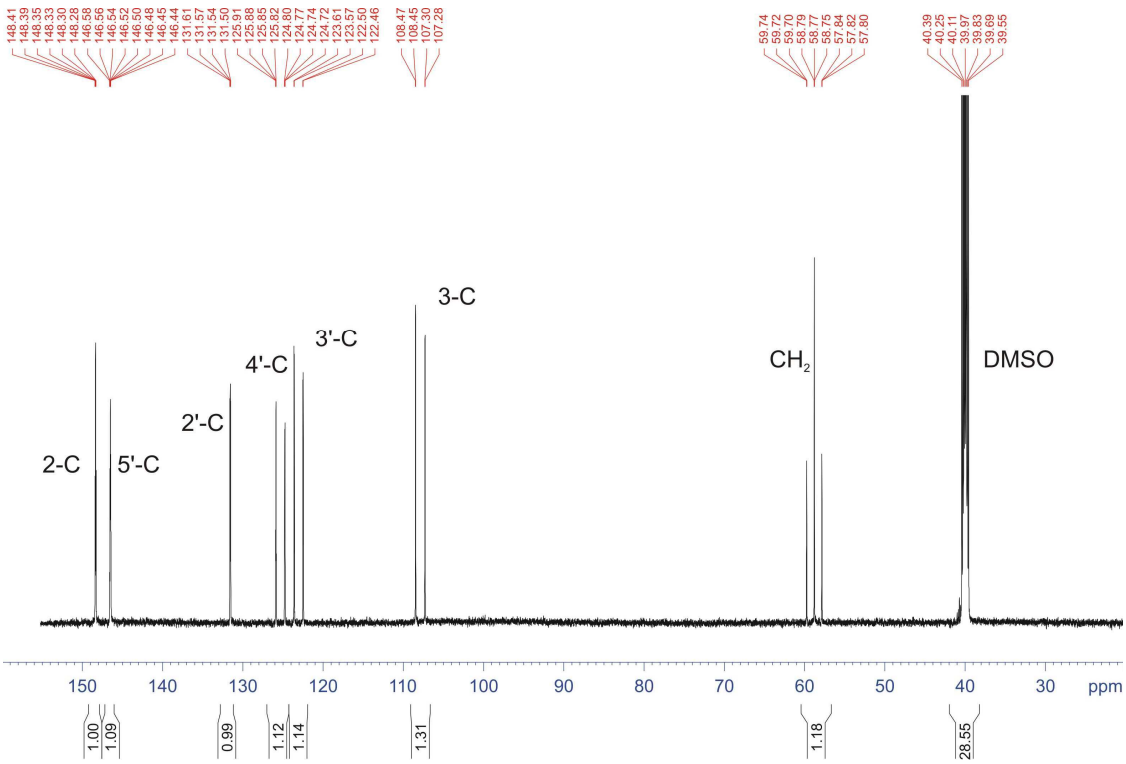

Spectrum 10 A natural abundance ^{13}C spectrum. A ^{13}C 1D NMR spectrum without decoupling and without NOESY enchancement was recorded on the DRX 600 MHz spectrometer. Nine different carbons (apart from the DMSO peak at 40 ppm) are seen. These are: CH_2 at 58.7 ppm, 3-C at 108 ppm, 3'-C at 123 ppm, 4'-C at 125.8 ppm, 2'-C at 131.5 ppm, 5' at 146.5 ppm, 2 at 148,3 ppm. The assignment was accomplished by selective decoupling at certain proton frequencies (Spectrum 11).

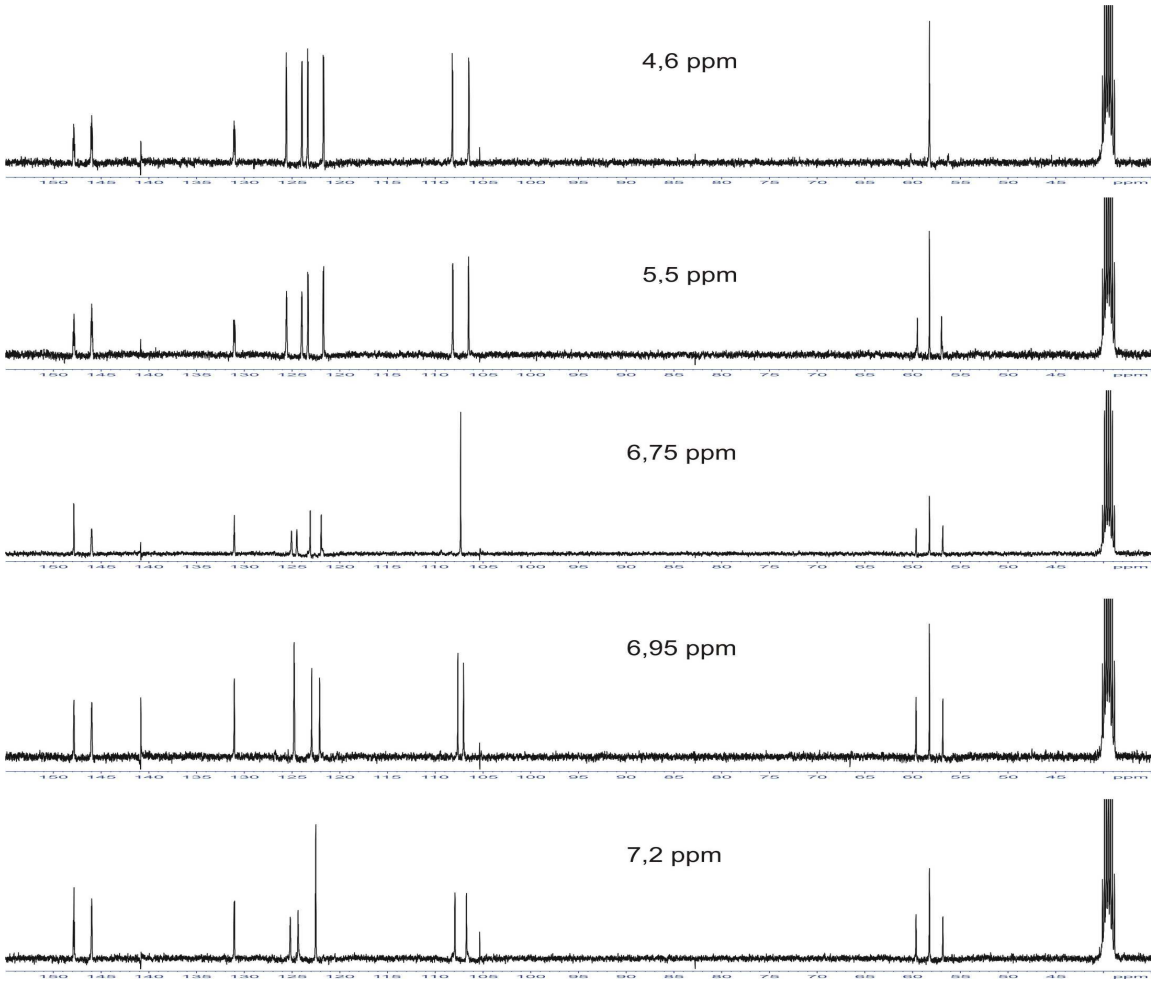

Spectrum 11 Selective proton-decoupling experiments. ^{13}C spectra were recorded on the AMX 400 MHz at 300 K, with the broadband proton presaturation prior to acquisition (NOESY enhancement) and selective CW irradiation at a single proton frequency indicated in ppm above the ^{13}C spectrum. The assignment of three signals from quaternary carbons (shown separately in Spectrum 12) can also be assigned by analysis of multiplet changes in these experiments (data not shown). The assignment of the OH proton resonance was also confirmed since no change to the carbon spectrum was observed upon decoupling of the OH proton signal.

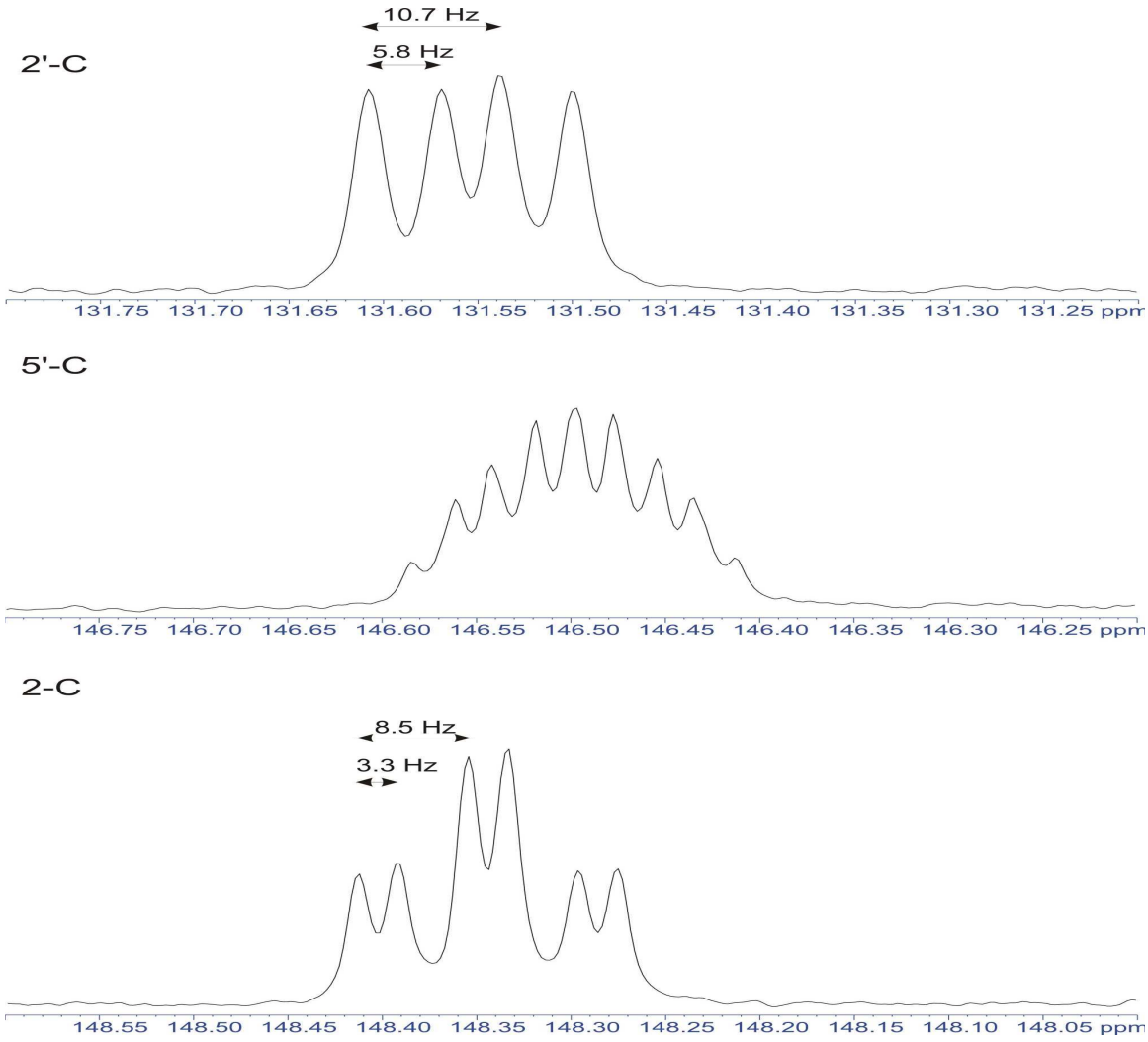

Spectrum 12 Multiplet structures of quaternary carbons in RITA.

Chapter 3

Results and Discussion

3.1 Protein crystallization (pRB)

Despite intensive trials of crystallization of the A/B pocket domain of pRb, these experiments failed. I did not obtain a single crystal of this protein from several screening condition delivered by Hampton. Screening was preformed also for different temperatures: 4℃ and room temperature. A potential result of failure could be due to a long and flexible tag of the construct (MRGSHHHHHHGMASMTGGQQMGRDLYDDDDKDPSSRSAAGTMEF). Flexibility of this tag is illustrated in *Figure 34*. Nevertheless, main proporties of the fusion protein, like the increased expression, enhanced solubility, and protein purification via affinity chromatography were obtained (Smyth et al., 2003).

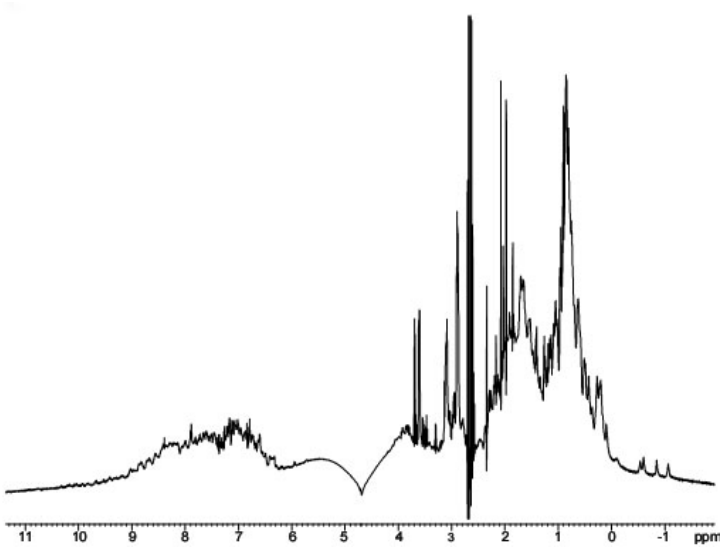

Figure 34 1D proton NMR spectrum of the A/B domain of human pRb showing the folded nature of the protein and a flexible long His-tag

3.2. E7

The E7 protein should form a dimer. The molecular weight for the ^{15}N labelled protein used for NMR studies corresponds to c.a. 28 kDa. This is in agreement with the literature data (Sanders and Maitland, 1994) and is not surprising because the construct includes, in the C-terminus, dimerization repeats Cys-X-X-Cys (McIntyre et al., 1993). A 1D NMR spectrum shows that E7 contains also large unstructured regions. The NMR spectrum in *Figure 35* is typical for unstructured, flexible polypeptides (Rehm et al., 2002). These properties of the E7 preparation did not allow for farther studies.

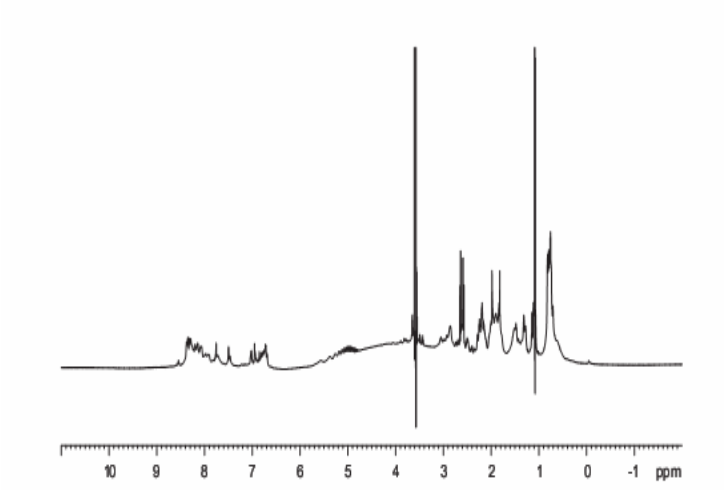

Figure 35 1D proton NMR spectrum of E7 showing the unfolded nature of the protein.

3.3 Preliminary investigations on nucleostemin

The recombinant full-length nucleostemin was optained from *Escherichia coli* BL21(DE3) pLys S expression system and contained the full length gene of nucleostemine (*Figure 21*) cloned in a pET 28 vector (Novagen) with a N-terminus His-Tag. The level of test expression of protein was low. The protein was purified under native conditions using a NiNTA (Qiagen) column. Eluted nucleostemine was collected and concentrated down to 1 ml and loaded onto size exclusion chromatography on a High Load 26/60 Superdex 200 column (Amersham Pharmacia Biotech) in 50 mM NaPCl (pH 7.4), 150 mM NaCl, 5 mM DTT. Protein eluted as a single monomeric peak (*Figure 36*).

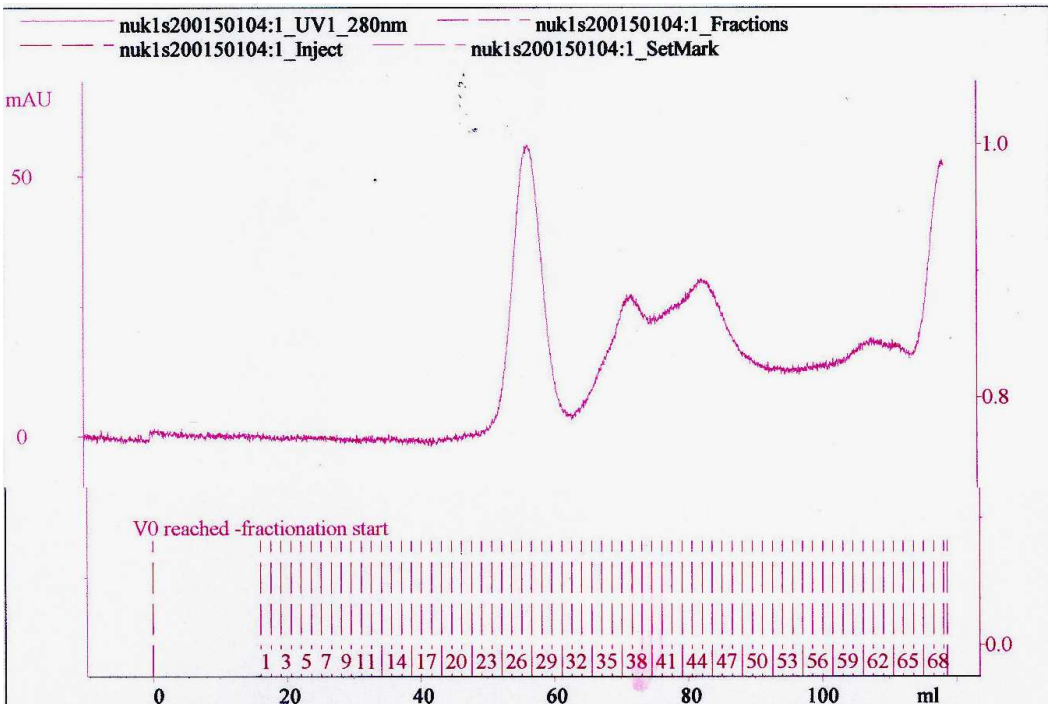

Figure 36 Purification of the native nucleostemin by gel filtration chromatography.

Levels of expression were very low and I have decided to make truncated constructs. Before planning new constructs, the amino acid sequence of the protein was checked for consensus motifs (*Figure 37 A*). Results of this search, as well as mutation analysis preformed by Tsai and McKay (2002), were important for the new constructs design. The list of sequences is shown in *Figure 37 B*. New fragments possess His-tag and GST-tag.

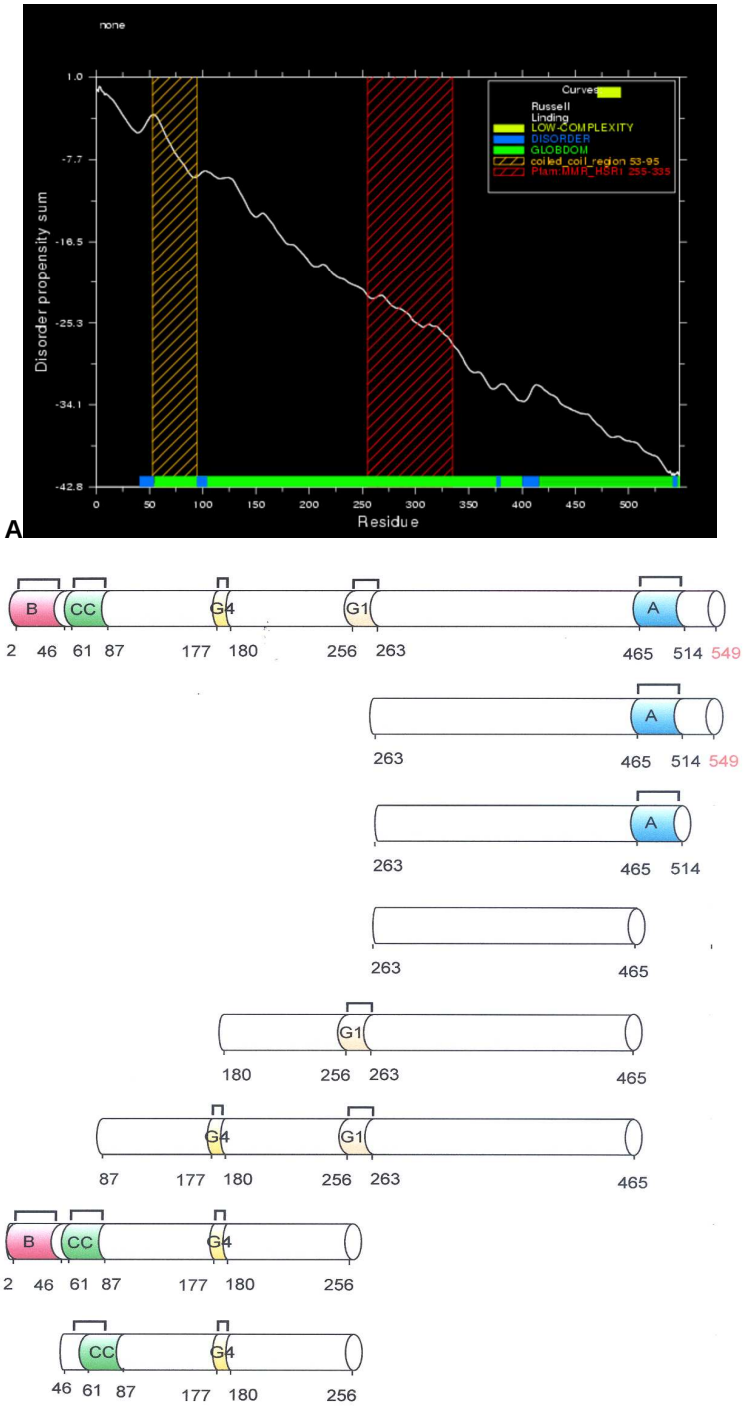

Figure 37 (**A**) Plot showing important motifs of nucleostemin, (**B**) Graphic representation of designed constructs.

3.4 CDK2 NMR binding experiments

NMR measurements consisted of monitoring changes in chemical shifts and line widths of backbone amide resonances of uniformly ^{15}N-enriched CDK2 samples in a series of HSQC spectra as a function of a ligand concentration (Shuker et al., 1996). We first tried to test the inhibitors with the ^{15}N uniformly labeled sample of full-length CDK2. CDK2 is a 34 kDa protein and it has 7 α-helices, 8 β-sheets and 16 loops (De Bondt et al., 1993). NMR signals from α helices are not resolved well in the proton NMR frequency due to overlap of resonances, so it was difficult to determine the (specific) binding site in the protein upon addition of compounds.

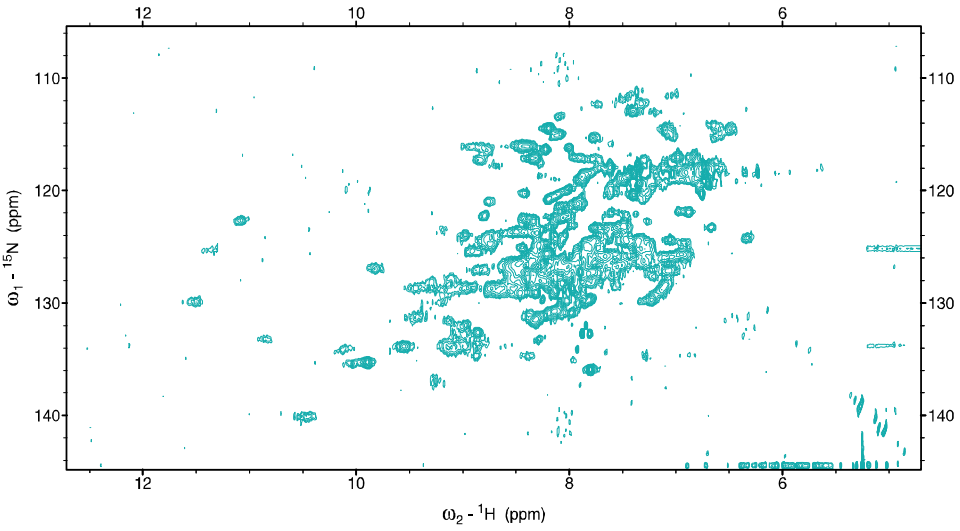

Figure 38 ^{1}H-^{15}N HSQC spectrum of the ^{15}N uniformly labeled CDK2.

Selective ^{15}N amino acid labelling was employed in order to overcome the problem of overlap. By comparing the crystal structure of the CDK2 bound to roscovitine and ATP, we found that the residues of CDK2 which make contacts to both of these

compounds were Lys33**,** IIe10, Val18, Ala31, Leu134, Phe 80, and Phe 82. In the ATP binding region of CDK2 there are two lysine residues that take part in the binding, Lys33 and Lys89 (for roscovitine) and Lys33 and Lys129 (for ATP) (*Figure 40*). Lys33 and Lys89 are present in the β3 and α2 helix, respectively (*Figure 40*). Lys33 is important for ATP binding because it forms salt bridges with γ-phosphate of ATP and Asp145 residue is involved in ATP-Mg^{2+} binding. This behaviour of the Lys33 side chain could be important for drug design because it is possible that the cavity formed (Val18, Ala31, Lys33, Val64, Phe80 and Asp145) can accommodate larger groups (Legraverend M et al., 2000);(Otyepka M et al., 2002). We chose to selectively label the lysines present in CDK2 (there are total 21 lysines in our construct) (De Bondt et al., 1993). In this construct the histidine-tag bound to the CDK2 has one more lysine. Of the total 22 peaks, 20 are visible in the 2D HSQC spectrum. In the spectrum the signals cluster around a ^{1}H frequency of 8.3 ppm, as expected for lysines in a helical part of the structure.

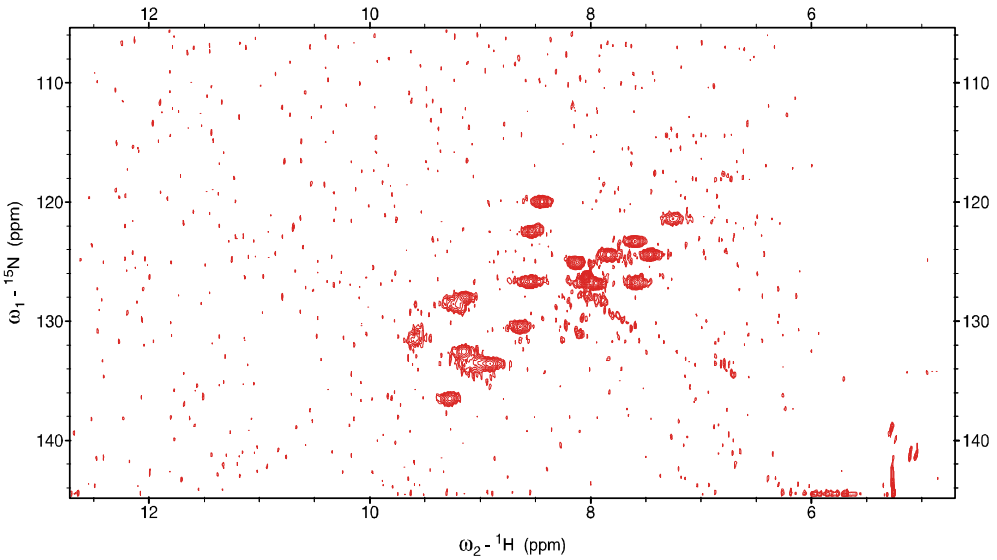

Figure 39 ^{1}H-^{15}N HSQC spectrum of the ^{15}N selectively labeled lysine sample of CDK2.

We titrated the ^{15}N lysine selectively labeled CDK2 with ATP. Addition of Mg-ATP caused 5 changes in the ^{1}H-^{15}N HSQC spectrum (*Figure 40,* **A**). Peaks numbered 1, 3, 4 and 5 showed shifts whereas the intensity of peaks numbered 2 and 6 weakened. When the ^{15}N lysine sample of CDK2 was titrated with roscovitine there were clear shifts noticeable in the ^{1}H-^{15}N HSQC spectra. In, peaks 1, 3, 4, 5, and 7 show distinct chemical shifts compared to the others. Whereas the intensity of peaks numbered 2 and 6 weakened. As roscovitine is a competitive analog of ATP, the binding of roscovitine with CDK2 is stronger than ATP which is clearly seen in the HSQC spectrum. We used ATP and roscovitine as positive control for our studies:

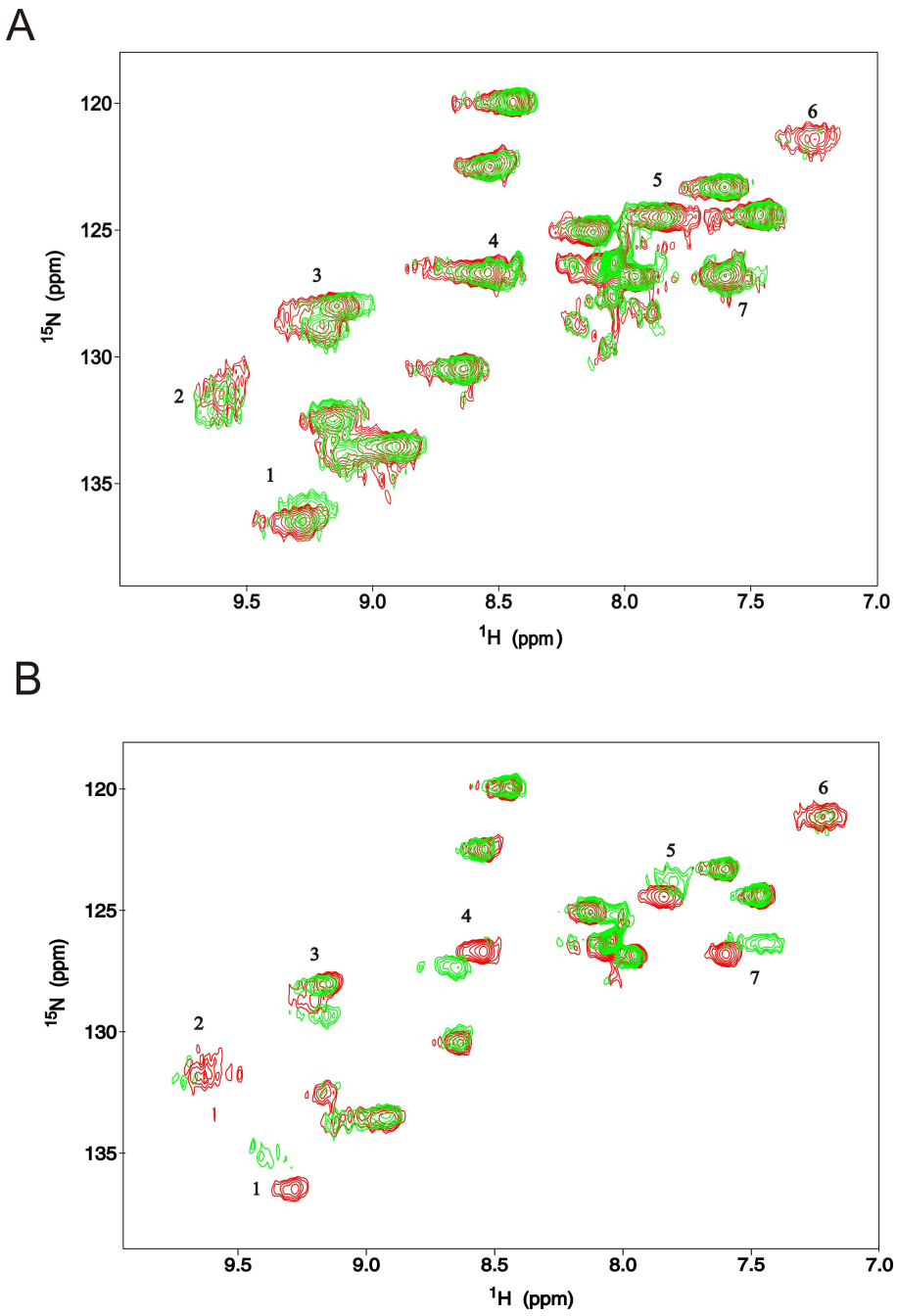

Figure 40 (**A**) ^{1}H-^{15}N HSQC spectrum of the ^{15}N selectively labeled lysine of CDK2 titrated with ATP. The reference is in red and the last step of the titration is in green. Both spectra are overlaid over each other to show the exact chemical shifts of the peak. For convenience the peaks, which show chemical shifts or disappear are numbered. (**B**) ^{1}H-^{15}N HSQC spectrum of the ^{15}N selectively labeled lysine of CDK2 titrated with roscovitine. Reference in red and the last step of titration is in green. For details consult the text.

Dichlorochalcone: (See *Figure 33,* page 64 2Cl) When ^{15}N lysine sample of specifically labeled CDK2 was titrated with this compound there were hardly any changes seen in the ^{1}H-^{15}N HSQC spectrum. The intensity of the peaks numbered 2 and 6 weakened whereas the peak numbered 1 showed an insignificant chemical shift. This compound also precipitated the protein at higher concentration. The binding of this compound with CDK2 was much weaker compared to the other inhibitors (*Figure 41,* **A**).

Butein: (See Appendix *Figure A* page 126) Butein inhibits the PKC (protein kinase C), which is a serine–threonine kinase and protein kinase A (cAMP dependent) (Yang. et al., 1998). The inhibition was competitive to ATP and non-competitive to the phosphate acceptor for EGF receptor (Yang. et al., 1998). This made us to test the compound on CDK2, which is also a serine threonine kinase. When the ^{15}N specifically labeled lysine of CDK2 was titrated with butein the peak numbers 1, 5 and 7 showed changes in chemical shift whereas the peaks 2 and 6 disappeared, confirming that the interaction was stronger compared to the chalcones (*Figure 41,* **B**).

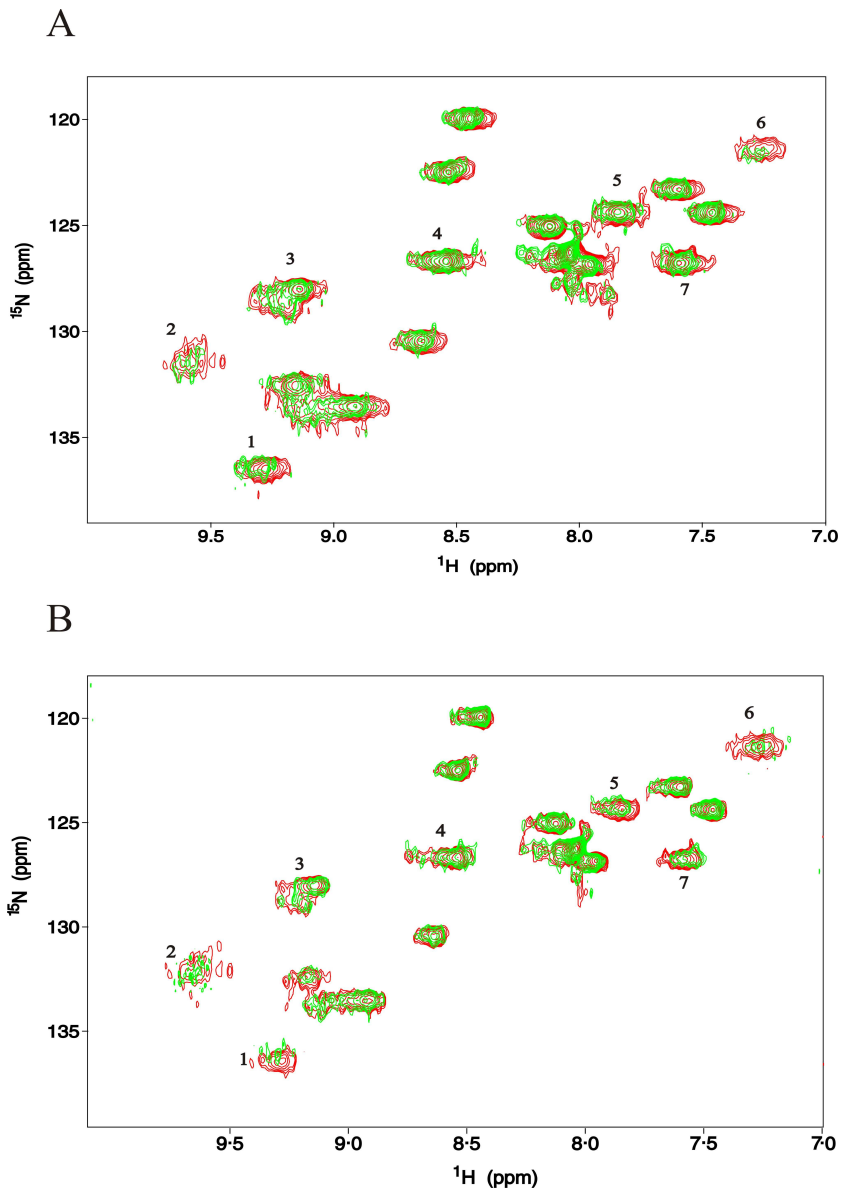

Figure 41 (**A**) ^{1}H-^{15}N HSQC spectrum of the ^{15}N selectively labeled lysine sample of CDK2 titrated with dichloro-chalcone. Reference in red and the last step of titration is in green. For details consult the text. (**B**) ^{1}H-^{15}N HSQC spectrum of the ^{15}N selectively labeled lysine sample of CDK2 titrated with butein. Reference in red and the last step of titration is in green. For details consult the text.

In above experiments it was possible to detect the binding of chalcones to the ATP binding site of CDK2. Butein proved to be the stronger binding partner compared to the

other chalcones. If we compare the chemical structure of chlorochalcones and butein, we can clearly visualize that OH groups in position 3 and 5 can make hydrogen bonds with the CDK2. Thus, we conclude that the presence of the OH groups in this region is important for binding to the ATP region of CDK2.

Table 2. NMR experiments with full-length CDK2.

Sample	Exp. type	Results
^{15}N CDK2	1D, HSQC	overlapping of resonances
CDK2 (^{15}N-Lys)	HSQC	peaks, 20 are visible
CDK2 (^{15}N-Lys) + roscovitine	HSQC	peaks 1, 3, 4, 5, and 7 shows distinct chemical shifts, intensity of peaks numbered 2 and 6 weakened
CDK2 (^{15}N-Lys) + 3-chlorochalkone	HSQC	The intensity of the peaks numbered 2 and 6 weakened, whereas the peak numbered 1 shows a small insignificant chemical shift. This compound also precipitated the protein
CDK2 (^{15}N-Lys) + 3,4 dichlorochalkone	HSQC	The intensity of the peaks numbered 2 and 6 weakened whereas the peak numbered 1 shows a small insignificant chemical shift. This compound also precipitated the protein
CDK2 (^{15}N-Lys)+ butein	HSQC	peak numbers 1, 5 and 7 showed changes in chemical shift whereas the peaks 2 and 6 disappeared

3.5 Inhibitors of the p53-Mdm2 complex

3.5.1 Preliminary investigations

We have tested several Mdm2 inhibitors. One group is chalcone derivatives shown in *Figure 42* and the second was obtained from the Developmental Therapeutics Program NCI/NIH (*Figure 43*).

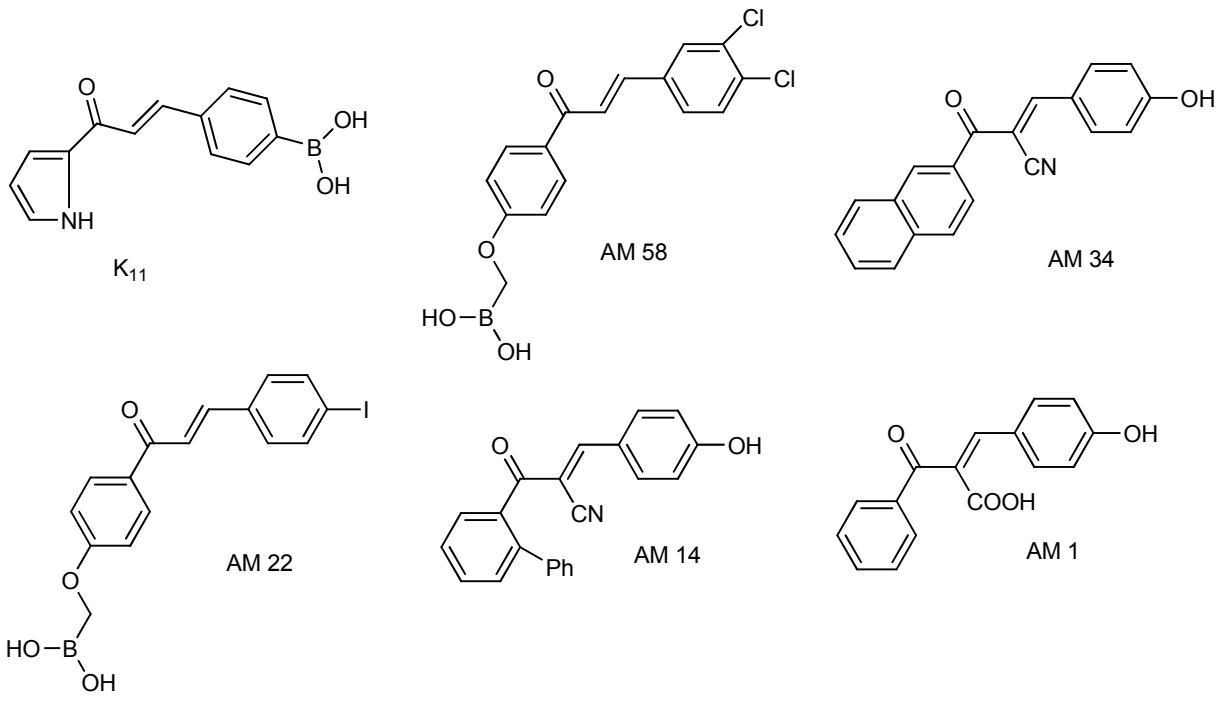

Figure 42 Chalcone derivatives

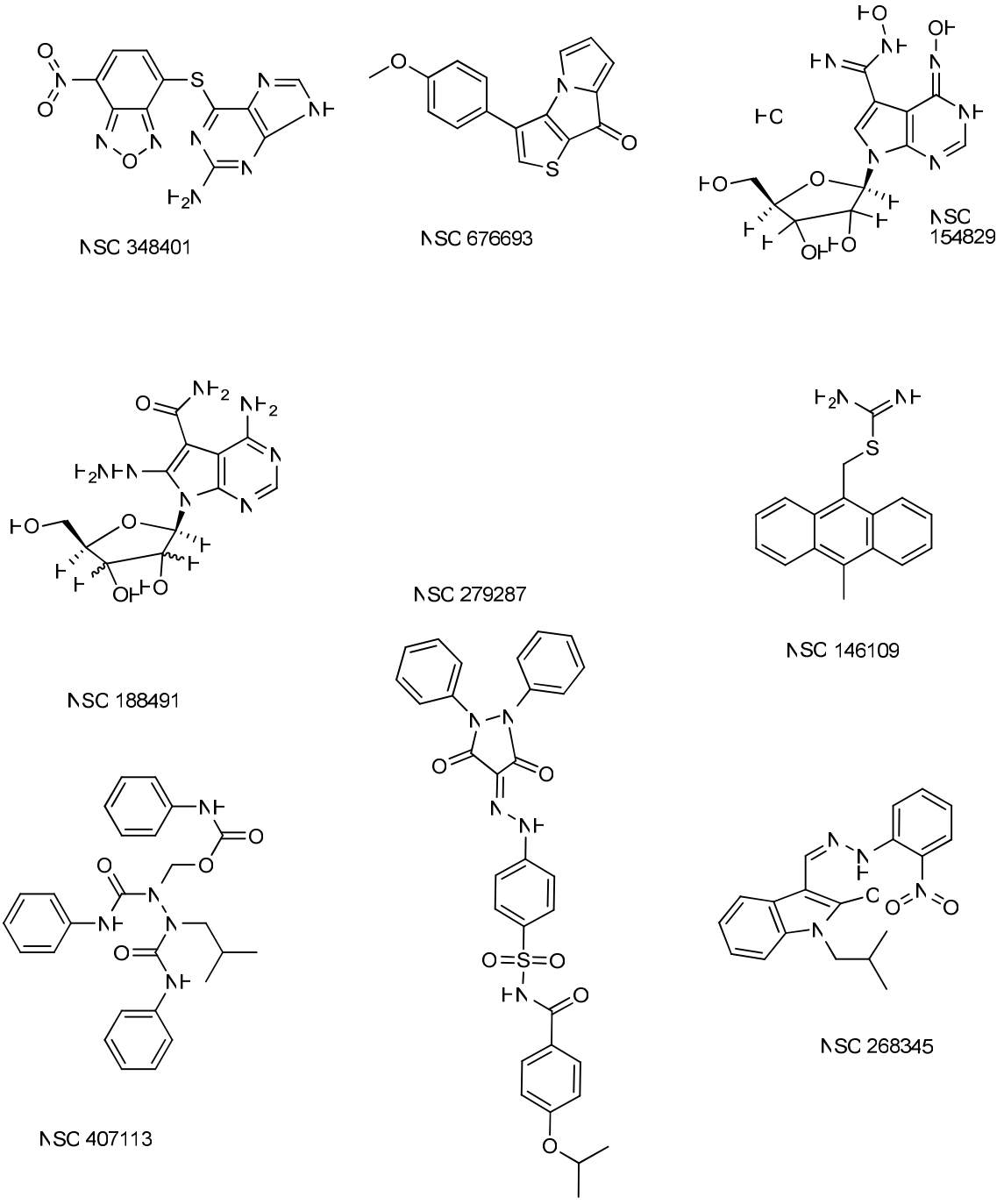

Figure 43 Compounds from the Developmental Therapeutics Program of the NCI/NIH

Ligand Binding

A total of 16 small molecular compounds were tested (*Figure 42 and 43*). NMR measurements consisted of monitoring changes in chemical shifts and line widths of the backbone amide resonances of uniformly ^{15}N-enriched Mdm2 samples in a series of HSQC spectra as a function of a ligand concentration. For free Mdm2 no changes in chemical shifts were observed between samples of different concentrations (0.03-0.5 mM) and pH values between 6.5 and 7.5. For titration experiments, 0.1-0.3 mM of human Mdm2 in 50 mM KH2-PO4, 50 mM Na2HPO4, 150 mM NaCl, pH 7.4, and 5 mM DTT was used. The componds were lyophilized and finally dissolved in DMSO-*d*6. No shifts were observed in the presence of 1% DMSO (the maximum concentration of DMSO in all NMR experiments after addition of inhibitors). All compound-Mdm2 complexes showed a continuous movement of several NMR peaks upon addition of increasing amounts of inhibitors. From these experiments, the spectra of compounds-Mdm2 could be assigned unambiguously. The complexes of human Mdm2 and the compond were prepared by mixing the protein and the ligand in the NMR tube. Typically, NMR spectra were recorded 15 min after mixing at room temperature. An initial screening of all compounds used in this studywas performed with a 10-fold molar excess of compond to human Mdm2. All subsequent titrations were carried out until no further shifts were observed in the spectra. Typically, the concentration of human Mdm2 was 0.1 mM and the final concentration of the ligand was 50 mM in each titration. In most cases we observed precipitation of Mdm2. All of tested compounds were useless for future studies.

3.5.2 Inhibiton of the p53-Mdm2 complex

The p53-Mdm2 complex

Figure 44 **A** shows the 2D ^{15}N -^{1}H spectrum of ^{15}N Mdm2. The Mdm2-p53 complex formation was observed by the stepwise addition of unlabeled p53 to ^{15}N-Mdm2. The disappearance of most of the Mdm2 peaks, as seen in *Figure 44* **B** indicates a complete complex formation between the two proteins.

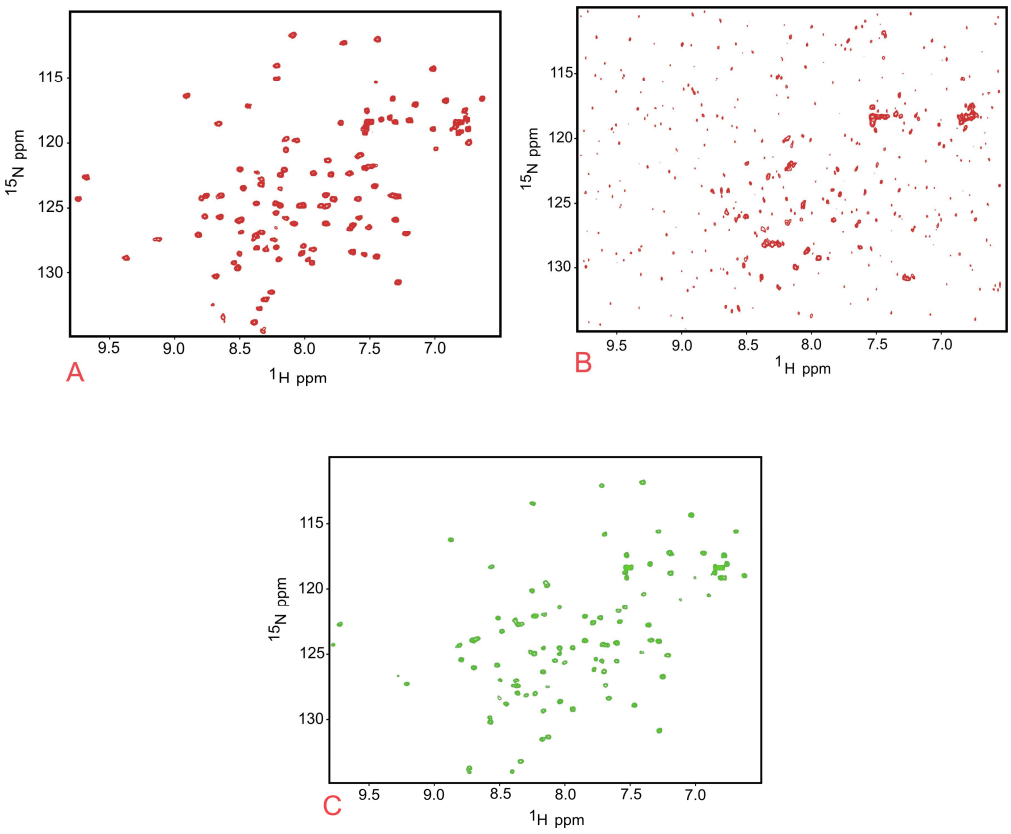

Figure 44 Spectra of the ^{15}N uniformly labeled Mdm2. (**A**) ^{1}H -^{15}N HSQC spectrum of ^{15}N Mdm2. (**B**) ^{1}H -^{15}N HSQC spectrum of ^{15}N Mdm2 complexed with p53, as seen, most of the cross peaks disappear. (**C**) ^{1}H-^{15}N HSQC spectrum of Mdm2 in complex with Nutlin-3. Some cross peaks are shifted due to binding of Nutlin to Mdm2.

As expected, majority of the backbone ^{15}N -^{1}H resonances of the structured regions of Mdm2 broadened and/or disappeared, while the leftover peaks originate from flexible residues of the complex and/or free Mdm2. Following our previous calculations, we found that, for the complex of Mdm2-p53 having a KD of 0.77 μM and a protein concentration of 0.1 mM, there is still 8.4% free Mdm2 present and the residual observed sharp signals could arise from this free protein. All these signals are located in the spectrum around "central 8.3 ppm NH amide" region, diagnostic for unstructured residues, plus flexible side chains at 7 and 7.5 ppm.

Nutlin-3

Nutlin-3 was added in a stepwise manner to the Mdm2/p53 complex and we found that it restores the Mdm2 spectrum, as seen in *Figure 44* **C**, with the sites involved in binding to Nutlin. A 1D spectrum of the dissociated complex revealed that the freed p53 is folded (the core domain) as judged by NMR. The experiment also shows that the Mdm2/Nutlin complex is soluble, and that Nutlin did not induce precipitation of Mdm2. To be sure of these results and to establish our methodology, we performed experiments on ^{15}N -labeled p53 and unlabeled Mdm2. *Figure 46* **A** shows the ^{1}H -^{15}N HSQC spectrum of the uniformly labeled p53.

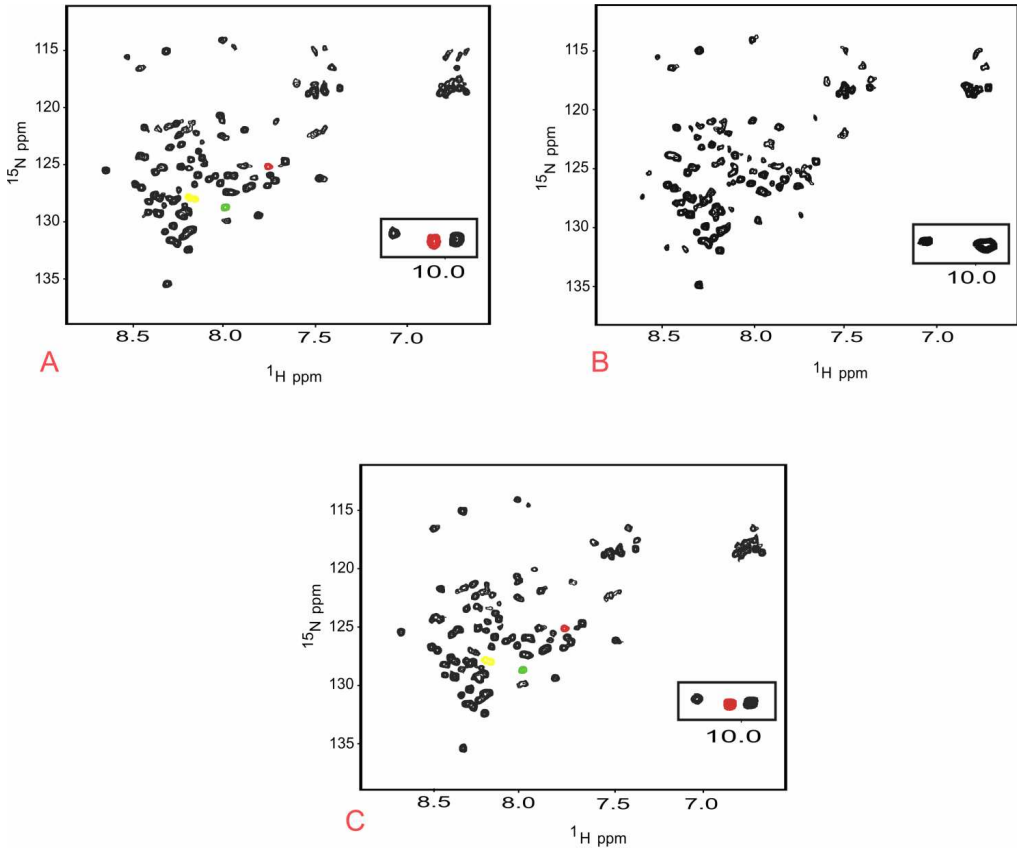

Figure 46 Spectra of the ^{15}N uniformly labeled p53. (**A**) ^{1}H -^{15}N HSQC spectrum of p53 (for assignments see (Ayed A et al., 2001);(Lee H et al., 2000). The cross peak of Phe19 is shown in yellow and Leu26 in green. The two cross peaks in red are from Trp23, with the side chain cross peak at the ^{1}H chemical shift of 10.10 ppm (inset) (**B**) ^{1}H -^{15}N HSQC spectrum of ^{15}N -p53 in complex with Mdm2. The complex formation is monitored by the disappearance of Phe19, Trp23 and Leu26 peaks. (**C**) ^{1}H -^{15}N HSQC spectrum of free p53 after addition of Nutlin-3. The spectrum corresponds to that of *Figure 46* (**A**), with all the "bound" peaks being restored, indicating the dissociation of the complex.

The spectrum indicates that the first 93 residues are flexible and mostly unstructured. These flexible residues are the ones that are mainly seen in the spectrum owing to their narrower line widths as compared to the p53 DNA core domain that have

broad line widths, and hence unobservable. The primary binding sites of p53 to Mdm2 are known and the complex formation can be monitored from the NMR spectrum by observing the three binding site residues (Phe19, Trp23 and Leu26 (Kussie et al., 1996)). A stepwise addition of Mdm2 resulted in the disappearance of these cross peaks and a complete disappearance indicated complex formation, as seen in *Figure 46* **B**. An interesting observation was that the N-terminal residues were still not structured when bound to the Mdm2 domain, with the exception of a 10 residue-binding site (residues 17 to 26). As before, Nutlin-3 was then added to the Mdm2/p53 complex in a stepwise manner and the reappearance of the three peaks (Phe19, Trp23 and Leu26) was monitored. *Figure 46* **C** shows the spectra of ^{15}N -p53 and the reappearance of the three binding sites indicating that Nutlin-3 dissociates the p53-Mdm2 complex by binding to Mdm2.

RITA

RITA is soluble in the buffer used for the NMR samples at around 0.15 mM therefore the DMSO-d_6 stock solution of RITA was used for NMR measurements. The effect of DMSO-d_6 on the proteins and the protein complex was checked separately and found to be negligible up to 15%/volume of DMSO-d_6. Highly concentrated RITA in DMSO was added to 500 ml of the Mdm2 solution, resulting in a saturated RITA solution as judged by a RITA precipitate. No major changes in the Mdm2 spectrum were observed. A stepwise addition of p53 followed. The DMSO stock solution of RITA was added again, up to the concentration of 15% DMSO; at this stage a high excess of RITA signals compared to the signals of the proteins, was seen in the proton 1D NMR spectrum. After each step an HSQC experiment was recorded. The details of the experiment are

summarised in *Figure 45*. In order to secure consistent results, we decided to test our experiments in the presence and absence of RITA. *Figures 45* **A**, **D** show the reference ^{15}N-Mdm2 spectra. A stepwise addition of p53 resulted in the disappearance of the Mdm2 (*Figure 45,* **B***,* **E**). The visible peaks originate from the remaining 8.4% free Mdm2. RITA was added to this complex up to a maximum of 5-fold molar excess relative to p53 and it did not prevent the Mdm2/p53 complex formation (*Figure 45,* **B**). RITA was administered to the complex using two strategies. In the first strategy p53 was pre-incubated with RITA at 37^{o}C for 80 min and then Mdm2 was added to the mixture (*Figure 45,* **B**). In the second strategy RITA was titrated into the Mdm2/p53 complex. RITA did not dissociate the complex. Addition of Nutlin-3 restores the Mdm2 spectrum, as seen in *Figure 45* **C**, **F** with the signals from Mdm2 sites involved in binding to Nutlin being however shifted. This was a clear indication that Nutlin-3 releases p53 from the complex by competing with p53 for binding to Mdm2, whereas RITA has no effect on this interaction.

In conclusion, we found that that RITA does not block the formation of the complex in vitro between p53 (residues 1-312) and the N-terminal p53-binding domain of Mdm2 (residues 1-118).

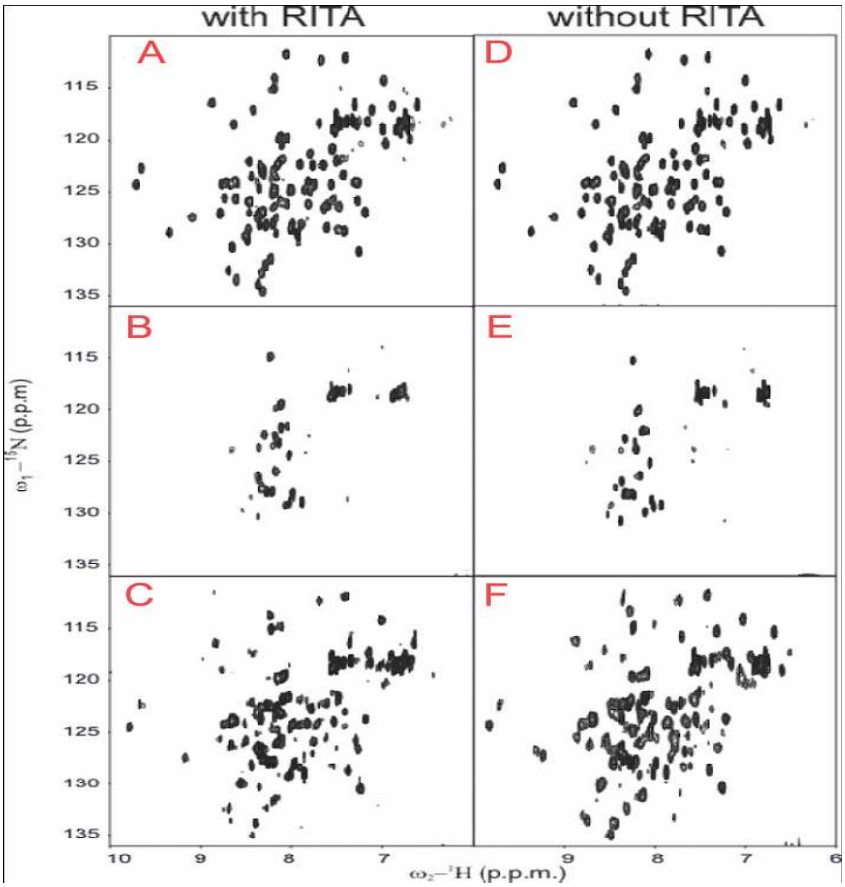

Figure 45 HSQC spectra of the ^{15}N labeled Mdm2 (residues 1-118). (**A-C**) with RITA, (**D-F**) without. (**A, D**) HSQC spectra of the ^{15}N labeled Mdm2. (**B, E**) Addition of p53 results in the disappearance of most of the peaks indicating complex formation. (**C, F**) Additions of Nutlin-3 dissociates the p53-Mdm2 complex.

Sulfonamide compound

Following the previous protocol for titrations, a stepwise addition of the sulfonamide to p53-^{15}N-Mdm2 complex did not result in the recovery of the free ^{15}N-Mdm2 spectrum, but resulted in the release of the folded p53. The release of p53 could also be monitored from the 1D proton NMR spectra.

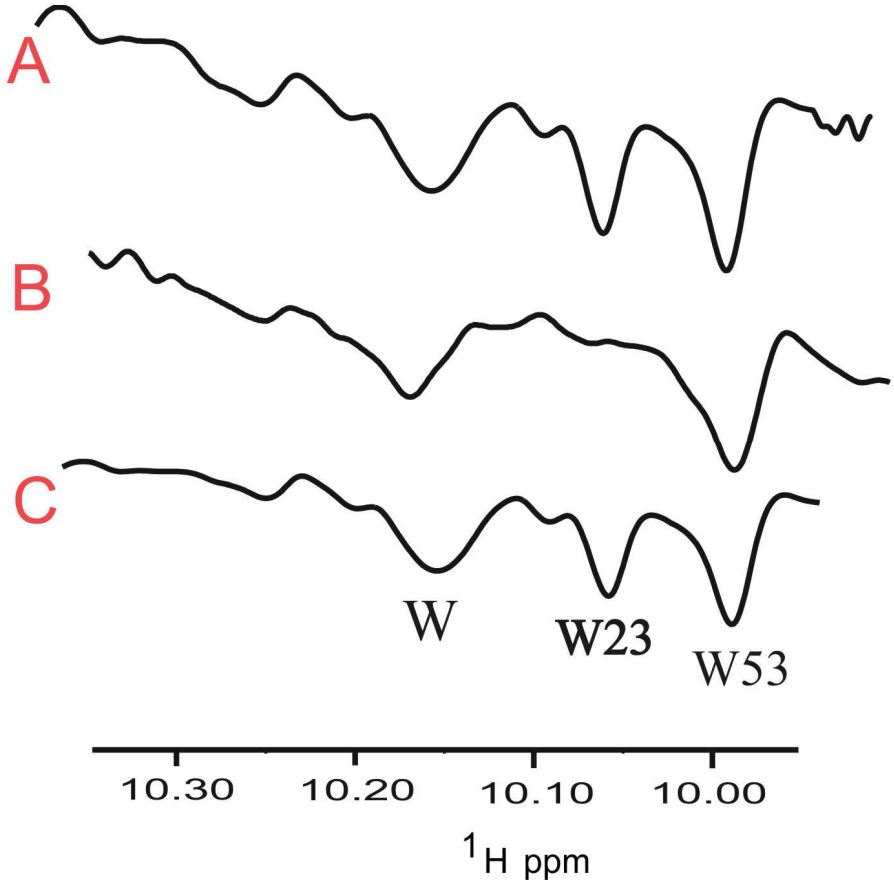

Figure 47 1D proton spectra of the side chains of tryptophans (W) (for assignment refer to Ayed et al., 2001). (**A**) Side chain peaks of free p53, showing W23, W53. W is the side chain peak from the tryptophan of the DNA binding region that is not assigned. (**B**) On forming a complex with Mdm2, the side chain of Trp23 disappears. The W53 peaks broaden as seen in the 2D spectrum also. (**C**) The peak reappears on addition of the sulfonamide, indicating that p53 has been released.

Figure 47 shows the 1D spectra of the region where the side chain of Trp23 resonates at 10.10 ppm. Before drawing conclusions about the inhibitory effect of sulfonamide we decided to test if preincubation of Mdm2 with sulfonamide would help inhibit its interaction with p53. We therefore added sulfonamide to the free ^{15}N -Mdm2 with the intention of adding p53 after the preincubation of Mdm2 with the compound;

however we observed only very small, insignificant induced chemical shift changes in the ^{15}N HSQC spectrum of Mdm2 on titration with sulfonomide. A closer inspection of the 1D proton spectra indicated that sulfonamide precipitated Mdm2, as no signals from Mdm2 were present in the final 1D proton spectrum. Mdm2 begins to precipitate at about 0.3 mM sulfonamide concentration, which is about three times the protein concentration, and the precipitation was complete at about 1 mM, which is about ten times the protein concentration.

Boronic chalcones

A boronic chalcone (*Figure 42 AM 58*) was titrated in order to study its effect on the Mdm2/p53 complex. This boronic chalcone did not dissociate the Mdm2-p53 complex even at concentrations of 2 mM, i.e. 20 times that of the protein complex (the HSQCs were all equivalent to those of *Figure 44* **B**). At this concentration of the ligand, the Mdm2-p53 complex completely precipitated in the NMR tube. However, direct titration of ^{15}N-Mdm2 with these chalcone showed that they bind to the tryptophan-binding subsite of the p53-binding cleft of human Mdm2 (Kussie et al., 1996);(Stoll et al., 2001) with very low, i.e. high micromolar, affinity, indicating that these compounds are extremely weak inhibitors for the Mdm2/p53 interaction, and exhibit their activity in cell lines via a mechanism that is different from the primary direct inhibition of p53- Mdm2 interaction.

3.6 The interaction of roscovitine and chalcones with CDK2

We have tested several lead compounds that have recently been reported as CDK2 inhibitors: ATP (De Bondt et al., 1993), roscovitine (Legraverend M et al., 2000), chalcones (Jang HS et al., 2005; Samoszuk M et al., 2005), and indole-3-carbinol

(Brandi et al., 2003). At first we have used a protocol that corresponds to the traditional "SAR by NMR" approach. Primary, we found that the residues of CDK2 which make contacts to ATP-Mg^{2+}, roscovitine were Lys33**,** IIe10, Val18, Ala31, Leu134, Phe 80, and Phe 82. In the ATP binding region of CDK2 there are two lysine residues that take part in the binding, Lys33 and Lys89 (for roscovitine) and Lys33 and Lys129 (for ATP) (*Figure 45*). Lys33 and Lys89 are present in the β3 and α2 helix, respectively (*Figure 45*). Lys33 is important for ATP binding because it forms salt bridges with γ-phosphate of ATP and Asp145 residue is involved in ATP-Mg^{2+} binding. This behavior of the Lys33 side chain could be important for drug design because it is possible that the cavity formed (Val18, Ala31, Lys33, Val64, Phe80 and Asp145) can accommodate larger groups (Legraverend M et al., 2000 ; Otyepka et al., 2002). However, we did not see possible binding for nucleoside mono- or di-phosphates. Our studies with the chalcone family have shown that it is possible to detect the binding of chalcones to the ATP binding site of CDK2. Butein proved to be a stronger binding partner compared to other chalcones. We can clearly visualize that OH groups in position 3 and 5 can make hydrogen bonds with CDK2. Thus, we conclude that the presence of the OH groups in this region is important for binding to the ATP region of CDK2. However, butein or dichloro- or chloro- chalcone prove to be extremely weak binding partners compared to ATP or roscovitine. We have shown also that selective labeling can simplify the HSQC protein spectrum.

3.7 General comments on the application of NMR for studying ligand-protein interactions

The advantage of the use of ^{15}N-HSQC spectra is ability to detect the binding of small, weakly bound ligands to ^{15}N-labeled target proteins. Because of the ^{15}N spectral editing, no signals from the ligand are observed. Another advantage is the ability to rapidly determine the different binding site locations of the fragments, which is critical for interpreting structure-activity relationships and for guiding the synthesis of related compounds. However, SAR by NMR method is limited by the solubility of compounds at milimolar concentrations and is applicable only to small proteins (MW < 30 kDa) that can be obtained in large quantities, measurable for NMR. The NMR chemical shift perturbation methods have also been successfully used for mapping binding interfaces in proteins The most popular protocol has been based on the use of chemical shift perturbations in 2D ^{1}H-^{15}N HSQC spectra of ^{15}N-labeled proteins upon addition of ligands or peptides/proteins. In general, a prerequisite for mapping these interactions is that the assignment of the NMR spectrum of the protein, at least for the nuclei that exhibit chemical shift changes, although a method has recently been described that allows mapping interfaces of protein complexes without the knowledge of chemical shift assignments provided that the 3D structures are known. The assignment is not needed if the only purpose of the NMR experiment is to detect the binding of ligands to target proteins.

3.8 An NMR-based antagonist induced dissociation assay for targeting the ligand-protein and protein-protein interaction in competition binding experiments

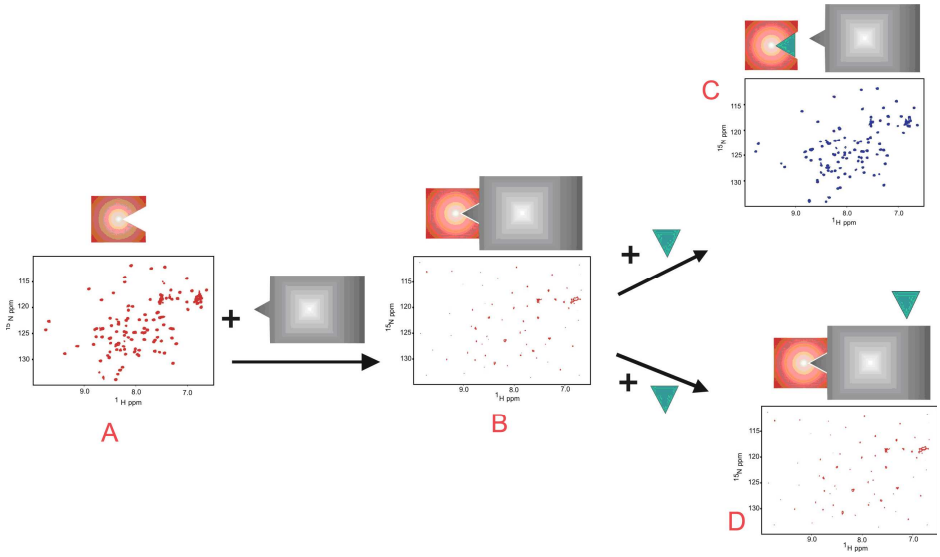

Figure 48 Schematic representation of our method for studying the effect of an antagonist on the interface between two proteins. (**A**) A ^{15}N HSQC spectrum of a ca. 10 kDa uniformly ^{15}N labeled protein (each amino acid gives a cross peak for the N-H pair. The side chain N-H resonances are observed at around 7 ppm ^{1}H and at 120 ppm ^{15}N chemical shifts). (**B**) The cross peaks disappear on addition of a large protein (ca. 35 kDa) that forms a complex with the smaller one. (**C**) The cross peaks reappear on addition of a strong inhibitor ligand that dissociates the complex. (**D**) A weak inhibitor does not dissociate the complex.

A schematic representation of our method for two-protein complex is shown in *Figure 48*. At least two protein components that make up a complex are monitored, with one component being small enough (less than ca. 15 kDa) to provide a good quality HSQC spectrum after ^{15}N or ^{13}C labeling of the protein (*Figure 48,* **A**). The size of the second component should be large enough so that the molecular weight of the

preformed complex is larger than ca. 40 kDa. On forming a complex, the smaller protein begins to exhibit characteristics of the larger one. The observed 1/T2 transverse relaxation rates of the bound protein in the complex increase significantly and broadening of NMR resonances results in the disappearance of most of the cross peaks in the HSQC spectrum (*Figure 48,* **B**). In order to restore the spectrum of the smaller component, one would have to add an antagonist that would dissociate this complex, as shown in *Figure 48* **C**, whereas a non-binder would not affect the HSQC spectrum of the complex as seen in *Figure 48* **D**. However, a weak inhibitor could partially release the labeled protein when added in large excess. A simple calculation (Wang Z. X, 1995) shows that an inhibitor of KD 5 μM would release about 40% of the protein at 250 μM concentration, assuming 100 μM each of proteins and a KD of 0.7 μM for the complex. Our approach lacks typical weaknesses of "SAR NMR" i.e.: too crowded HSQC spectra for proteins larger then ca. 30 kDa or the problems of detecting NMR signals for intermediate exchanges when the lifetime of the free and bound states is approximately equal to the differences in chemical shift and/or transverse relaxation rates between the free and ligand-bound forms. We have tested four lead compounds that were reported to inhibit the p53-Mdm2 interaction: Nutlin-3, the sulfonamide compound, boronic chalcone, and RITA. Only Nutlin-3 was found to be an inhibitor of the p53- Mdm2 interaction and therefore is a potential candidate for drug development in cancer treatment. Our experiments with Nutlin-3 showed that Nutlin-3 releases p53 from the complex by competing with p53 for binding to Mdm2. By monitoring the 1D/2D spectra we could conclude that the freed p53 was folded, the Mdm2/Nutlin complex was soluble, and that Nutlin did not induce precipitation of Mdm2. The dissociation constant (K_d) of Nutlin-3 for Mdm2/p53 complexes estimated from NMR is in the low micro-molar

range (< 1 μM), indicating tight binding. The sulfonamide compound precipitates Mdm2 and releases folded p53. The boronic chalcone precipitated p53 and Mdm2 at high ligand concentrations. This boronic chalcone is an extremely weak binder for Mdm2. In case of sulfonamide, the precipitation was selective for Mdm2, but not for p53. RITA was found to be a nonbinder and hence cannot be used as an antagonist for the primary p53- Mdm2 interaction. The studies with sulfonamide and the boronic chalcone provide for a more rigorous detection of inhibition of protein-protein interactions than the approaches based on affinity chromatography pull down assays, immunoprecipitation, as these methods are known to give false positive results. In addition, these methods provide very limited information about the structural status of proteins. The correct structure of a protein is a universal requirement for its function. An interesting side-result of these experiments is the determination of the folding status of the p53 when free or bound to Mdm2. Characterization of these forms has been a subject of several recent studies (Ayed et al., 2001; Bell et al., 2002; Dyson and Wright, 2005; Lee et al., 2000; Mulder et al., 2000). Our NMR spectra indicate that the first 93 residues of p53 are flexible and unstructured in agreement with the findings which showed that the full-length p53 contains large unstructured N- and C- terminal regions in its native state (Ayed et al., 2001; Bell et al., 2002; Lee et al., 2000). Since the HSQC spectrum of these 93 residues is almost identical to that of the isolated N-terminal domain Lee et al. (2000), the conformations of these residues have to be the same as those found in (Lee et al., 2000) i.e. although the p53 transactivation domain does not have tertiary structure, it is nevertheless populated by a nascent helix and turns (Ayed et al., 2001; Lee et al., 2000; Uesugi and Verdine, 1999). A new finding is that our NMR spectra unequivocally show that, with the exception of a 10 residue-binding site (residues 17 to

26), the bulk of the N-terminal residues is still not structured when bound to the Mdm2 domain.

Several modifications of our approached are possible. In few favorable cases (flexible residues), 1D proton NMR spectra may suffice for monitoring the states of proteins in complexes upon treatment with ligands. The regions of the proton NMR spectra at ppm 8.7 to 12 and 0.0 to -0.5 could be used for these purposes. A protocol that would start first with the titration of the small ^{15}N labeled component of the complex would correspond to the traditional "SAR by NMR" approach. Adding the second larger protein would then follow. Finally, a part of the large protein fragment could be replaced by GST, which has 226 amino acids. For example, a GST tagged N-terminal 93-residue p53 domain could replace the 1-312 residue p53 fragment.

Summary

The work presented in this thesis was carried out at the Department of Structural Research, Max Planck Institute of Biochemistry, Martinsried, from April 2003 to December 2005.

The NMR screening studies for lead compounds so far concentrated on binary interactions of lead compounds with small to middle size domains of target proteins, but not on protein-protein complexes. In order to study the effect of antagonists on a protein-protein complex, we developed a new approach based on differentials of 1/T2 relaxation rates of the proteins forming the complex. The size of one component should be small enough (less than ~ 15 kDa) to provide a good quality HSQC spectrum for ^{15}N or ^{13}C labelled proteins. The size of the second component should be large enough so that the molecular weight of the preformed complex is larger than ~ 40 kDa. We have illustrated our method by studying lead compounds that have been reported to block the p53-Mdm2 interaction. p53, the “guardian of the genome”, is a tetrameric allosterically regulated protein that is activated by a number of genotoxic factors. In response to these signals, p53 promotes the transcription of genes responsible for cell-cycle arrest, DNA repair, and apoptosis. The importance of p53 in cancer prevention development is implicated by the fact that over 50% of clinically detected tumors display mutations in one or both p53 alleles. p53 can be inactivated by other mechanisms besides mutation, however. There are a number of cancers, which have wild-type p53 and overexpressed Mdm2, a protein which can inhibit p53's ability to bind to DNA and activate transcription. Inhibition of the p53-Mdm2 interaction is a potential avenue of targeted anticancer therapy.

Four compounds that were reported to inhibit this interaction were tested using this method and only one of them was found to be a good inhibitor of the p53-Mdm2

complex. Apart from monitoring inhibition, we can also monitor the folded state of the protein on being released. This method should provide an important extension to the traditional "SAR by NMR" technique.

Very often the mechanisms by which transformed cells can override checkpoints are closely related to CDK function (Zhu et al., 2004). For this reason, restoration of cell cycle control through pharmacological inhibition of CDKs has been actively pursued over the last decade as a new strategy for the treatment of cancer (Balasubramanian et al., 2005; Owa et al., 2001). We have tested several lead compounds that have recently been reported as CDK2 inhibitors: ATP (De Bondt et al., 1993), roscovitine (Legraverend M et al., 2000), chalcones (Jang HS et al., 2005; Samoszuk M et al., 2005), and indole-3-carbinol (Brandi et al., 2003). Our studies with the chalcone family have shown that it is possible to detect the binding of chalcones to the ATP binding site of CDK2. Butein proved to be a stronger binding partner compared to other chalcones. We could propose that OH groups in position 3 and 5 can make hydrogen bonds with CDK2. Thus, we conclude that the presence of the OH groups in this region is important for binding to the ATP region of CDK2. On the other hand, butein or dichloro- or chloro-chalcone proved to be extremely weak binding partners compared to ATP or roscovitine.

Zusammenfassung

Die vorliegende Arbeit wurde in der Abteilung Strukturbiologie am Max-Planck-Institut für Biochemie, Martinsried, zwischen April 2003 und Dezember 2005 angefertigt.

Die NMR Screening Studien für potentielle Wirkstoffe (Leitstrukturen) konzentrierten sich bislang auf die paarweise Interaktion dieser Verbindungen mit kleinen bis mittelgroßen Zielproteindomänen, aber nicht auf Protein-Protein-Komplexe. Um den Effekt eines Antagonisten auf einen Protein-Protein-Komplexe zu untersuchen, haben wir eine neue Methode, basierend auf den Unterschieden der $1/T_2$ Relaxations-Raten der komplexbildenden Proteine, entwickelt. Die Größe der ersten Proteinkomponente sollte klein genug (kleiner 15 kDa) sein um eine gutes HSQC-Spektrum für ^{15}N oder ^{13}C markierte Proteine zu liefern. Die zweite Komponente sollte groß genug sein, damit der vorgeformte Komplex ein Molekulargewicht von mehr als 40 kDa erreicht. Wir haben unsere Methode veranschaulicht, indem wir Leitstrukturen untersucht haben über die berichtet wurde, dass sie die p53-Mdm2-Jnterakiton blockieren. p53, der „Wächter des Genoms“, ist ein tetrameres, allosterisches Regulatorprotein, das von einer Vielzahl von genotoxischen Faktoren aktiviert wird. Als Antwort auf diese Signale treibt p53 die Transkription der für den Zellzyklusarrest, DNA Reparatur und Apoptose verantwortlichen Gene voran. Die Wichtigkeit von p53 bei der Entwicklung von Krebspräventionen wird klar durch die Tatsache, dass über 50% der klinisch festgestellten Tumore Mutationen in einem oder beiden p53 Allelen zeigen. Jedoch kann p53 auch durch andere Mechanismen neben direkter Mutation inaktiviert werden. In einigen Tumoren mit funktionalem Wildtyp p53 wird Mdm2 überexpremiert, ein Protein, das die Fähigkeit von p53 an DNA zu binden und die Transkriptions-Maschinerie zu starten, inaktivieren kann. Die Inhibition der p53-Mdm2 Interaktion ist eine potentielle Möglichkeit für eine zielgerichtete Antikrebstherapie.

Vier Komponenten, die diese Interaktionen inhibieren sollen, wurden mit dieser NMR-Methode getestet, aber nur eine von ihnen wurde als guter Inhibitor des p53-Mdm2 Komplexes befunden. Weiterhin konnte auch der Faltungszustand dieses Proteins bestimmt werden. Diese Methode stellt eine wichtige Erweiterung für die traditionelle „SAR by NMR“ Technik dar.

Häufig stehen Mechanismen, nach denen transformierte Zellen Checkpoints umgehen, in engem Zusammenhang mit der CDK Funktion (Zhu et al., 2004). Aus diesem Grund wurde im letzen Jahrzehnt die Wiederherstellung der Zellzykluskontrollen mit Hilfe der pharmakologischen Inhibition von CDKs als neue Strategie der Krebsbehandlung (Balasubramanian et al., 2005; Owa et al., 2001) aktiv verfolgt. Wir haben verschiedene Leitstrukturen getestet die als mögliche CDK2 Inhibitoren in Frage kommen: ATP (De Bondt et al., 1993), Roscovitine (Legraverend M et al., 2000), Chalcones (Jang HS et al., 2005; Samoszuk M et al., 2005) und Indole-3-carbinol (Brandi et al., 2003). Unsere Studien an der Chalcone-Familie haben gezeigt, dass es möglich ist eine Interaktion von Chalcone mit der ATP-Bindungsstelle von CDK2 nachzuweisen. Dabei hat sich Butein als ein stärkerer Bindungspartner im Vergleich zu anderen Chalcone Mitgliedern herausgestellt. Eine Wasserstoffbrückenbindung von CDK2 mit den OH-Gruppen an 3. und 5. Position konnte klar visualisiert werden. Daraus schließen wir, dass das Vorhandensein der OH-Gruppen in diesem Bereich für die Bindung an die ATP-Bindungsregion des CDK2 wichtig ist. Andererseits haben sich Butein, Dichloro- oder Chloro-Chalcone als sehr schwache Bindungspartner im Vergleich mit ATP oder Roscovitine herausgestellt.

References

Ahn, Y.M., Vogeti, L., Liu, C.J., Santhapuram, H.K., White, J.M., Vasandani, V., Mitscher, L.A., Lushington, G.H., Hanson, P.R., Powell, D.R.*, et al.* (2007). Design, synthesis, and antiproliferative and CDK2-cyclin a inhibitory activity of novel flavopiridol analogues. Bioorg. Med. Chem. *15*, 702-713.

Alessi, F., Quarta, S., Savio, M., Riva, F., Rossi, L., Stivala, L.A., Scovassi, A.I., Meijer, L., and Prosperi, E. (1998). The cyclin-dependent kinase inhibitors olomoucine and roscovitine arrest human fibroblasts in G1 phase by specific inhibition of CDK2 kinase activity. Exp. Cell. Res. *245*, 8-18.

Anto, R.J., Sukumaran, K., Kuttan, G., Rao, M.N., Subbaraju, V., and Kuttan, R. (1995). Anticancer and antioxidant activity of synthetic chalcones and related compounds. Cancer Lett. *97*, 33-37.

Arkin, M.R., and Wells, J.A. (2004). Small-molecule inhibitors of protein-protein interactions: progressing towards the dream. Nat. Rev. Drug. Discov. *3*, 301-317.

Arris, C.E., Boyle, F.T., Calvert, A.H., Curtin, N.J., Endicott, J.A., Garman, E.F., Gibson, A.E., Golding, B.T., Grant, S., Griffin, R.J.*, et al.* (2000). Identification of novel purine and pyrimidine cyclin-dependent kinase inhibitors with distinct molecular interactions and tumor cell growth inhibition profiles. J. Med. Chem. *43*, 2797-2804.

Ayed A, Mulder FA, Yi GS, Lu Y, Kay LE, and CH., A. (2001). Latent and active p53 are identical in conformation. Nat. Struct. Biol. *8*, 756-760.

Baddoo, M., Hill, K., Wilkinson, R., Gaupp, D., Hughes, C., Kopen, G.C., and Phinney, D.G. (2003). Characterization of mesenchymal stem cells isolated from murine bone marrow by negative selection. J. Cell. Biochem. *89*, 1235-1249.

Balasubramanian, S., Chandraratna, R.A., and Eckert, R.L. (2005). A novel retinoid-related molecule inhibits pancreatic cancer cell proliferation by a retinoid receptor independent mechanism via suppression of cell cycle regulatory protein function and induction of caspase-associated apoptosis. Oncogene *24*, 4257-4270.

Beekman, C., Nichane, M., De Clercq, S., Maetens, M., Floss, T., Wurst, W., Bellefroid, E., and Marine, J.C. (2006). Evolutionarily Conserved Role of Nucleostemin (NS): Controlling Proliferation of Stem/Progenitor Cells during Early Vertebrate Development. Mol. Cell. Biol.

Bell, S., Klein, C., Muller, L., Hansen, S., and Buchner, J. (2002). p53 contains large unstructured regions in its native state. J. Mol. Biol. *322*, 917-927.

Berezutskaya, E., Yu, B., Morozov, A., Raychaudhuri, P., and Bagchi, S. (1997). Differential regulation of the pocket domains of the retinoblastoma family proteins by the HPV16 E7 oncoprotein. Cell Growth Differ. *8*, 1277-1286.

Berkson, R.G., Hollick, J.J., Westwood, N.J., Woods, J.A., Lane, D.P., and Lain, S. (2005). Pilot screening programme for small molecule activators of p53. Int. J. Cancer *115*, 701-710.

Bramson, H.N., Corona, J., Davis, S.T., Dickerson, S.H., Edelstein, M., Frye, S.V., Gampe, R.T., Jr., Harris, P.A., Hassell, A., Holmes, W.D.*, et al.* (2001). Oxindole-based inhibitors of cyclin-dependent kinase 2 (CDK2): design, synthesis, enzymatic activities, and X-ray crystallographic analysis. J. Med. Chem. *44*, 4339-4358.

Brandi, G., Paiardini, M., Cervasi, B., Fiorucci, C., Filippone, P., Marco, C.D., Zaffaroni, N., and Magnani, M. (2003). A New Indole-3-Carbinol Tetrameric Derivative Inhibits Cyclin-dependent Kinase 6 Expression, and Induces G1 Cell Cycle Arrest in Both Estrogen-dependent and Estrogen-independent Breast Cancer Cell Lines Cancer Res. *63*, 4028-4036.

Bringold, F., and Serrano, M. (2000). Tumor suppressors and oncogenes in cellular senescence. Exp. Geront. *35*, 317-329.

Cai, J., Cheng, A., Luo, Y., Lu, C., Mattson, M.P., Rao, M.S., and Furukawa, K. (2004). Membrane properties of rat embryonic multipotent neural stem cells. J. Neurochem. *88*, 212-226.

Chan, H.M., Smith, L., and La Thangue, N.B. (2001). Role of LXCXE motif-dependent interactions in the activity of the retinoblastoma protein. Oncogene *20*, 6152-6163.

Chellappan, S., Kraus, V.B., Kroger, B., Munger, K., Howley, P.M., and Nevins, J.R. (1992). Adenovirus E1A, Simian Virus 40 Tumor Antigen, and Human Papillomavirus E7 Protein Share the Capacity to Disrupt the Interaction Between Transcription Factor E2F and the Retinoblastoma Gene Product. Proc. Nat. Acad. Sci. *89*, 4549-4553.

Chen, C.-Y., Oliner, J.D., Zhan, Q., Fornace, A.J., Jr., Vogelstein, B., and Kastan, M.B. (1994). Interactions between p53 and Mdm2 in a mammalian cell cycle checkpoint pathway. Proc. Nat. Acad. Sci. *91*, 2684-2688.

D'Silva, L., Ozdowy, P., Krajewski, M., Rothweiler, U., Singh, M., and Holak, T.A. (2005). Monitoring the Effects of Antagonists on Protein-Protein Interactions with NMR Spectroscopy J. Am. Chem. Soc. *127* 13220-13226.

Davies, T.G., Bentley, J., Arris, C.E., Boyle, F.T., Curtin, N.J., Endicott, J.A., Gibson, A.E., Golding, B.T., Griffin, R.J., Hardcastle, I.R.*, et al.* (2002a). Structure-based design of a potent purine-based cyclin-dependent kinase inhibitor. Nat. Struct. Biol. *9*, 745-749.

Davies, T.G., Pratt, D.J., Endicott, J.A., Johnson, L.N., and Noble, M.E. (2002b). Structure-based design of cyclin-dependent kinase inhibitors. Pharmacol. Ther. *93*, 125-133.

Davies, T.G., Tunnah, P., Meijer, L., Marko, D., Eisenbrand, G., Endicott, J.A., and Noble, M.E. (2001). Inhibitor binding to active and inactive CDK2: the crystal structure of CDK2-cyclin A/indirubin-5-sulphonate. Structure *9*, 389-397.

De Azevedo, W.F., Leclerc, S., Meijer, L., Havlicek, L., Strnad, M., and Kim, S.H. (1997). Inhibition of cyclin-dependent kinases by purine analogues: crystal structure of human CDK2 complexed with roscovitine. Eur. J. Biochem. *243*, 518-526.

De Bondt, H.L., Rosenblatt, J., Jancarik, J., Jones, H.D., Morgan, D.O., and Kim, S.-H. (1993). Crystal structure of cyclin-dependent kinase 2. Nature *363*, 595-602.

De Vincenzo, R., Ferlini, C., Distefano, M., Gaggini, C., Riva, A., Bombardelli, E., Morazzoni, P., Valenti, P., Belluti, F., Ranelletti, F.O*., et al.* (2000). In vitro evaluation of newly developed chalcone analogues in human cancer cells. Cancer Chemother.Pharmacol. *46*, 305-312.

Deb, S.P. (2002). Function and dysfunction of the human oncoprotein Mdm2 [Review]. Front. Biosci. *7*, D235-D243.

Dreyer, M.K., Borcherding, D.R., Dumont, J.A., Peet, N.P., Tsay, J.T., Wright, P.S., Bitonti, A.J., Shen, J., and Kim, S.H. (2001). Crystal structure of human cyclin-dependent kinase 2 in complex with the adenine-derived inhibitor H717. J. Med. Chem. *44*, 524-530.

Dyson, H.J., and Wright, P.E. (2005). Intrinsically unstructured proteins and their functions. Nat. Rev. Mol. Cell. Biol. *6*, 197-208.

Dyson, N. (1998). The regulation of E2F by pRB-family proteins. Genes Dev. *12*, 2245-2262.

Dyson, N., Guida, P., Munger, K., and Harlow, E. (1992). Homologous sequences in adenovirus E1A and human papillomavirus E7 proteins mediate interaction with the same set of cellular proteins. J. Virol. *66*, 6893-6902.

Elledge, S.J., and Spottswood, M.R. (1991). A new human p34 protein kinase, CDK2, identified by complementation of a cdc28 mutation in Saccharomyces cerevisiae, is a homolog of Xenopus Eg1. EMBO J. *10*, 2653-2659.

Fischer, P.M. (2004). The use of CDK inhibitors in oncology: a pharmaceutical perspective. Cell Cycle *3*, 742-746.

Fischer, P.M., and Lane, D.P. (2000). Inhibitors of cyclin-dependent kinases as anti-cancer therapeutics. Curr. Med. Chem. *7*, 1213-1245.

Fry, D.C., Emerson, S.D., Palme, S., Vu, B.T., Liu, C.M., and Podlaski, F. (2004). NMR structure of a complex between Mdm2 and a small molecule inhibitor. J. Biomol. NMR *30*, 163-173.

Fu, Y., Hsieh, T.C., Guo, J., Kunicki, J., Lee, M.Y., Darzynkiewicz, Z., and Wu, J.M. (2004). Licochalcone-A, a novel flavonoid isolated from licorice root (Glycyrrhiza glabra), causes G2 and late-G1 arrests in androgen-independent PC-3 prostate cancer cells. Biochem. Biophys. Res. Commun. *322*, 263-270.

Fukai, T., Sakagami, H., Toguchi, M., Takayama, F., Iwakura, I., Atsumi, T., Ueha, T., Nakashima, H., and Nomura, T. (2000). Cytotoxic activity of low molecular weight polyphenols against human oral tumor cell lines. Anticancer Res. *20*, 2525-2536.

Furet, P., Zimmermann, J., Capraro, H.G., Meyer, T., and Imbach, P. (2000). Structure-based design of potent CDK1 inhibitors derived from olomoucine. J. Comput. Aided Mol. Des. *14*, 403-409.

Galatin, P.S., and Abraham, D.J. (2004). A nonpeptidic sulfonamide inhibits the p53-Mdm2 interaction and activates p53-dependent transcription in Mdm2-overexpressing cells. J. Med. Chem. *47*, 4163-4165.

Giacinti, C., and Giordano, A. (2006). RB and cell cycle progression. Oncogene *25*, 5220-5227.

Glab, N., Labidi, B., Qin, L.X., Trehin, C., Bergounioux, C., and Meijer, L. (1994). Olomoucine, an inhibitor of the cdc2/CDK2 kinases activity, blocks plant cells at the G1 to S and G2 to M cell cycle transitions. FEBS Lett. *353*, 207-211.

Go, M.L., Wu, X., and Liu, X.L. (2005). Chalcones: An update on cytotoxic and chemoprotective properties [Review]. Curr. Med. Chem. *12*, 483-499.

Gotz, C., and Montenarh, M. (1995). P53 and its implication in apoptosis (Review). Int. J. Oncol. *6*, 1129-1135.

Gray, N., Detivaud, L., Doerig, C., and Meijer, L. (1999). ATP-site directed inhibitors of cyclin-dependent kinases. Curr. Med. Chem. *6*, 859-875.

Gray, N.S., Wodicka, L., Thunnissen, A.M., Norman, T.C., Kwon, S., Espinoza, F.H., Morgan, D.O., Barnes, G., LeClerc, S., Meijer, L.*, et al.* (1998). Exploiting chemical libraries, structure, and genomics in the search for kinase inhibitors. Science *281*, 533-538.

Guadagno, T.M., Ohtsubo, M., Roberts, J.M., and Assoian, R.K. (1993). A link between cyclin A expression and adhesion-dependent cell cycle progression. Science *262*, 1572-1575.

Gulliver, G.A., Herber, R.L., Liem, A., and Lambert, P.F. (1997). Both conserved region 1 (CR1) and CR2 of the human papillomavirus type 16 E7 oncogene are required for induction of epidermal hyperplasia and tumor formation in transgenic mice. J. Virol. *71*, 5905-5914.

Han, C., Zhang, X., Xu, W., Wang, W., Qian, H., and Chen, Y. (2005). Cloning of the nucleostemin gene and its function in transforming human embryonic bone marrow mesenchymal stem cells into F6 tumor cells. Int. J. Mol. Med. *16*, 205-213.

Harbour, J.W., Luo, R.X., Dei Santi, A., Postigo, A.A., and Dean, D.C. (1999). Cdk phosphorylation triggers sequential intramolecular interactions that progressively block Rb functions as cells move through G1. Cell *98*, 859-869.

Hardcastle, I.R., Golding, B.T., and Griffin, R.J. (2002). Designing inhibitors of cyclin-dependent kinases. Annu. Rev. Pharmacol. Toxicol. *42*, 325-348.

Hawley-Nelson, P., Vousden, K.H., Hubbert, N.L., Lowy, D.R., and Schiller, J.T. (1989). HPV16 E6 and E7 proteins cooperate to immortalize human foreskin keratinocytes. EMBO J. *8*, 3905-3910.

Howley, P.M., Munger, K., Werness, B.A., Phelps, W.C., and Schlegel, R. (1989). Molecular mechanisms of transformation by the human papillomaviruses. Princess Takamatsu Symp. *20*, 199-206.

Issaeva, N., Bozko, P., Enge, M., Protopopova, M., Verhoef, L.G., Masucci, M., Pramanik, A., and Selivanova, G. (2004). Small molecule RITA binds to p53, blocks p53-HDM-2 interaction and activates p53 function in tumors. Nature Med. *10*, 1321-1328.

Jang HS, Kook SH, Son YO, Kim JG, Jeon YM, Jang YS, Choi KC, Kim J, Han SK, Lee KY*, et al.* (2005). Flavonoids purified from Rhus verniciflua Stokes actively inhibit cell growth and induce apoptosis in human osteosarcoma cells. Biochim. Biophys. Acta. *1726*, 309-316.

Jones, S.N., Hancock, A.R., Vogel, H., Donehower, L.A., and Bradley, A. (1998). Overexpression of Mdm2 in mice revelas a p53-independent role for Mdm2 in tumorigenesis. Proc. Nat. Acad. Sci. *95*, 15608-15612.

Ke Ding, Yipin Lu, Zaneta Nikolovska-Coleska, Su Qiu, Yousong Ding, Wei Gao, Jeanne Stuckey, Krzysztof Krajewski, Peter P. Roller, York Tomita*, et al.* (2005). Structure-Based Design of Potent Non-Peptide Mdm2 Inhibitors. J. Am. Chem. Soc. *127* 10130-10131.

Kim, K.S., Kimball, S.D., Misra, R.N., Rawlins, D.B., Hunt, J.T., Xiao, H.Y., Lu, S., Qian, L., Han, W.C., Shan, W.*, et al.* (2002). Discovery of aminothiazole inhibitors of cyclin-dependent kinase 2: synthesis, X-ray crystallographic analysis, and biological activities. J. Med. Chem. *45*, 3905-3927.

Kitagawa, M., Higashi, H., Takahashi, I.S., Okabe, T., Ogino, H., Taya, Y., Hishimura, S., and Okuyama, A. (1994). A cyclin-dependent kinase inhibitor, butyrolactone I, inhibits phosphorylation of RB protein and cell cycle progression. Oncogene *9*, 2549-2557.

Kitagawa, M., Okabe, T., Ogino, H., Matsumoto, H., Suzuki-Takahashi, I., Kokubo, T., Higashi, H., Saitoh, S., Taya, Y., Yasuda, H.*, et al.* (1993). Butyrolactone I, a selective inhibitor of CDK2 and cdc2 kinase. Oncogene *8*, 2425-2432.

Klein, C., and Vassilev, L.T. (2004). Targeting the p53-Mdm2 interaction to treat cancer. Br. J. Cancer *91*, 1415-1419.

Krajewski, M., Ozdowy, P., D'Silva, L., Rothweiler, U., and Holak, T.A. (2005). NMR indicates that the small molecule RITA does not block p53-Mdm2 binding in vitro. Nature Med. *11*, 1135-1136.

Kussie, P.H., Gorina, S., Marechal, V., Elenbaas, B., Moreau, J., Levine, A.J., and Pavletich, N.P. (1996). Structure of the Mdm2 oncoprotein bound to the p53 tumor suppressor transactivation domain. Science *274*, 948-953.

Lang, S.E., McMahon, S.B., Cole, M.D., and Hearing, P. (2001). E2F transcriptional activation requires TRRAP and GCN5 cofactors. J. Biol. Chem. *276*, 32627-32634.

Lawrence, N.J., McGown, A.T., Ducki, S., and Hadfield, J.A. (2000). The interaction of chalcones with tubulin. Anticancer Drug Des. *15*, 135-141.

Lee H, Mok KH, Muhandiram R, Park KH, Suk JE, Kim DH, Chang J, Sung YC, Choi KY, and KH., H. (2000). Local structural elements in the mostly unstructured transcriptional activation domain of human p53. J. Biol. Chem. *275*, 29426-29432.

Lee, J.O., Russo, A.A., and Pavletich, N.P. (1998). Structure of the retinoblastoma tumour-suppressor pocket domain bound to a peptide from HPV E7. Nature *391*, 859-865.

Legraverend M, Tunnah P, Noble M, Ducrot P, Ludwig O, Grierson DS, Leost M, Meijer L, and J., E. (2000). Cyclin-dependent kinase inhibition by new C-2 alkynylated purine derivatives and molecular structure of a CDK2-inhibitor complex. J. Med. Chem. *43*, 1282-1292.

Liu, S.J., Cai, Z.W., Liu, Y.J., Dong, M.Y., Sun, L.Q., Hu, G.F., Wei, Y.Y., and Lao, W.D. (2004). Role of nucleostemin in growth regulation of gastric cancer, liver cancer and other malignancies. World J. Gastroenterol. *10*, 1246-1249.

Makita, H., Tanaka, T., Fujitsuka, H., Tatematsu, N., Satoh, K., Hara, A., and Mori, H. (1996). Chemoprevention of 4-nitroquinoline 1-oxide-induced rat oral carcinogenesis by the dietary flavonoids chalcone, 2-hydroxychalcone, and quercetin. Cancer Res. *56*, 4904-4909.

Martin, L.G., Demers, G.W., and Galloway, D.A. (1998). Disruption of the G1/S transition in human papillomavirus type 16 E7-expressing human cells is associated with altered regulation of cyclin E. J. Virol. *72*, 975-985.

May, P., and May, E. (1995). P53 and Cancers. Pathologie et Biologie *43*, 165-173.

McIntyre, M.C., Frattini, M.G., Grossman, S.R., and Laimins, L.A. (1993). Human papillomavirus type 18 E7 protein requires intact Cys-X-X-Cys motifs for zinc binding, dimerization, and transformation but not for Rb binding. J. Virol. *67*, 3142-3150.

McIntyre, M.C., Ruesch, M.N., and Laimins, L.A. (1996). Human papillomavirus E7 oncoproteins bind a single form of cyclin E in a complex with CDK2 and p107. Virology *215*, 73-82.

Meijer, L., and Raymond, E. (2003). Roscovitine and other purines as kinase inhibitors. From starfish oocytes to clinical trials. Acc. Chem. Res. *36*, 417-425.

Misteli, T. (2005). Going in GTP cycles in the nucleolus. J. Cell. Biol. *168*, 177-178.

Momand, J., Wu, H.H., and Dasgupta, G. (2000). Mdm2 - master regulator of the p53 tumor suppressor protein [Review]. Gene *242*, 15-29.

Mulder, F.A., Ayed, A., Yang, D., Arrowsmith, C.H., and Kay, L.E. (2000). Assignment of 1H(N), 15N, 13C(alpha), 13CO and 13C(beta) resonances in a 67 kDa p53 dimer using 4D-TROSY NMR spectroscopy. J. Biomol. NMR *18*, 173-176.

Nevins, J.R. (1992). E2F: a link between the Rb tumor suppressor protein and viral oncoproteins. Science *258*, 424-429.

Nikolaev, A.Y., Papanikolaou, N.A., Li, M., Qin, J., and Gu, W. (2004). Identification of a novel BRMS1-homologue protein p40 as a component of the mSin3A/p33(ING1b)/HDAC1 deacetylase complex. Biochem. Biophys. Res. Commun. *323*, 1216-1222.

Normile, D. (2002). Cell proliferation. Common control for cancer, stem cells. Science *298*, 1869.

Nugiel, D.A., Vidwans, A., Etzkorn, A.M., Rossi, K.A., Benfield, P.A., Burton, C.R., Cox, S., Doleniak, D., and Seitz, S.P. (2002). Synthesis and evaluation of indenopyrazoles as cyclin-dependent kinase inhibitors. 2. Probing the indeno ring substituent pattern. J. Med. Chem. *45*, 5224-5232.

O'Connor, P.M., Jackman, J., Bae, I., Myers, T.G., Fan, S., Mutoh, M., Scudiero, D.A., Monks, A., Sausville, E.A., Weinstein, J.N.*, et al.* (1997). Characterization of p53 tumor suppressor pathway cell lines of the National Cancer Institute anticancer drug screen and correlations with the growth-inhibitory potency of 123 anticancer agents. Cancer Res. *57*, 4285-4300.

Oliner, J.D., Pietenpol, J.A., Thiagalingram, S., Gyuris, J., Kinzler, K.W., and Vogelstein, B. (1993). Oncoprotein Mdm2 conceals the activation domain of tumour suppressor p53. Nature *362*, 857-860.

Otyepka M, Kriz Z, and J., K. (2002). Dynamics and binding modes of free CDK2 and its two complexes with inhibitors studied by computer simulations. J. Biomol. Struct. Dyn. *20*, 141-154.

Owa, T., Yoshino, H., Yoshimatsu, K., and Nagasu, T. (2001). Cell cycle regulation in the G1 phase: a promising target for the development of new chemotherapeutic anticancer agents. Curr. Med. Chem. *8*, 1487-1503.

Pagano, M., Draetta, G., and Jansen-Durr, P. (1992). Association of CDK2 kinase with the transcription factor E2F during S phase. Science *255*, 1144-1147.

Palleros, D.R. (2004). Solvent-Free Synthesis of Chalcones. J. Chem. Educ. *81*, 1345-1347.

Pan, Y., and Haines, D.S. (2000). Identification of a tumor-derived p53 mutant with novel transactivating selectivity. Oncogene *19*, 3095-3100.

Radulescu, R.T., Bellitti, M.R., Ruvo, M., Cassani, G., and Fassina, G. (1995). Binding of the LXCXE insulin motif to a hexapeptide derived from retinoblastoma protein. Biochem. Biophys. Res. Commun. *206*, 97-102.

Rafi, M.M., Rosen, R.T., Vassil, A., Ho, C.T., Zhang, H., Ghai, G., Lambert, G., and DiPaola, R.S. (2000). Modulation of bcl-2 and cytotoxicity by licochalcone-A, a novel estrogenic flavonoid. Anticancer Res. *20*, 2653-2658.

Rehm, T., Huber, R., and Holak, T.A. (2002). Application of NMR in structural proteomics: screening for proteins amenable to structural analysis. Structure *10*, 1613-1618.

Riek, R., Fiaux, J., Bertelsen, E.B., Horwich, A.L., and Wüthrich, K. (2002). Solution NMR techniques for large molecular and supramolecular structures. J. Am. Chem. Soc. *124* 12144-12153.

Riek, R., Pervushin, K., and Wüthrich, K. (2000). TROSY and CRINEPT: NMR with large molecular and supramolecular structures in solution. Trends Biochem. Sci. *25*, 462-468.

Sabzevari, O., Galati, G., Moridani, M.Y., Siraki, A., and O'Brien, P.J. (2004). Molecular cytotoxic mechanisms of anticancer hydroxychalcones. Chem. Biol. Interact. *148*, 57-67.

Samoszuk, M., Tan, J., and Chorn, G. (2005). The chalcone butein from Rhus verniciflua Stokes inhibits clonogenic growth of human breast cancer cells co-cultured with fibroblasts. BMC Complement Altern. Med. *5*.

Sanders, C.M., and Maitland, N.J. (1994). Kinetic and equilibrium binding studies of the human papillomavirus type-16 transcription regulatory protein E2 interacting with core enhancer elements. Nucleic Acids Res. *22*, 4890-4897.

Satomi, Y. (1993). Inhibitory effects of 3'-methyl-3-hydroxy-chalcone on proliferation of human malignant tumor cells and on skin carcinogenesis. Int. J. Cancer *55*, 506-514.

Schon, O., Friedler, A., Bycroft, M., Freund, S.M.V., and Fersht, A.R. (2002). Molecular mechanism of the interaction between Mdm2 and p53. J. Mol. Biol *323*, 491-501.

Schutte, B., Nieland, L., van Engeland, M., Henfling, M.E., Meijer, L., and Ramaekers, F.C. (1997). The effect of the cyclin-dependent kinase inhibitor olomoucine on cell cycle kinetics. Exp. Cell. Res. *236*, 4-15.

Schwartz, P.H., Nethercott, H., Kirov, II, Ziaeian, B., Young, M.J., and Klassen, H. (2005). Expression of neurodevelopmental markers by cultured porcine neural precursor cells. Stem Cells *23*, 1286-1294.

Shapiro, G.I. (2006). Cyclin-dependent kinase pathways as targets for cancer treatment. J. Clin. Oncol. *24*, 1770-1783.

Shuker, S.B., Hajduk, P.J., Meadows, R.P., and Fesik, S.W. (1996). Discovering High-Affinity Ligands for Proteins: SAR by NMR. Science *274*, 1531 - 1534.

Sielecki, T.M., Johnson, T.L., Liu, J., Muckelbauer, J.K., Grafstrom, R.H., Cox, S., Boylan, J., Burton, C.R., Chen, H., Smallwood, A.*, et al.* (2001). Quinazolines as cyclin dependent kinase inhibitors. Bioorg. Med. Chem. Lett. *11*, 1157-1160.

Singh, M., Krajewski, M., Mikolajka, A., and Holak, T.A. (2005). Molecular determinants for the complex formation between the retinoblastoma protein and LXCXE sequences. J. Biol. Chem. *280*, 37868-37876.

Smyth, D.R., Mrozkiewicz, M.K., McGrath, W.J., Listwan, P., and Kobe, B. (2003). Crystal structures of fusion proteins with large-affinity tags. Protein Sci. *12*, 1313-1322.

Soni, D.V., and Jacobberger, J.W. (2004). Inhibition of cdk1 by alsterpaullone and thioflavopiridol correlates with increased transit time from mid G2 through prophase. Cell Cycle *3*, 349-357.

Stiegler, P., and Giordano, A. (2001). The family of retinoblastoma proteins. Crit Rev Eukaryot. Gene Expr. *11*, 59-76.

Stoll, R., Renner, C., Hansen, S., Palme, S., Klein, C., Belling, A., Zeslawski, W., Kamionka, M., Rehm, T., Muehlhahn, P*., et al.* (2001). Chalcone derivatives antagonize interactions between the human oncoprotein Mdm2 and p53. Biochemistry *40*, 336-344.

ter Haar, E., Hamel, E., Balachandran, R., and Day, B.W. (1997). Cellular targets of the anti-breast cancer agent Z-1,1-dichloro-2,3-diphenylcyclopropane: type II estrogen binding sites and tubulin. Anticancer Res. *17*, 1861-1869.

Toda, F., Tanaka, K., and Hamai, K.A. (1990). Aldo condensations in the absence of solvent: Acceleration of the reaction and enhancement of the stereoselectivity. J. Chem. Soc., Perkin Trans 1, 3207-3209.

Toogood, P.L. (2001). Cyclin-dependent kinase inhibitors for treating cancer. Med. Res. Rev. *21*, 487-498.

Tsai, L.H., Harlow, E., and Meyerson, M. (1991). Isolation of the human CDK2 gene that encodes the cyclin A- and adenovirus E1A-associated p33 kinase. Nature *353*, 174-177.

Tsai, R.Y., and McKay, R.D. (2002). A nucleolar mechanism controlling cell proliferation in stem cells and cancer cells. Genes Dev. *16*, 2991-3003.

Tsai, R.Y., and McKay, R.D. (2005). A multistep, GTP-driven mechanism controlling the dynamic cycling of nucleostemin. J. Cell. Biol. *168*, 179-184.

Uesugi, M., and Verdine, G.L. (1999). The alpha-helical FXXPhiPhi motif in p53: TAF interaction and discrimination by Mdm2. Proc. Nat. Acad. Sci. *96*, 14801-14806.

Vassilev, L.T., Vu, B.T., Graves, B., Carvajal, D., Podlaski, F., Filipovic, Z., Kong, N., Kammlott, U., Lukacs, C., Klein, C.*, et al.* (2004). In vivo activation of the p53 pathway by small-molecule antagonists of Mdm2. Science *303*, 844-848.

Wang, Y., Bai, Y., Li, X., Hu, Q., Lin, C., Xiao, Z., Liu, Y., Xu, J., Shen, L., and Li, L. (2004). Fetal human neural progenitors can be the target for tumor transformation. Neuroreport *15*, 1907-1912.

Wang Z. X (1995). An exact mathematical expression for describing competitive binding of two different ligands to a protein molecule. FEBS Lett. *360*, 111-114.

Webster, K., Taylor, A., and Gaston, K. (2001). Oestrogen and progesterone increase the levels of apoptosis induced by the human papillomavirus type 16 E2 and E7 proteins. J. Gen. Virol. *82*, 201-213.

Xiao, B., Spencer, J., Clements, A., Ali-Khan, N., Mittnacht, S., Broceno, C., Burghammer, M., Perrakis, A., Marmorstein, R., and Gamblin, S.J. (2003). Crystal structure of the retinoblastoma tumor suppressor protein bound to E2F and the molecular basis of its regulation. Proc. Nat. Acad. Sci. *100*, 2363-2368.

Xiong, Y., Zhang, H., and Beach, D. (1992). D type cyclins associate with multiple protein kinases and the DNA replication and repair factor PCNA. Cell *71*, 505-514.

Xu, W., Qian, H., Zhu, W., Chen, Y., Shao, Q., Sun, X., Hu, J., Han, C., and Zhang, X. (2004). A novel tumor cell line cloned from mutated human embryonic bone marrow mesenchymal stem cells. Oncol. Rep. *12*, 501-508.

Yaghoobi, M.M., Mowla, S.J., and Tiraihi, T. (2005). Nucleostemin, a coordinator of self-renewal, is expressed in rat marrow stromal cells and turns off after induction of neural differentiation. Neurosci. Lett. *390*, 81-86.

Yamamoto, S., Aizu, E., Jiang, H., Nakadate, T., Kiyoto, I., Wang, J.C., and Kato, R. (1991). The potent anti-tumor-promoting agent isoliquiritigenin. Carcinogenesis *12*, 317-323.

Yang, Y.L., Li, C.C.H., and Weissman, A.M. (2004). Regulating the p53 system through ubiquitination [Review]. Oncogene *23*, 2096-2106.

Yili Yang, Robert L. Ludwig, Jane P. Jensen, Shervon A. Pierre, Maxine V. Medaglia, Ilia V. Davydov, Yassamin J. Safiran, Pankaj Oberoi, John H. Kenten, Andrew C. Phillips*, et al.* (2005). Small molecule inhibitors of HDM2 ubiquitin ligase activity stabilize and activate p53 in cells. Cancer Cell *7* 547-559.

Yin H, Gui-in Lee, Hyung Soon Park, Gregory A. Payne, Johanna M. Rodriguez, Sebti, S.M., and D, H.A. (2005). Terphenyl-Based Helical Mimetics That Disrupt the p53/HDM2 Interaction. Angew. Chem. Int. Ed. *44*, 2704 -2707.

Yue, E.W., Higley, C.A., DiMeo, S.V., Carini, D.J., Nugiel, D.A., Benware, C., Benfield, P.A., Burton, C.R., Cox, S., Grafstrom, R.H.*, et al.* (2002). Synthesis and evaluation of indenopyrazoles as cyclin-dependent kinase inhibitors. 3. Structure activity relationships at C3(1,2). J. Med. Chem. *45*, 5233-5248.

Zaharevitz, D.W., Gussio, R., Leost, M., Senderowicz, A.M., Lahusen, T., Kunick, C., Meijer, L., and Sausville, E.A. (1999). Discovery and initial characterization of the paullones, a novel class of small-molecule inhibitors of cyclin-dependent kinases. Cancer Res. *59*, 2566-2569.

Zauberman, A., Barak, Y., Ragimov, N., Levy, N., and Oren, M. (1993). Sequence-specific DNA binding by p53: Identification of target sites and lack of binding to p53-Mdm2 complexes. EMBO J. *12*, 2799-2808.

Zhao, J.H., Wang, M.J., Chen, J., Luo, A.P., Wang, X.Q., Wu, M., Yin, D.L., and Liu, Z.H. (2002). The initial evaluation of non-peptidic small-molecule HDM2 inhibitors based on p53-HDM2 complex structure. Cancer Lett. *183*, 69-77.

Zhu, L., Enders, G., Lees, J.A., Beijersbergen, R.L., Bernards, R., and Harlow, E. (1995). The pRB-related protein p107 contains two growth suppression domains: independent interactions with E2F and cyclin/cdk complexes. EMBO J. *14*, 1904-1913.

Zhu, Y., Alvarez, C., Doll, R., Kurata, H., Schebye, X.M., Parry, D., and Lees, E. (2004). Intra-S-phase checkpoint activation by direct CDK2 inhibition. Mol. Cell. Biol. *24*, 6268-6277.

Zini, N., Trimarchi, C., Claudio, P.P., Stiegler, P., Marinelli, F., Maltarello, M.C., La Sala, D., De Falco, G., Russo, G., Ammirati, G.*, et al.* (2001). pRb2/p130 and p107 control cell growth by multiple strategies and in association with different compartments within the nucleus. J. Cell. Physiol. *189*, 34-44.

Zwerschke, W., Joswig, S., and Jansen-Durr, P. (1996). Identification of domains required for transcriptional activation and protein dimerization in the human papillomavirus type-16 E7 protein. Oncogene *12*, 213-220.

Appendix

Abbreviations and Symbols

- aa amino acid
- ATP adenosine triphosphate
- 1D one-dimensional
- bp base pair
- CDK cyclin-dependent kinase
- chalcone 1,3-diphenyl-2-propen-1-one
- COSY correlation spectroscopy
- δ chemical shift
- Da Dalton (g mol^{-1})
- DMSO dimethylsulfoxide
- DNA deoxyribonucleic acid
- DNaseI deoxyribonuclease I
- DTT Dithiothreitol
- EDTA ethylenediamine tetraacetic acid
- G gravity (9.81 m s^{-2})
- GSH reduced glutathione
- GSSG oxidized glutathione
- GST glutathione S-transferase
- HSQC heteronuclear single quantum coherence
- Hz Hertz
- IPTG isopropyl-β-thiogalactopyranoside
- LB Luria-Broth medium
- M mol l^{-1}
- Mdm2 murine double minute clone 2

- MM minimal medium
- MW molecular weight
- NiNTA nickel-nitrilotriacetic acid
- NLS nuclear localization signal
- NMR nuclear magnetic resonance
- NOE nuclear Overhauser effect
- NOESY nuclear Overhauser enhancement spectroscopy
- OD optical density
- PAGE polyacrylamide gel electrophoresis
- PBS phosphate-buffered saline
- ppm parts per million
- RNaseA ribonuclease A
- SAR structure-activity relationship
- SDS sodium dodecyl sulfate
- TEMED N,N,N’,N’-tetramethylethylendiamine
- TOCSY total correlation spectroscopy

Amino acids and nucleotides are abbreviated according to either one or three letter IUPAC code.

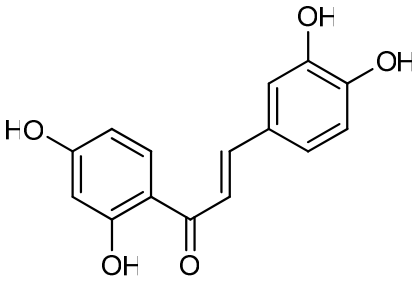

Figure A Chemical structures of butein

Tabel 1. From selection to validated hits

Step	Property of inhibitory	Suggested methods	Comments
1	Functional inhibition	Typically how compounds are identified, by ELISA, SPA, DELFIA	Deglycosylation of target proteins and conjugation of reporter proteins can reduce protein solubility and. introduce artefacts; proteins should be kept as close to native state as possible.
2	Inhibition in orthogonal assay	SPA, FRET, inhibition of antibody binding	Eliminates detection-specific artefacts from primary assay. screen.
3	Aggregation of compounds and/or protein	Extreme sensitivity to conditions, for example detergents, concentration of protein. Functional inhibition of unrelated proteins. AUC	Bona fide, hydrophobic or amphiphilic compound may also be sensitive to detergents, so can produce false negatives. Non-selectivity is often a sign of aggregation or denaturation Equilibrium sedimentation diagnoses aggregation of compound and compound-dependent aggregation of proteins. Requires optical absorbance of compound for direct detection of protein–compound interaction.
4	Reversibility	Surface plasmon resonance (SPR) Mass spectrometry Radioligand binding Concentration/dilution.	Allows measurement of kinetic constants; can be sensitive to nonspecific binding to the SPR surface. Allows detection of covalently bound compounds. Measuring the binding kinetics of a radiolabelled compound is most useful for tight-binding compounds.

			Compound is incubated with concentrated solution of protein; mixture is then diluted so that the compound concentration is well below the IC50 and the activity of the protein is measured. Identifies covalent modifiers, but might not identify aggregators (which are sensitive to compound/protein ratio).
5	Binding stoichiometry, Kd	Isothermal calorimetry. SPR, radioligand binding. Fluorescence. Equilibrium dialysis. NMR AUC Mass spectrometry of complex	Gives highly validated stoichiometry and/or Kd, but requires high compound solubility and can be difficult for weak binders or entropy-driven binding. See step 4 above. Straightforward method when either compound or protein have significant fluorescence that changes on compound binding. Compound detected by UV, HPLC, or radioligand binding. Ligand-based methods monitor binding of ligands with weak–moderate affinity (10^{-3} –10^{-6} M); can be used even with large proteins. Can determine K_d for moderate affinities (10^{-4} –10^{-6}) and stoichiometry for higher affinities. Not always feasible, especially for binding driven. by hydrophobic interactions.
6	Binding site	X-ray crystallography. NMR	Gives high-resolution image of binding interactions; a static view of binding. HSQC identifies

		Functional inhibition of known ligands Site-directed mutagenesis Photoaffinity labelling/MS.	protein residues affected by compound binding; NOESY experiments can lead to a three-dimensional model of the interaction in solution. These NMR methods require well-expressed, soluble, small proteins. Inhibiting the binding of antibodies, peptides or other small molecules with known binding sites could indicate same-site binding, but is subject to interpretation. Mutations that do not affect the structure of the protein but alter binding could indicate that the residue is in the small-molecule binding site. Compound is conjugated to a photoaffinity label in a way that does not affect its binding to the protein. The compound and protein are incubated in the presence of light, the protein is digested by a protease, and the location of the label is determined by changes in the digestion pattern. Incomplete or multiple labelling might complicate the analysis.